Spacecraft Dynamics as Related to Laboratory Experiments in Space

NASA

Spacecraft Dynamics as Related to Laboratory Experiments in Space

Edited by
G. H. Fichtl
B. N. Antar
and F G. Collins

George C. Marshall Space Flight Center
Marshall Space Flight Center, Alabama

NΛSΛ

National Aeronautics
and Space Administration

Scientific and Technical
Information Branch

1981

FOREWORD

The Space Shuttle era will facilitate the conduct of scientific experiments in space on a routine basis. Many physics and chemistry laboratory experiments that will be performed in space will utilize the "low-gravity" feature of Earth orbit. However, the dynamic nature of spaceflight necessitates that scientists and engineers consider the effects of spacecraft dynamics in the design of experiments and planning of spaceflight missions. Prior to the meeting, the subject of spacecraft dynamics in the context of laboratory experiments in space had not been considered in a unified manner. The Physics and Chemistry Experiments in Space (PACE) Working Group sponsored this meeting for scientists and engineers to discuss the nature of spacecraft dynamics and its impact on the design and performance of laboratory experiments in space, and to identify engineering and scientific deficiencies in our knowledge of the subject. The meeting proved to be an effective forum. It is anticipated that the proceedings will serve as an introduction to the subject for those new to the use of space as a laboratory environment and as a reference to those currently planning to use space for scientific experimentation.

The support of Dr. Ellis Whiting, Program Manager for PACE, NASA Headquarters Office of Aeronautics and Space Technology, and the PACE Working Group for the successful completion of this workshop is gratefully acknowledged, as well as the participants for the preparation of their presentations, manuscripts, and lively discussion.

TABLE OF CONTENTS

I. EXECUTIVE SUMMARY

INTRODUCTORY COMMENTS TO WORKSHOP ON SPACECRAFT

DYNAMICS AS RELATED TO LABORATORY

EXPERIMENTS IN SPACE

During the 1980's the Space Shuttle will provide a platform for scientists and technologists to perform experiments in space. In particular, the Space Shuttle will provide new opportunities for the performance of laboratory experiments in space which could not otherwise be performed on Earth because of the constraining effects of the Earth's gravitational field. However, the environment associated with Earth orbiting vehicles is not quiescent but, rather, is a dynamic environment which results from many sources, i.e., spacecraft maneuvers, vernier thrusters, atmospheric drag, crew activity, venting of liquids and gases, operation of machinery (blowers, fans, pumps, etc.) experiments, etc. (Table 1, p. 120). The frequency bandwidth of this dynamic environment is broad, ranging from zero to frequencies associated with audible sound. It has been recognized that spacecraft dynamics constitutes a major forcing function which could significantly affect the outcome of experiments in space and, as such, must be taken into account during the development, planning, operation, and postflight analysis of spaceflight experiments. However, the subject has not been fully discussed and explored in the context of spacecraft/ experiment interaction. This is particularly true for laboratory experiments to be performed in spacecraft that involve fluid dynamic processes, combustion processes, quantum fluids, crystal growth, life sciences, etc. The NASA Office of Aeronautics and Space Technology (OAST), Physics and Chemistry Experiments in Space (PACE) Working Group, has recognized the need for scientists, technologists, and engineers to address the subject of spacecraft/experiment interaction. In this regard, the PACE Working Group has supported the conduct of this workshop relative to accomplishing the following objectives:

1) To provide a forum wherein scientists and technologists who are involved with the development and performance of experiments in space and specialists in the field of spacecraft dynamics can exchange ideas with a view toward clarifying the nature of spacecraft dynamics/experiment interaction and developing understanding of the impact of spacecraft dynamics on experiments in space.

2)   To assess the knowledge that is available on the subject of spacecraft dynamics and to identify areas where important deficiencies exist in our information with respect to both spacecraft dynamics and the associated impact on experiments anticipated to be performed in space in the 1980's.

3)   To develop recommendations on needed research and technology development to eliminate these deficiencies.

Because of the broad nature of the subject of spacecraft dynamics/experiment interaction the meeting was restricted to laboratory experiments, e.g., free and contained fluids, quantum fluids, combustion processes, general relativity, and life sciences. The meeting was not concerned with Earth- or space-viewing experiments, except as related to viewing experiments' requirements which result in vehicle dynamics effects that might impact the laboratory experiments in question. The subsequent sections in this proceedings provide the papers presented at the meeting and deal with the following subjects: Part II - Low Gravity Experiments, Part III - Effects of Spacecraft Dynamics on Experiments, and Part IV - Spacecraft Dynamic Environment. A meeting agenda is provided in Appendix A. A list of participants in the workshop is available in Appendix B.

During the first day of the workshop, a common frame of reference was established through presentations on laboratory experiments and spacecraft dynamics. Scientists and technologists provided a brief description of laboratory experiments that are being planned for performance in space in the 1980's, including goals, objectives, and potential effects of spacecraft dynamics on these experiments. Presentations were also provided on effects of spacecraft dynamics on fluids in space by representatives from the scientific community. Subsequent to these presentations, lectures were provided on spacecraft dynamics encompassing orbital mechanics, rigid and elastic body dynamics, acoustic and vibration environments, and related subjects. In addition, on the morning of the second day two lectures were provided by Dr. Donald Drever of the California Institute of Technology on relativity experiments in space involving transmission of signals between satellites to detect gravitation waves, and by Mr. William Lange of the Bell Aerospace/Textron Corporation on spacecraft acceleration measurements with the Miniature Electrostatic Accelerometer (MESA) scheduled to fly on Spacelab Mission 2. The second day was devoted to open discussion aimed at accomplishing the previously stated objectives. Scientific and engineering deficiencies were identified and the necessary developments needed to eliminate these deficiencies were identified. A summary of the deficiencies and needed developments is provided in the conclusions and recommendations section of Part I.

<div align="right">

George H. Fichtl
Basil N. Antar
Frank G. Collins

</div>

CONCLUSIONS AND RECOMMENDATIONS

As a result of the presentations and discussions, important conclusions and recommendations were formulated. Major deficiencies were found to exist in our knowledge of spacecraft dynamics and in the potential effect of spacecraft dynamics upon laboratory experiments in space. Recommendations were made concerning technological and scientific developments that are needed to eliminate these deficiencies. These deficiencies and recommendations are summarized in this section.

It was concluded by the workshop participants that there is an urgent need for a comprehensive description of the anticipated dynamic state of spacecraft for experiment definition. This should include a complete description of the dynamic disturbance sources and strengths, and the description should encompass a sufficiently wide bandwidth, i.e., 0 to 50 Hz. For rotating fluid dynamic experiments wherein the angular velocity of a vessel is Ω (rad sec^{-1}) the description of the dynamics of spacecraft should encompass bandwidth 0 to $\Omega/2\pi$ (in units of Hertz). Statistical descriptions of the dynamic environment of spacecraft (angular and rectilinear accelerations, angular rates, and attitude) are needed, including mean values, frequency spectra, discrete disturbance signatures as a function of risk of exceedance during the experiment duration time, distribution functions, peak-to-peak values, etc. A major item upon which there was general agreement is the need for typical examples of time histories and frequency spectra of spacecraft accelerations ("g-jitter"). It was further recommended that every effort be made by the NASA to acquire these profiles during early Shuttle missions (e.g., OFT missions, Spacelab 1 Mission). Instrumentation should be provided on these early missions as well as all later missions to measure and record time histories of vehicle attitude, angular rates, and angular and rectilinear accelerations. Furthermore, event times of disturbances like thruster firings, gas venting, etc., should be recorded for postflight analysis. In addition to the data above, information about high-frequency disturbances, e.g., acoustic disturbances, is needed. The information described above is needed in general terms for experiment definition studies. Once a specific mission is identified for performance of the experiment, predictions of the dynamic environment for that mission are needed for experiment planning. Subsequent to flight, measurements of the dynamic environment are required for postflight experiment data analysis.

It was concluded that an assessment of the behavior of fluids in space in response to spacecraft dynamic behavior is required for experiment planning. The range of possible fluid flow/spececraft dynamics interactions that could occur is broad. Nevertheless, systematic development of a body of knowledge is possible, and it appears that it will be developed in part as a result of experiment payload definition and planning activities. It was pointed out that assessments of the role of spacecraft accelerations ("g-jitter") on fluids may be required relative to destabilization of fluid experiments as a result of "g-jitter," effect of "g-jitter" with zero mean value on convection, and masking of desired effects of "g-jitter" deposition of energy into experiment systems. It was noted that in the case of experiments involving rotating fluids, important effects could occur from (1) precession of the angular velocity vector of the experiment about the angular velocity vector of the orbit of the spacecraft, (2) changes in vehicle attitude, and (3) periodicities in the rectilinear and angular accelerations of the vehicle at frequencies which are multiples of the magnitude of the angular velocity vector of the experiment. In the case of the latter, there appears to be essentially no information on the subject in the literature on rotating fluid mechanics. Finally, it was concluded that in certain cases the effect of spacecraft dynamics on experiments may not be predictable and could only be assessed by performing the spaceflight experiment. This is especially true of life sciences experiments.

It was concluded that the following technological and scientific developments are required to help eliminate the deficiencies noted above.

1) The available data on spacecraft dynamics from the Apollo, Skylab, and the Apollo-Soyuz missions should be analyzed and documented. The results of these studies should be made available to the scientists who are planning experiments for space.

2) Every attempt should be made to acquire data on spacecraft dynamics in the planned Shuttle flights in the 1980's. These data should include recordings from 3-axis low-g (10^{-9} g) accelerometers encompassing frequencies up to 50 Hz. Also, to aid in experiment design it was recommended that VFI quality instruments to measure the dynamic environment should be flown on Shuttle flights.

3) It was recommended that simulations be made of the dynamic environment of Spacelab using data from previous missions. Such simulations should take into account the forcing functions anticipated to be present during an experiment (e.g., crew activity, venting, etc.), as well as our

6

current knowledge of Orbiter systems (thruster time interval, specific impulse, limit cycles, etc.).

4) It was concluded that improved understanding of the experiments can be made through more use of available ground-based facilities such as drop towers, laboratory simulation, computer simulation, intensive analytical models, and KC 135 flights. It was concluded that information of this type would aid significantly in experiment design and planning.

5) It was agreed that effort should be applied to the development of techniques for isolating experiments from spacecraft dynamic effects.

II. LOW-GRAVITY EXPERIMENTS

10

DEFINING CRITICAL POINT EXPERIMENTS

FOR A SPACE LABORATORY

by
M. R. Moldover
Thermophysics Division
National Bureau of Standards

ABSTRACT

We are defining three representative low-gravity experiments for a fluid near its liquid-vapor critical point. Two of these experiments require very careful measurements of properties of the fluid in thermodynamic equilibrium, while the third experiment is a series of optical observations of the phenomena which occur as a fluid is changed from one phase to two phases, either by cooling through the critical point, or by adiabatic expansion. We are concerned with spacecraft dynamics insofar as residual spacecraft motions may complicate the interpretation of the data from the proposed experiments. It is possible that the spacelab environment will render certain desirable experiments impractical.

INTRODUCTION

This experiment definition study has been sponsored by NASA Lewis Research Center under Interagency Agreement C-62861-C. An interim report has been prepared giving an overview of research in critical phenomena and phase transitions in fluids with emphasis on the opportunities for experimental research that will become available in Spacelab [1]. A definitive review of gravity effects in fluids near the gas-liquid critical points has been published [2]. A brief overview and bibliography have also been published [3, 4].

A low-g environment greatly reduces certain constraints on the design of scientifically exciting experiments near critical points [1]. To establish the feasibility and utility of low-g experiments it is necessary to show that other likely constraints can be overcome. We are attempting to identify these constraints and methods of dealing with them for three representative experiments.

REPRESENTATIVE EQUILIBRIUM EXPERIMENTS

Under normal gravity conditions, efforts to measure these equilibrium properties of fluids are ultimately frustrated by the fluid's extraordinarily strong response to pressure gradients. This response is so strong near the critical point that the density at the bottom of a 1 mm high sample of fluid will be about 6% greater than the density at the top of the sample because of the sample's own weight. Thus any experiment which requires a sample at least 1 mm tall cannot yield meaningful results within ±3% of the critical density at the critical temperature. The density difference scales as $g^{0.26}$; hence low-g experiments might yield meaningful results closer to the critical density. Residual steady spacecraft accelerations will prevent the experimental fluid samples from achieving the uniform density expected in the absence of such accelerations.

The first equilibrium experiment we have studied in detail is a careful measurement of the angular dependence of the intensity and spectrum of light scattered from fluid near its critical point. This gives information about the size and lifetime of the transient "clusters" which occur near the critical point and are manifest as critical opalescence. A schematic diagram of the experiment is shown in Figure 1.

The second equilibrium experiment under consideration is a measurement of one of the theoretically important but experimentally "weak" anomalies which occur in several properties of fluids near critical points. (The dielectric constant is our prototypical example of such a property; however, the viscosity and constant volume specific heat, C_V, are other properties of similar importance.) A schematic diagram of a dielectric constant experiment is shown in Figure 2. A high-quality Earth-based dielectric constant measurement has been completed [5].

Under steady conditions near the critical point, a temperature gradient of 1 mK/cm will alter the fluid's density distribution about as much as an acceleration of 1 g. It is conceivable that unsteady spacecraft motion could deposit energy in fluid samples, leading to undesired temperature gradients. (Fluids near their critical points are extremely poor heat conductors.) A rate of energy deposition as small as 0.1 erg $cm^{-3}s^{-1}$ would probably be a severe design constraint for the proposed equilibrium measurements. Thus we need a method of estimating the rate of energy deposition in very compressible fluids samples from spacecraft motion.

Specific heat experiments, which require a complete record of energy inputs into a quite small fluid sample, will be particularly sensitive to unsteady motion. To establish the feasibility of a C_V experiment near the critical point, consideration must be given to stray energy inputs to the fluid sample from mechanical vibrations of the system supporting the experiment and from acoustic sources in the air surrounding the experiment. (Comparable Earth-based measurements are carried out in rather quiet laboratories.) Thus we require not only a thorough characterization of spacecraft dynamics, but also some sort of realistic upper bounds on the spectrum of noise and structural vibrations in Spacelab.

NONEQUILIBRIUM EXPERIMENT

A fluid near its critical density and temperature will be caused to phase separate by steady cooling and/or by increasing the volume of the cell several percent (see Figure 3).

Under normal gravity conditions, the later stages of the phase separation experiment are dominated by sedimentation. Once bubbles (or droplets) are several microns in size, they rise (or fall) to the end of the cell within a few seconds. Under low-g conditions it should be possible to observe bubble and droplet growth for much longer periods of time. The growth regimes dominated by heat conduction and Marangoni convection should be more easily observed than on Earth. A detailed discussion of the role of spacecraft dynamics on this phase separation experiment must await a more complete understanding of the mechanisms dominating bubble motion under the nonequilibrium conditions of the proposed experiment.

REFERENCES

1. Moldover, M. R., Hocken, R. J., and Gammon, R. W.: Spacelab Experiment Definition Study on Phase Transition and Critical Phenomena in Fluids: Interim Report on Experimental Justification, NASA CR-135070, August 1976.

2. Moldover, M. R., Sengers, J. V., Gammon, R. W., and Hocken, R. J.: Gravity Effects in Fluids Near the Gas-Liquid Critical Point, Rev. Modern Physics, 51:79-99 (1979).

3. Sengers, J. V., and Moldover, M. R.: Critical Phenomena in Space? Z. Flugwiss Weltraunforsch, $\underline{2}$:371-379 (1978).

4. Sengers, J. V., and Moldover, M. R.: Critical Phenomena in a Low Gravity Environment, in M. J. Rycroft and A. C. Strickland (Eds.). Cospar: Space Research. Vol. XVIII, pp. 495-506. Pergamon Press, Oxford, New York, 1978.

5. Thijsse, B. J.: The Dielectric Constant of SF_6 Near the Critical Point. Submitted to J. Chem. Phys. (1980); and Thijsse, B. J., Doiron, T. D., and Sengers, J. M. H. Levelt: A New Upper Bound for a Critical Anomaly in the Dielectric Constant of SF_6, Phys. Chem. Letters $\underline{72}$, 546 (1980).

LIGHT SCATTERING EXPERIMENT

CHOPPER

MASK

TRAP

PM TUBE

SCATTERING CELL

MULTISTAGE THERMOSTAT

AMPLIFIER DISCRIMINATOR

LASER

CORRELATOR OR COUNTER

COMPUTER
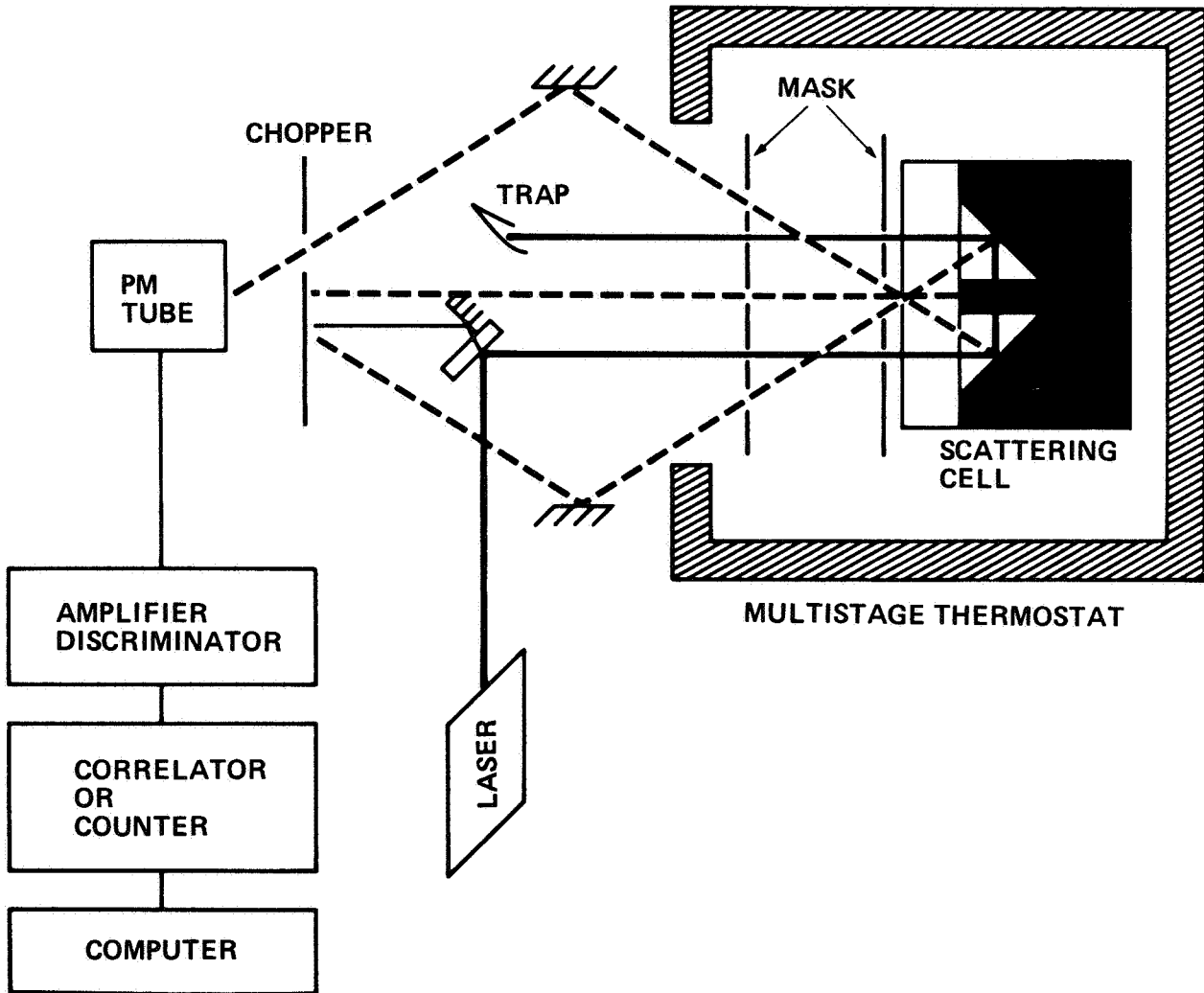
FIGURE 1

DIELECTRIC CONSTANT EXPERIMENT

MULTISTAGE THERMOSTAT

FIGURE 2

PHASE SEPARATION EXPERIMENT

FIGURE 3

17
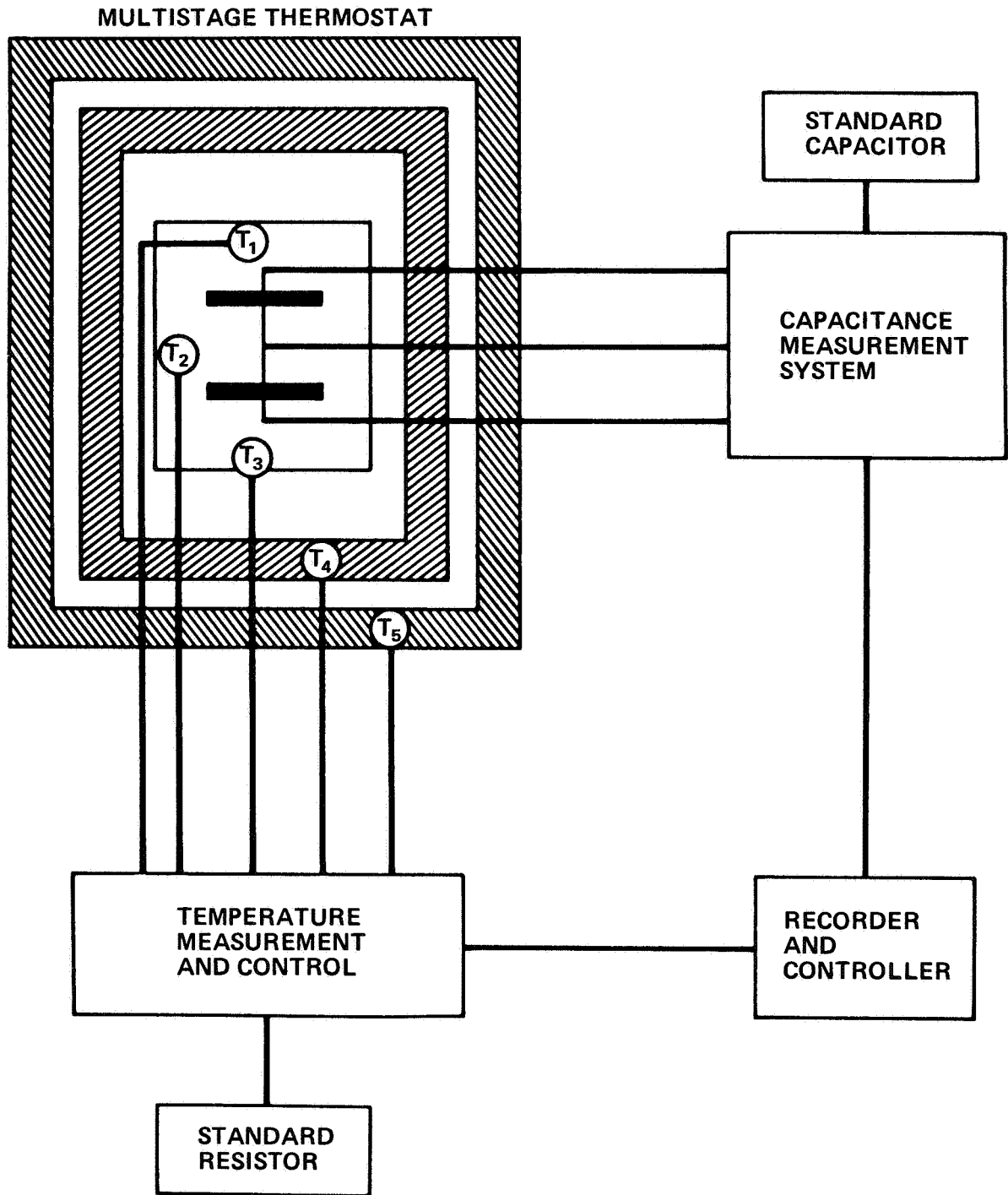
DYNAMICS OF SUPERFLUID HELIUM

IN ZERO GRAVITY

by
Peter V. Mason
Low-Temperature Physics Group
Jet Propulsion Laboratory

Liquid helium becomes superfluid (HeII) when its temperature is reduced below 2.2 K. In this state, it has a number of unusual properties which are of technological and scientific interest. These include near-zero viscosity, thermal superconductivity, and the thermomechanical or fountain pressure.

HeII is composed of two interpenetrating phases--the superfluid phase has zero viscosity, carries no heat, and has zero entropy. The other phase is a normal fluid with normal viscosity and entropy. The fraction of superfluid is determined by temperature, rising rapidly from zero at 2.2 K to 1 at 0 K. HeII has an extremely high thermal conductivity--about 1000 times that of copper--and can maintain temperature uniformity in a working volume of several centimeters uniform to a few milliKelvin.

HeII may support several different sound waves, five or six at last count. First sound, the ordinary pressure-density wave of classical physics, is the synchronous motion of the two fluids. Second sound is the anti-synchronous motion of the two fluids without a change in density. It is a thermal wave; heat travels in a coherent manner described by a wave equation rather than the usual diffusion equation.

Third sound is still another form; in thin films the normal component is clamped to the substrate by its viscosity, but the superfluid, being frictionless, moves as a surface wave. In one gravity and at low frequency, this surface wave is a gravitational wave, similar to long-period ocean waves. High-frequency, short-period capillary waves, similar to wind-driven ripples on a water surface, are theoretically possible, but in actuality are so highly damped by energy exchange between the liquid and the gas above the surface that they cannot be observed.

It is this capillary wave that we propose to observe in space. The low-gravity environment provides two essential experimental conditions. First, as shown in Figure 1, the

capillary wave behavior is extended to the long-period, low-frequency region, where attenuation is low enough to permit it to be observed. Secondly, the films must be about one micron thick over an area of several square centimeters, a condition impossible to obtain in the 1-g laboratory, due to tilts and irregularities in the substrate on which the films are formed.

As shown in Figure 2, a time of flight technique will be used to measure the velocity and damping of the capillary waves. A pulsed heater will generate the wave, and a capacitance thickness detector will observe its passage. If the damping is low, the wave will pass over the sensors several times, permitting highly accurate determination of its velocity and amplitude loss. If the damping is high, only one passage will be observed, permitting determination but with reduced accuracy.

Superfluid helium will be used as a cryogen to maintain the optics and detectors of space-borne far IR telescopes such as the free-flying Infrared Astronomical Satellite (due for launch in 1982) and the Shuttle Infrared Telescope Facility (planned for flight in the mid-to-late 1980's). For these missions, it is important to understand the sloshing motion of the bulk liquid in near-zero gravity, for it may have deleterious effects on the sensors and the attitude control system. A preliminary 10-minute experiment has been performed on a rocket [1] supplemented by 15-second observations in a NASA zero-g aircraft. A much longer and more accurate experiment will be flown on the Shuttle in conjunction with the surface wave experiment described above.

As shown in Figure 3, the helium can be expected to pass from regions where surface tension dominates to regions where gravity dominates. Thus the behavior will be complex. In the surface tension region, the free surface will tend to take the shape of the vessel, while in the gravitational region, it will tend to be planar. Since the viscosity is low and nonlinear, theoretical predictions are difficult and direct observation is essential. The thruster and maneuvering systems of the Shuttle will provide the excitations of the liquid, and a large number of superconducting liquid vapor sensors will define the motion of the free surface.

A third experiment will measure temperature distributions in the liquid and their correlations with the bulk motions. One expects variations of only millidegrees in volumes of the order of a cubic meter. We will use a number of sensors with a sensitivity of 10 microKelvin.

The overall system is shown in Figure 4. A helium cryostat will contain a sensor head with the experiments. A microcomputer will provide electrical excitations and gather and transmit the resultant responses to the experiment team on the ground. Astronaut intervention will be possible, but will be used primarily for turn-on and shutdown, and for necessary commands when out of communcation with the experimenters.

REFERENCES

1. Mason, P. V., Collins, D., Petrac, D., Yang, L., Edeskuty, F., Schuch, A., and Williamson, K.: The Behavior of Superfluid Helium in Zero Gravity, Proceedings of the 7th International Cryogenic Engineering Conference, 99. IPC Science and Technology Press, Surrey, 1978.

WAVE	g	FILM THICKNESS
a	1g	10^{-3}
b	$10^{-4}g$	10^{-3}
c	$10^{-4}g$	10^{-4}

$\sigma = 0.3$ DYNES/CM

$\rho = 0.14$ GM/CM^3
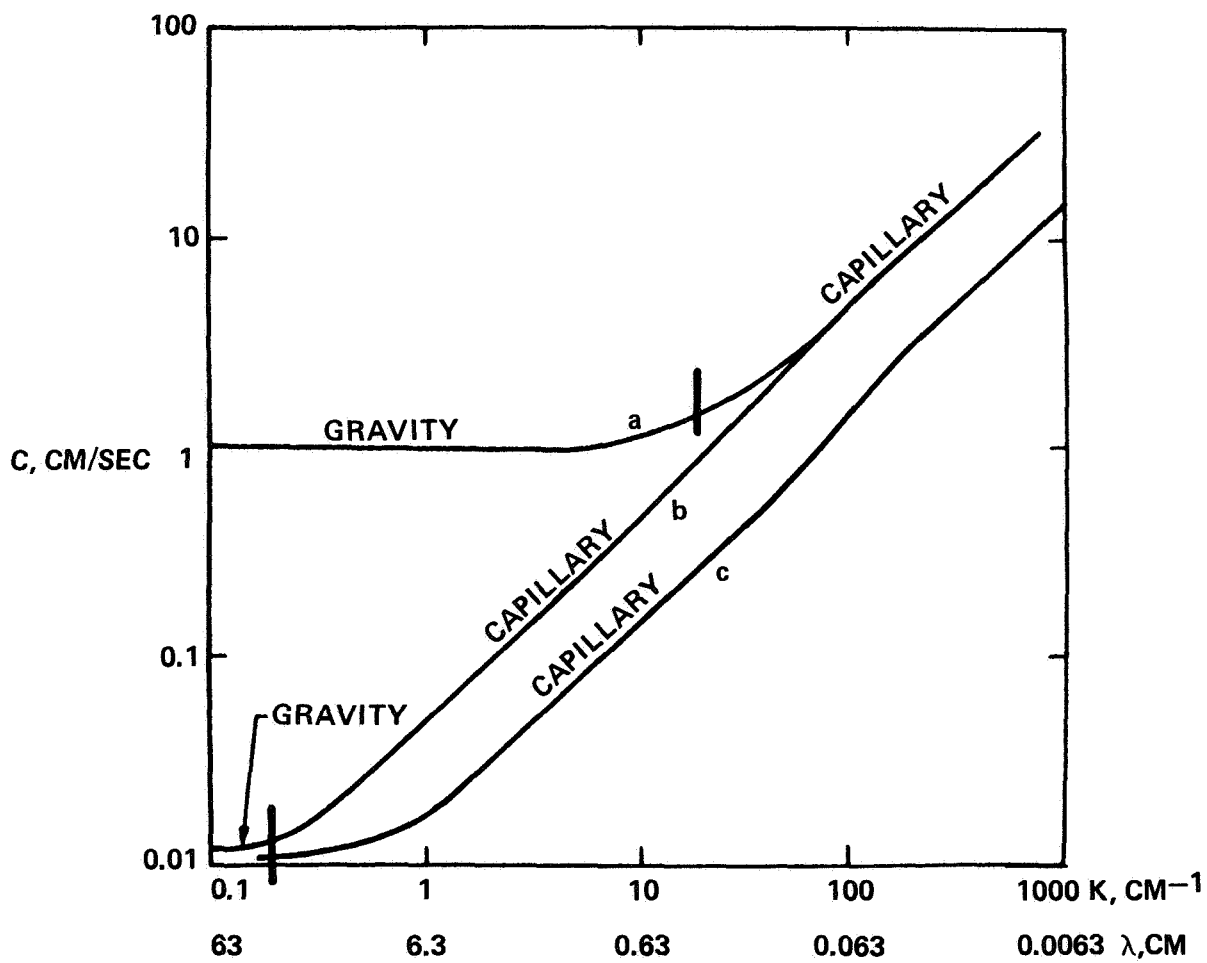
FIGURE 1. DISPERSION CURVE OF SURFACE WAVES

21

40 μ METER

0.4 CM

0.4 CM

SENSOR CAPACITOR
2 PLACES

SENSOR OUTPUT

CO-AXES

EXCITATION
INPUT WIRES

EXCITATION
HEATER
2 PLACES

WAVE CHANNEL

76 MM DIA

5 MM

18 MM

FILL LINE
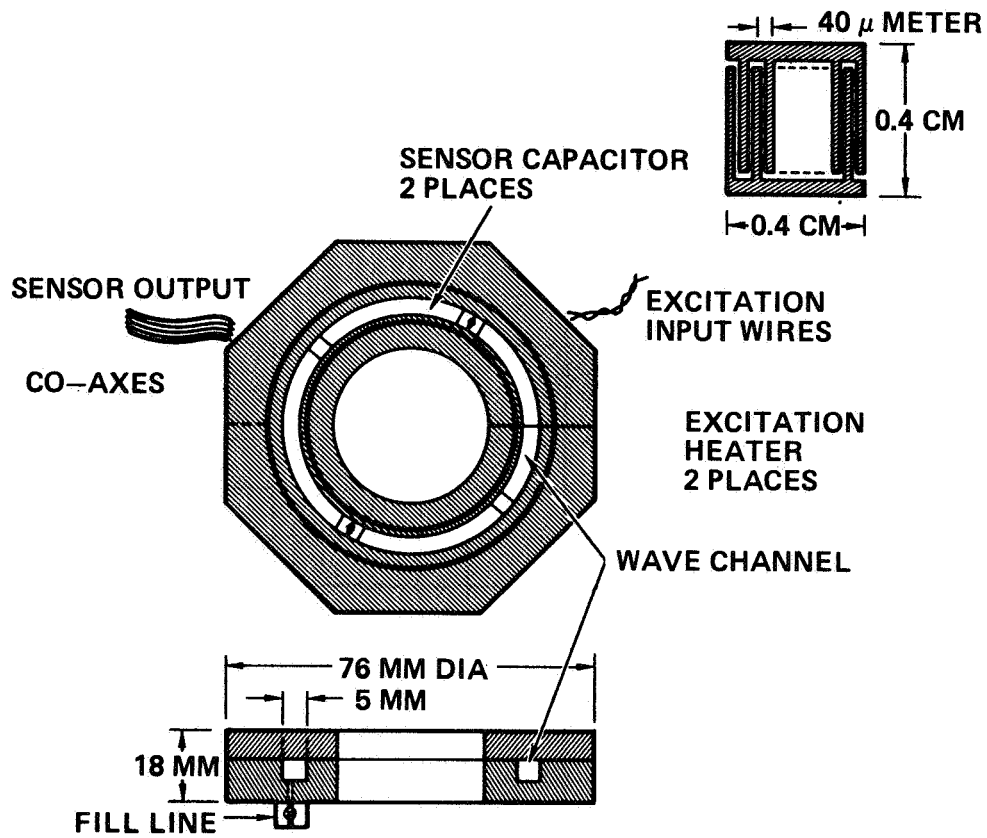
FIGURE 2. QUANTIZED SURFACE WAVE EXPERIMENT CELL
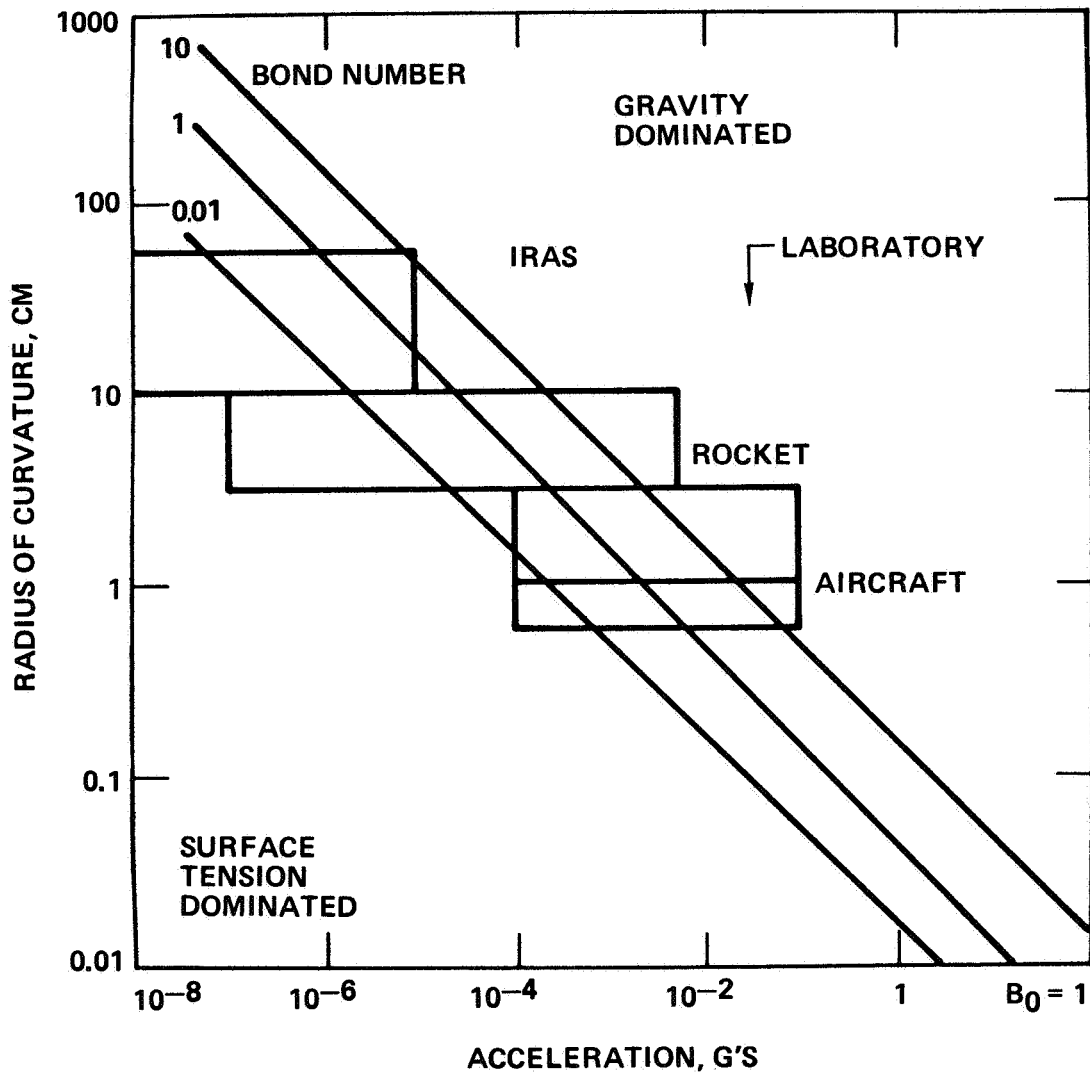
FIGURE 3. BOND DOMAIN OF EXPERIMENTS

23

SPACELAB 2 SUPERFLUID HELIUM EXPERIMENT
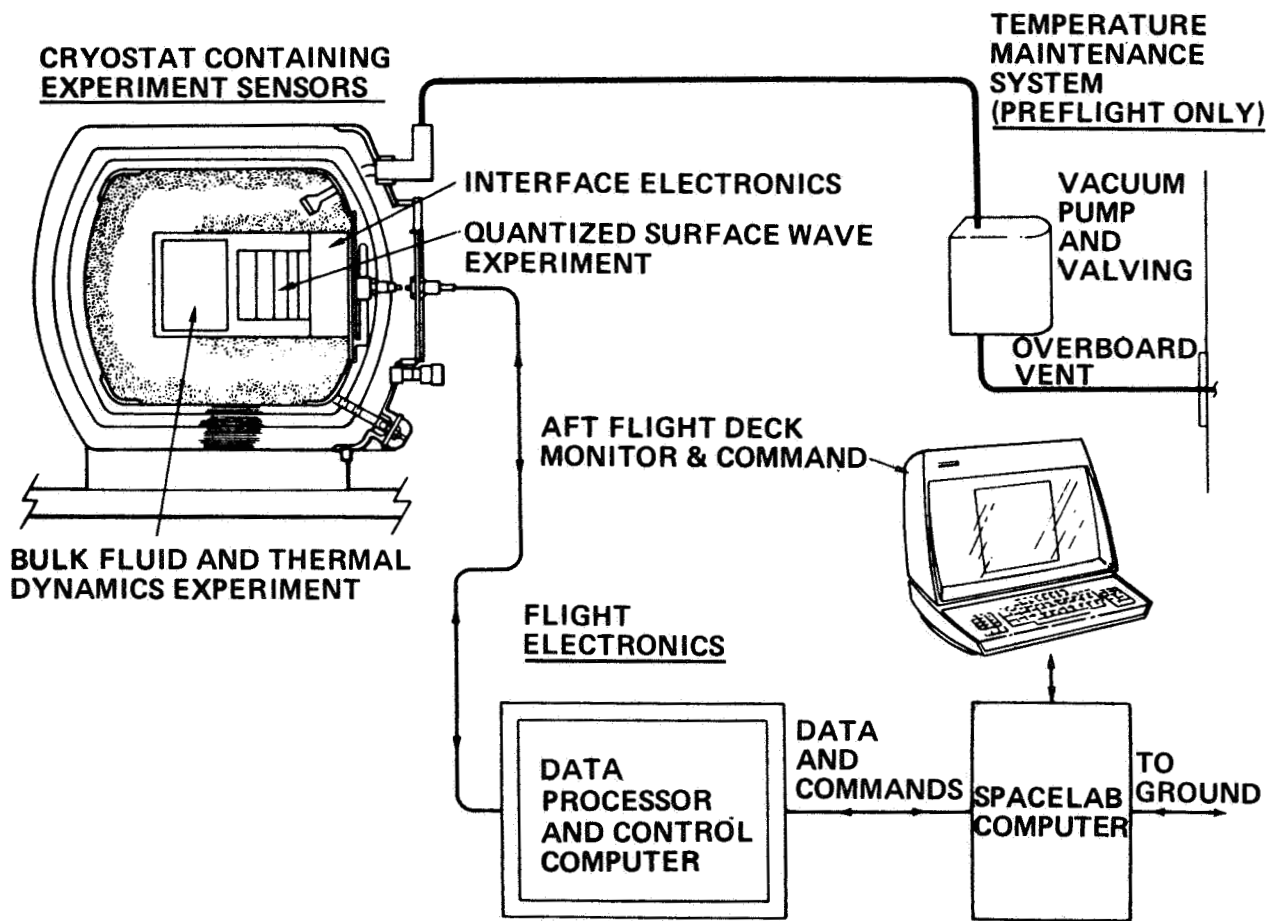
FIGURE 4. FLIGHT INSTRUMENT BLOCK DIAGRAM

GEOPHYSICAL FLUID DYNAMICS

by
William W. Fowlis
NASA/George C. Marshall Space Flight Center

INTRODUCTION

Geophysical fluid dynamics includes the study of large mass geophysical fluid flows, such as stellar circulations, planetary atmospheric circulations and ocean circulations. Systematic scaling or dimensional analysis reveals that certain scales of these flows can be accurately modeled in the laboratory. Note that the procedure of laboratory geophysical fluid flow modeling with which we are concerned is different from conventional engineering modeling. Rather than building a model to obtain numbers for a specific design problem, the relative effects of the significant forces are systematically varied in an attempt to deepen our understanding of the effects of these forces.

An area of geophysical fluid flow modeling that has received substantial attention is the modeling of large-scale planetary atmospheric flow in a rotating cylindrical annulus [1]. Figure 1 is a schematic diagram of the annulus. The boundary cylinders are maintained at different temperatures and the apparatus is mounted on a turntable. The volume between the cylinders is filled with a low-viscosity liquid which has usually been water. Motions in the annulus have been made visible by adding aluminum powder to the liquid. Figure 2 is a photograph of an annulus flow taken with a camera rotating with the turntable and using a time exposure. An irregular jet flow showing a remarkable similarity to the atmospheric jet stream is observed. However, this similarity does not necessarily imply that the dynamics of the two flows are the same. Systematic scaling of the governing equations using characteristic values for both systems must be performed before we can conclude that the annulus is a model of the atmosphere. Such scaling of the horizontal momentum equation for the large-scale atmospheric motions and the annulus motions reveals a primary balance between the Coriolis force and the horizontal pressure gradient force for both systems. This is the geostrophic balance. A similar scaling of the vertical momentum equation reveals a hydrostatic balance for both systems. A complete study of all the equations involved shows that the annulus is a model of the synoptic-scale atmospheric flow.

A major limitation of this annulus work is that it does not allow for the effects of spherical geometry. This is clearly important. For the annulus the rotation vector and gravity are always parallel, whereas for the Earth they vary from being parallel at the poles to being perpendicular at the equator.

THE DIELECTRIC BODY FORCE

There is no known way in which a true radial gravitational force can be obtained in a fixed geometry in the laboratory. However, a radial dielectric body force can be achieved. An analysis of the forces on a dielectric fluid in an electric field, E, reveals a dielectric force of the form, $\frac{1}{2}E^2\nabla_\varepsilon$, due to variations in the dielectric constant [2]. For the geometry of a spherical capacitor (radii, R_I and R_0, $R_0 > R_I$) filled with a dielectric liquid and subjected to a voltage difference, V, across the spheres and thermal gradients on the boundaries, this dielectric body force, g_E, is given by Equation (1), where ε_0 and ρ_0 are the dielectric constant and density

$$ g_E = \frac{2\varepsilon_0\gamma}{\rho_0\alpha} \left(\frac{R_I\,R_0}{R_0 - R_I} \right)^2 \frac{V^2}{r^5} \tag{1} $$

of the liquid, respectively, at some reference temperature. The terms γ and α are the thermal coefficients of dielectric constant and density, respectively; r is any radius between R_I and R_0 [3].

A calculation for g_E using realistic values reveals that it is not possible to make g_E dominate terrestrial gravity. Thus, the need to perform these experiments in an orbiting laboratory like Spacelab becomes clear [4].

SPACELAB GEOPHYSICAL FLUID
DYNAMICS EXPERIMENTS

At the present time two spherical geophysical fluid dynamics experiments are being designed and prepared for Spacelab flights:

1) The Geophysical Fluid Flow Cell (GFFC). Principal Investigator: J. Hart, University of Colorado.

2)   The Atmospheric General Circulation Experiment
(AGCE).   Principal Investigator: W. Fowlis, NASA, Marshall
Space Flight Center.

It is anticipated that other geophysical fluid dynamics
experiments will be proposed for later Spacelab flights.

These two experiments are designed to examine different
flows that have essentially different dynamics or physics.

In the GFFC, the liquid between the spheres will be
subjected to an unstable radial temperature gradient and
rotation.   The unstable gradient will be achieved by having
the inner sphere everywhere warmer than the outer sphere.
This is a model of stellar convection.   For some experiments
a latitudinal gradient will be imposed in addition to the
unstable radial gradient.   This may be a model of the Jovian
atmospheric circulation.   In the AGCE the liquid will be sub-
jected to a stable radial gradient and an unstable latitudi-
nal gradient and rotation.   This is a model of the Earth's
atmospheric circulation and extends the previous work per-
formed in cylindrical geometry to spherical geometry.   The
thermal gradients will be imposed by maintaining temperature
differences and gradients on the inner and outer spherical
boundaries.

MEASUREMENT AND DISTURBANCES

A photochromic dye technique will be used for flow
measurement [5].   When a small amount of a compatible photo-
chromic dye (0.01% by weight) has been added to the working
fluid, it will darken upon exposure to ultraviolet radiation
and then spontaneously clear again.   Successive photographs
showing the dye movement will reveal the flow.   Figure 3 is a
photograph showing photochromic dye sheets created in the
working fluid in a spherical apparatus.   This apparatus is
being used for development work for the Spacelab experiments.

A double-grid Schlieren system will be used for tempera-
ture measurement [5].   In this system the image of a Ronchi
ruling will be superposed back on the original ruling so that
only light refracted by temperature gradients within the
working fluid will pass through and be observed.   For this
system the inner sphere must behave like a mirror, and optics
to correct for the spherical curvature are needed.

Since these flows are thermally driven by temperature
differences of about 10C° in confined volumes, flow rates
will be small, 1 cm/sec and sometimes 0.1 cm/sec.   Clearly,

27

any disturbance of a rotational or precessional form to the rotating spherical containers could seriously affect the flows.

REFERENCES

1. Hide, R., and Mason, P. J.: Sloping Convection in a Rotating Fluid, Advances in Physics, 24:47 (1975).

2. Stratton, J.: Electromagnetic Theory. McGraw-Hill Book Co., New York, 1941.

3. Hart, J. E.: Studies of Earth Simulation Experiments, NASA Contractor Report No. 2753, 1976.

4. Fowlis, W. W., and Fichtl, G. H.: Geophysical Fluid Flow Model Experiments in Spherical Geometry. Proceedings of the Third NASA Weather and Climate Program Science Review, NASA Conference Publication 2029, Paper No. 32, 1977.

5. Fowlis, W. W.: Remote Optical Techniques for Liquid Flow and Temperature Measurement for Spacelab Experiments, Optical Engineering, 18(No. 3):281 (1979).
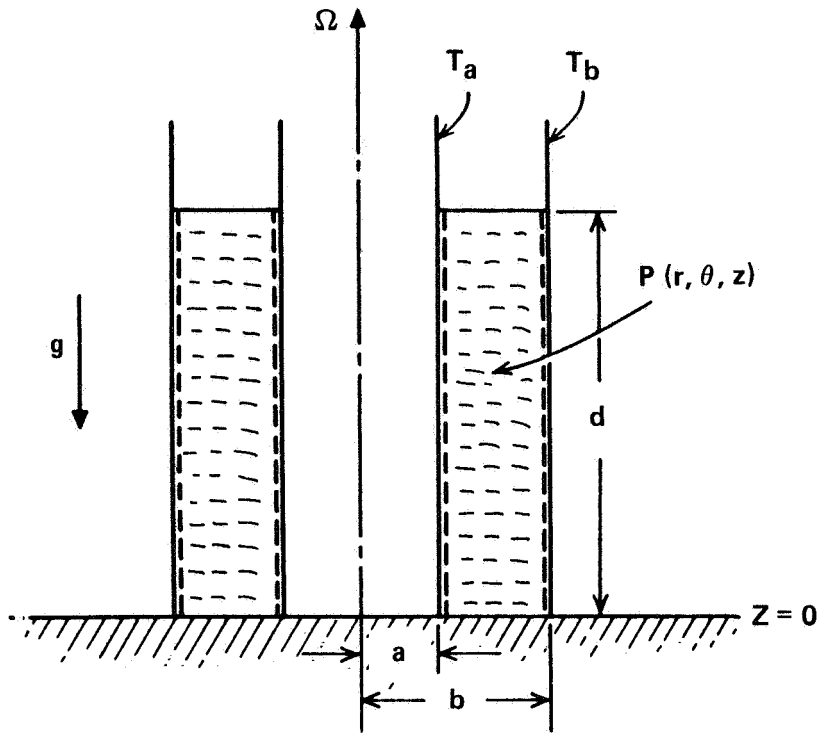
P — GENERAL POINT HAVING CYLINDRICAL POLAR
COORDINATES (r, θ, z) IN FRAME ROTATING
WITH THE APPARATUS

Ω = (0, 0, Ω) — ROTATION VECTOR

g = (0, 0, −g) — ACCELERATION OF GRAVITY

b, a, d — FLUID OCCUPIES REGION

$$a < r < b, 0 < z < d \ [1 + \Omega^2(r^2 - 1/2 \ (b^2 + a^2) \ ) \ / \ 2 \ gd] \simeq d$$

T (r, θ, z,t) — TEMPERATURE AT GENERAL POINT P AND TIME t

T_a, T_b — T (a, θ, z, t); T (b, θ, z, t) RESPECTIVELY

FIGURE 1. SCHEMATIC DIAGRAM ILLUSTRATING ROTATING FLUID ANNULUS.

29
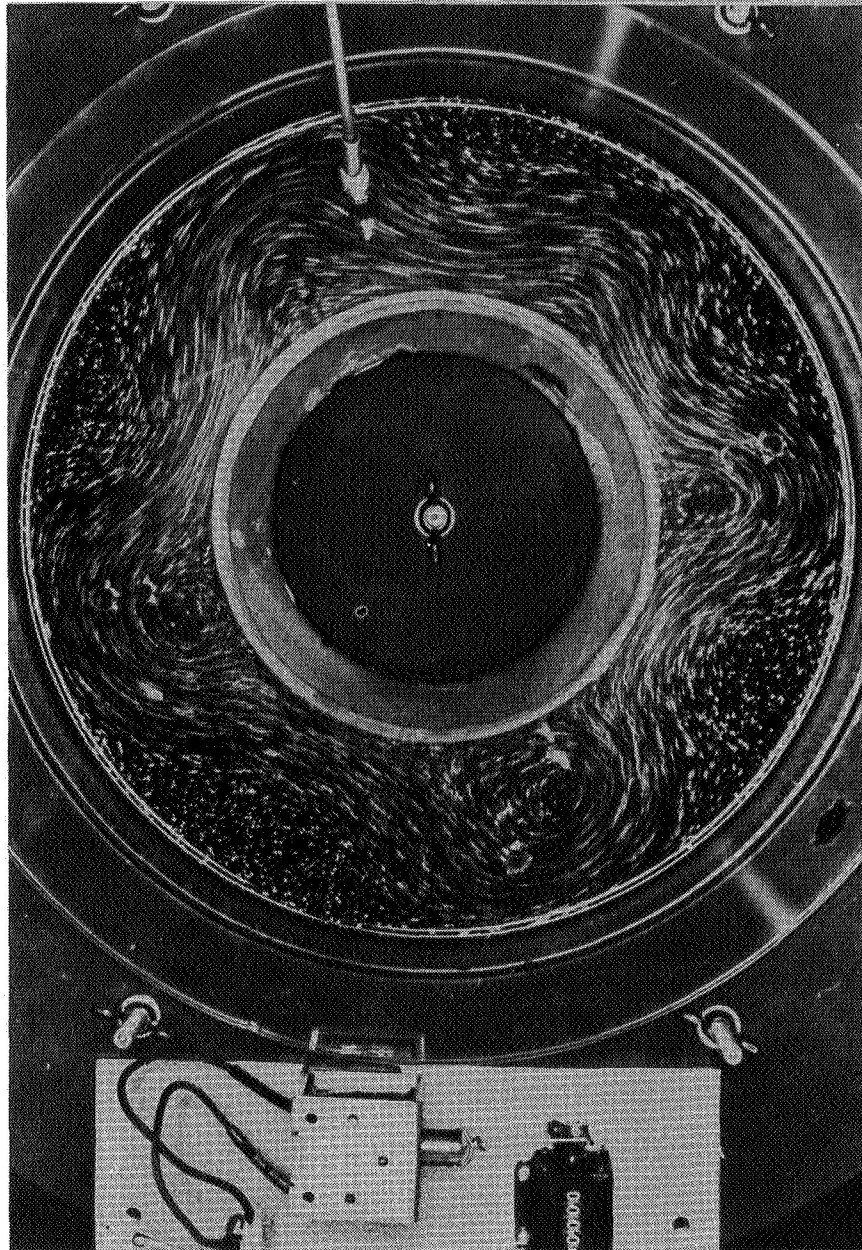
FIGURE 2.   A TIME EXPOSURE SHOWING AN UPPER SURFACE WAVE FLOW
IN THE ANNULUS.
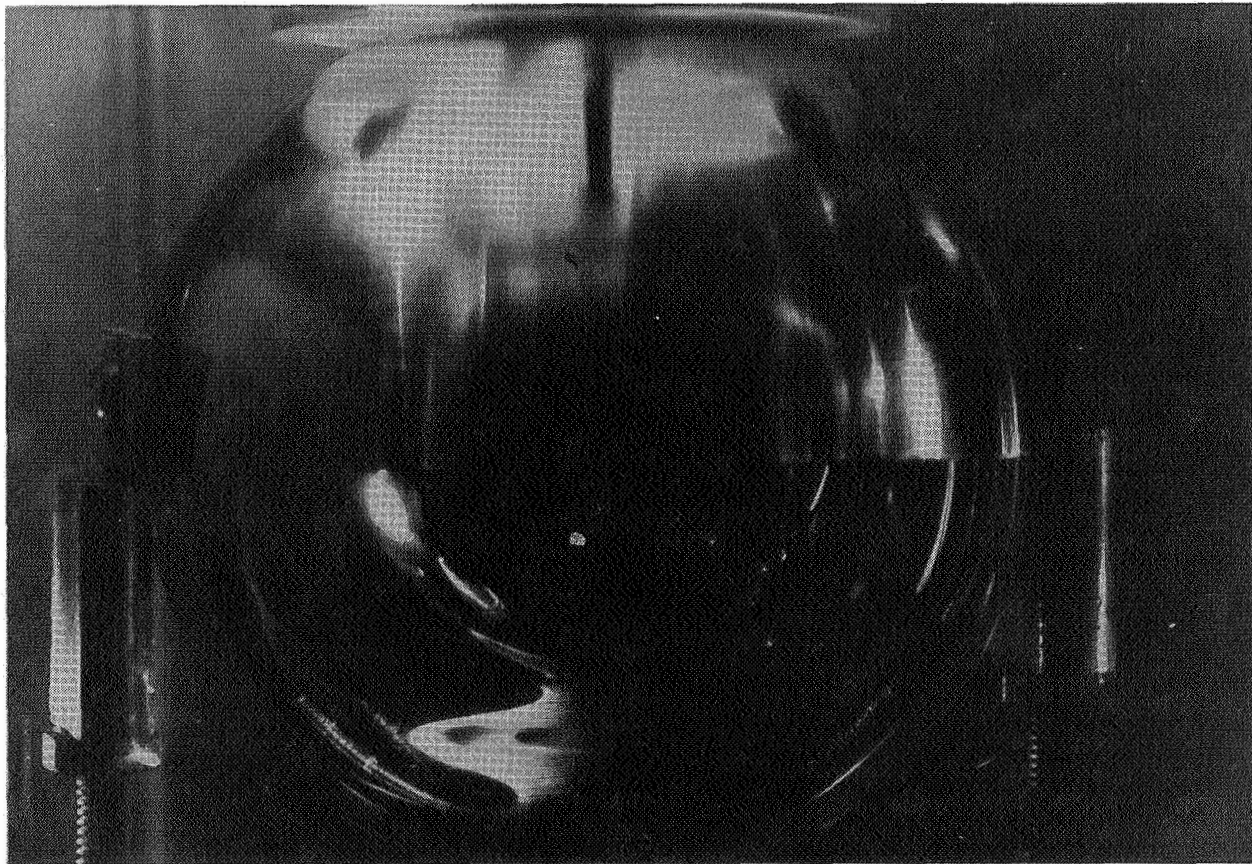
FIGURE 3. PHOTOCHROMIC DYE SHEETS CREATED IN SPHERICAL APPARATUS
BY EXPOSURE TO AN ULTRAVIOLET SOURCE.

DROP DYNAMICS

by
D. D. Elleman
Jet Propulsion Lab
Pasadena, California

The Drop Dynamics Module is a Spacelab-compatible acoustic positioning and control system for conducting drop dynamics experiments in space. It consists basically of a chamber, a drop injector system, an acoustic positioning system, and a data collection system. The principal means of collecting data is by a cinegraphic camera. The drop is positioned in the center of the chamber by forces created by standing acoustic waves generated in the nearly cubical chamber (about 12 cm on a side). The drop can be spun or oscillated up to fission by varying the phase and amplitude of the acoustic waves. The system will be designed to perform its experiments unattended, except for start-up and shutdown events and other unique events that require the attention of the Spacelab Payload Specialist.

The proposed drop dynamics experiments will utilize the unique zero-g (low gravity) environment provided by space flight to investigate the dynamics of a free drop quantitatively for the first time. Aside from its fundamental academic interest, understanding of the behavior of a free drop will contribute to the sciences of nuclear physics, chemical processing, material processing and meteorology. This type of experiment is such a natural candidate for implementation in a manned Earth satellite that astronauts have already, on their own initiative, carried out limited qualitative experiments of this kind. The proposed experiments aim at obtaining precise data on the behavior of liquid drops by means of high-resolution cinematography in three orthogonal views.

The theory of the dynamics of a free drop has been well studied in the approximation that dynamic quantities deviate linearly from a resting drop. With special exceptions to be discussed below, there is no nonlinear theory of the dynamics of a fluid drop. Not only are definitive experiments for the large amplitude behavior of fluid drops lacking but there is a deficit of definitive experiments even for linear behavior. This is a consequence of the limitations involved in conducting experiments in an Earth laboratory. Among these limitations are insufficient droplet sizes for accurate

observation, limited available time for experiments, and perturbing effects due to the method of suspending the droplets.

In the DDM a 1-cm radius drop will be positioned and held in an acoustic rotational well which can exert a force as large as 3 dynes on the drop. This is equivalent to the drops being able to withstand constant accelerations of the Spacelab of approximately 5×10^{-4} g. Acceleration forces larger than this will result in the drop striking the well of the chamber and a termination of that experiment. Dynamic accelerations smaller than the above level can also result in termination of the experiment and will be discussed.

INTERACTIONS BETWEEN SPACECRAFT MOTIONS AND THE

ATMOSPHERIC CLOUD PHYSICS

LABORATORY EXPERIMENTS

by
B. J. Anderson
NASA/George C. Marshall Space Flight Center

The Atmospheric Cloud Physics Laboratory (ACPL) is a set of equipment for studying a variety of atmospheric micro-physical processes in the low-gravity space environment. It will consist of three experiment chambers, an aerosol gener-ation and characterization system, and extensive support sub-systems. The experimentation planned for the first three ACPL missions will involve studies of the following processes: the transport of heat, water vapor, and aerosol particles through air; cloud drop nucleation and growth; ice crystal growth from the vapor and within a cloud; drop freezing dynamics, aerosol production within clouds (SO_2 oxidation); and air turbulence decay. For each of these studies the advantage of working in space is a result of the absence of fluid motion in the experiment chamber, either fluid motion with respect to the chamber or with respect to the cloud particles themselves. On Earth these motions arise so easily from sedimentation and buoyancy forces that they are diffi-cult or impossible to suppress or eliminate. It follows then in the evaluation of the effects of spacecraft motions on ACPL experimentation that the motions of concern are those which will result in the movement of the fluid or cloud particles within the experiment chambers.

Of the various vehicle motions and residual forces which can and will occur, three types appear most likely to damage the experimental results: non-steady rotations through a large angle, long-duration accelerations in a constant direction, and vibrations. Non-steady rotations present a problem because, for a fluid in a chamber, rotational motion of the chamber is poorly coupled to the fluid. The result is a long-duration rotation with respect to the chamber. The time constant for damping this motion is likely to be on the order of $L^2/j^2\nu$ = 200 seconds for the ACPL expansion chamber. L is about 21 cm, j is the first Bessel function zero, and ν is the kinematic viscosity. It appears that it is better to use the thrusters to stabilize the vehicle in a solid body rotation than to allow it to drift through large angular motions.

Constant accelerations, even of low magnitude, present a problem primarily because they may give rise to buoyancy forces when there are temperature gradients in the fluid. Apparently these forces do not fall off faster than $\sqrt{g}$. From a quick review of the literature it appears that the problem has not been adequately solved. If you calculate the Rayleigh numbers for situations typical of ACPL (lengths of a few tens of centimeters, temperature differences on the order of 1°C, and $10^{-4}g$), you find the values are only slightly less than the critical Rayleigh number after correction for a distributed heat source in the gas. Thus, it is possible to do the experiments without convection, but one must be careful. Some preliminary experiments may be called for to remove any doubt. Constant accelerations may also cause particle drift by sedimentation, but this concern is not critical for most ACPL work because cloud particles are generally quite small and viscous forces are significant.

Concern over spacecraft vibrations arises in consideration of the ice crystal growth experiments. For most of the early ACPL work the crystals will be suspended near the end of a long fiber (20 cm long by 200 micron diameter) of glass or similar material. Clearly, small vibrations of the supported end of the fiber could cause extensive motions of the ice crystal, if care is not taken to avoid this problem.

COMBUSTION EXPERIMENTS IN SPACE

by
A. L. Berlad
State University of New York at Stony Brook

Combustion phenomena of practical and fundamental interest occur primarily at normal gravitational conditions (g = 1). The underlying natural convection-free (g = 0) combustion processes are obscured by gravitationally associated body forces. Accordingly, the Space Shuttle Laboratory could provide the laboratory conditions required for observation of fundamental combustion phenomena. These g = 0 observations, and associated analyses, are then expected to provide understanding of combustion phenomena (at g ≥ 0) which is not accessible by other means. A list of pivotal areas for needed combustion observations (available through Space Shuttle experimentation) includes:

1) Single- and two-phase premixed flame propagation and extinction limits.

2) Noncoherent flame propagation and extinction.

3) Autoignition of premixed single-phase and two-phase combustible reactants.

4) Upper pressure limit combustion phenomena and ignition, propagation and extinction processes in the neighborhood of such limits.

5) Oscillatory combustion associated with the hydrocarbon-oxygen and with the carbon monoxide-oxygen systems.

6) Two-phase flame spread and extinction phenomena involving large liquid-gas or solid-gas interfaces.

7) Radiative ignition of solids and liquids.

8) Pool burning.

9) Smoldering of solid combustibles and the associated transition to flaming (or extinction).

10) Laminar gas jet combustion.

11) Transient responses of combustible systems to time variations in gravitational field strengths.

A number of the preceding experiments may be impacted by undesirably high g-jitter effects.

There are a number of compelling reasons, both experimental and theoretical, for taking combustion experiments into space. The first three that are listed in Figure 1 are general experimental considerations and the last three are general theoretical considerations. When combustion experiments are conducted under normal gravitational conditions, large free convective forces tend to obscure the underlying combustion processes which are themselves determined by chemical kinetics, heat and mass and momentum transfer. The underlying molecular transport processes are thus generally clouded by these free convective processes.

One of the really important experimental motivations for space-based experimentation is to assure the adequate/proper/ desirable preparation of the combustion experiment. For example, two-phase combustion experiments can be prepared in such a way that particulates don't settle. Accordingly, initial conditions for two-phase combustion experiments can be made uniform and homogeneous in space and time. Then, of course, the suppression of natural convection during the combustion process itself is made possible. Thus, one can characterize the space-based experimental observation of the combustion phenomenon as one which is not dominated by free convective forces, but rather one which is determined by the underlying chemical kinetics and molecular transport processes. From a theoretical point of view, this permits the resolution of a variety of key questions. These questions vary from experiment to experiment. Also, the theoretical representations of g = 1 combustion phenomena almost invariably become truncated or intractable when we try to include free convective processes at normal gravitational conditions. Space-based combustion experiments permit the use of realistic theoretical representations which do not suffer from such problems.

As a practical matter, most of us are interested in combustion behavior at normal gravitational conditions. Thus, a theoretical basis for g = 0 experimentation is that more meaningful, undistorted observation and more tractable theory can then be used to build on to understand the nonzero cases. This is the central feature of the space-based research in general, and, as indicated, detailed rationales vary from experiment to experiment. Twelve experiments are listed in Figure 2. Some of these we expect to be impacted by fluctuations in gravitational fields.

Item (1) of Figure 2 refers to a class of experiments in which one looks at single- and two-phase flame propagation

and flame extinction. Here we do not expect to have significant effects due to some small perturbation in the gravitational field when $g \doteq 0$.

Item (2) refers to another class of experiments, so-called noncoherent flame propagation and extinction. This is an experiment for which one finds that rather than simply connected flame surfaces, the surface comes apart, flame propagation is noncoherent. Non-simply connected flame surfaces are observed (at $g = 1$), and natural convection as well as molecular diffusion play a role in the experiment. Thus, the motivation for experiments of this kind would be to see whether in fact this phenomenon occurs at all and, if so, whether extinction limits are changed by the absence of a gravitational field. This phenomenon is particularly important at the so-called lean limit for H_2-O_2.

Autoignition or explosion is a criticality phenomenon (item 3). One always worries about criticality phenomena if, in fact, we have perturbations in the neighborhood of a critical condition.

The autoignition experiment for single- and two-phase systems is an experiment for which we have rather good $g = 0$ theory. We do not have observations that are generally free of significant gravitational conditions. We expect that the observed autoignition condition would be affected by fluctuations in gravitational conditions. Heat loss mechanisms are very important in defining autoignition conditions, and where these are nonsteady or have average values which are somewhat different from what they ought to be at $g = 0$, this criticality condition can be affected. However, for g-values of the order of 10^{-4}, substantial effects on this experiment are not expected.

Item (4) is a very interesting experiment for which there is no current proposal. It is well known that at normal gravitational conditions and at very high pressures (of the order of 10-100 atmospheres) there is an upper pressure limit extinction phenomenon. It is difficult or impossible to propagate some flames under some conditions of high pressure. In fact, one of the effects of normal gravitational conditions is that natural convective and momentum losses can be large, at high pressures. Extinction phenomena are generally associated with loss mechanisms. Thus, it would make a substantial difference on the operating body forces of these high-pressure, nonisothermal systems if we were to vary g-value over a substantial range, down to identically zero. There is no upper-pressure limit experiment currently proposed, though it would be a very interesting experiment indeed.

J

Oscillatory combustion (item 5) is a very interesting and important theoretical and experimental issue in the field of combustion. We find oscillatory phenomena in the combustion of hydrocarbons with oxygen and in the oxidation of carbon monoxide with oxygen. The hydrocarbon-oxygen case is thought to be a largely thermokinetic oscillation, due to an interplay between a heat release rate and a heat transport rate through boundaries. The carbon monoxide-oxygen case is thought to be a purely kinetic phenomenon. This is perhaps the most isothermal of all nontrivial combustion phenomena. For the oscillatory combustion of carbon monoxide with oxygen, we find cycles of the order of several hundred. As many as 450 have been observed in one experiment in which temperature in the middle of this oscillating system was perhaps only $1°C$ warmer than that of the wall. Now, because mass transport of reactive species to walls is so important, one would like to experiment with some very large systems. However, as we go to very large systems, we will run into natural convective processes. Although there appears to be an effect of physical scale and an effect of the chemical nature of walls $g = 1$, experiments of such a system are subject to free convective effects.

Pool burning (item 6) is one combustion phenomenon where the effect of 1 to 10 Hz g-jitter may indeed be significant. Pool burning experimentation involves the propagation of a flame (that may be subject to extinction) over a stabilized pool of fuel. In such experiments, the ability to establish a very well defined initial condition and maintain it during the course of the experiment is important.

Item (7) is concerned with two-phase flame spread and extinction phenomena. Such an experiment may involve a matrix-like structure of particulates, with flame spreading occurring over the particulates. Such an experiment has been identified previously as one of significant interest from both fundamental and applied points of view.

Item (8), radiative ignition of solids and liquids, is thought to be an important experiment, to be done at reduced gravitation or zero gravity fields.

Smoldering (item 9) is perhaps one of the most important phenomena from the point of view of fire safety at $g = 1$. Combustion characteristics of cigarette, cigar, and mattress burning processes involve transitions of smoldering to extinction, smoldering to flaming, or just continued smoldering. Smoldering itself is not well understood theoretically. Neither are smoldering-related transitions to flaming or extinction. An experiment which is designed to study the transition of smoldering to either flaming or

extinction which is going to develop over a period of time could, in fact, be significantly influenced by whether or not we have a gravitational field. All of the processes which participate in the smoldering phenomenon appear to be rather slow. Mass and heat transport as well as chemical kinetic and heat release rates are all slow. Natural convective processes, though modest, may still be very important for this class of phenomena.

Laminar gas jet combustion (item 10) studies have already been conducted in drop tower experiments. Many of these studies involve rather substantial forced convective conditions and we don't expect that small gravitational perturbations will create significant effects.

Criticality conditions of various kinds are common in combustion phenomena. There are flames that do exist; others don't exist; there are transitions to extinctions; there are transitions to detonation from ordinary flame propagation; and one would expect that those transition conditions may be affected if time-dependent gravitational conditions are present. This is indicated for the class of item (12).

COMBUSTION EXPERIMENTS IN SPACE

OBSERVATION AT $g \sim 0$ PERMITS

(1) PROPER/DESIRED PREPARATION OF EXPERIMENT.

(2) SUPPRESSION OF NATURAL CONVECTION — PRIOR TO & DURING COMBUSTION.

(3) CHARACTERIZATION OF UNDERLYING COMBUSTION PHENOMENON.

(4) RESOLUTION OF A CENTRAL QUESTION IN COMBUSTION THEORY/EXPERIMENT.

(5) MORE REALISTIC — MORE TRACTABLE THEORY.

(6) THEORETICAL BASES FOR $g > 0$.

FIGURE (1)

EXPERIMENTS

(1)   SINGLE/TWO—PHASE FLAME PROPAGATION AND EXTINCTION.

(2)   NONCOHERENT FLAME PROPAGATION AND EXTINCTION.

*(3)   AUTOIGNITION — SINGLE/TWO—PHASE.

*(4)   UPPER PRESSURE LIMITS — IGNITION, EXTINCTION, PROPAGATION.

*(5)   OSCILLATORY COMBUSTION:

        [HYDROCARBON — OXYGEN] + [CARBON MONOXIDE — OXYGEN]

*(6)   POOL BURNING.

*(7)   TWO—PHASE FLAME SPREAD AND EXTINCTION.

(8)   RADIATIVE IGNITION OF SOLIDS AND LIQUIDS.

*(9)   SMOLDERING OF SOLID COMBUSTIBLES AND TRANSITIONS TO
        FLAMING/EXTINCTION.

(10)   LAMINAR GAS JET COMBUSTION.

*(11) $0 < g \ll 1$. LOW (g) STUDIES.

*(12)   TRANSIENT RESPONSES OF COMBUSTIBLE SYSTEMS TO TIME VARIATIONS IN
        GRAVITATIONAL FIELD STRENGTHS.

---

*POSSIBLE g—GITTER EFFECTS OF SIGNIFICANCE.

FIGURE (2)

TWO-PHASE FLOW AND HEAT TRANSFER

UNDER LOW GRAVITY

by
Walter Frost
The University of Tennessee Space Institute
Tullahoma, Tennessee

The two-phase flow and heat transfer program for the space laboratory in which I am involved is outlined in Figure 1. General Dynamics is under contract with NASA, Lewis Research Center, to design a two-phase fluid mechanics heat transfer facility for spacecraft. I'm listed as the lead scientist for the two-phase flow patterns, pressure drop, and flow boiling experiment. Three other projects being considered under this same conceptual design study are listed in Figure 2; liquid reorientation, pool boiling, and bubble dynamics. Only liquid-vapor, two-phase flows are considered in this paper.

The needs for the spacecraft experiment described above are twofold. One is for space transportation systems which will begin to develop in the 1980's. A number of these systems will involve processes containing two-phase fluid flow and heat transfer. General Dynamics in their previous study [1] has identified the five areas shown on Figure 3 for which some 45 different applications where two-phase flow will occur have been identified. An example of one common occurrence of two-phase flow and heat transfer in these applications is cryogenic transfer lines where a cryogen is pumped into a warm line and undergoes boiling until the line cools to the appropriate temperature. Power generation systems utilizing boilers and condensers in which two-phase flow and heat transfer occur are also an example of typical applications. Since two-phase phenomena occur in these applications for a variety of fluids ranging from hydrogen to liquid metals, two-phase flow and heat transfer predictive models are needed for the design of space transportation systems.

Current design correlations for predicting two-phase flow pressure drops and heat transfer are primarily empirical and have been in most all cases developed under standard gravity. The flow process is generally so complex that writing the exact governing equations is prohibited and consequently we can't look fundamentally at how variation in the dependent variable will affect the heat transfer process.

Thus, there is a need to carry out experiments under reduced gravity to determine how it influences these correlations.

A second need to study two-phase flow and heat transfer in space is to improve our fundamental understanding of this phenomenon. By isolating gravity forces from surface tension forces, inertia forces, and other forces that are involved in the flow and boiling process, we will be able to establish a meaningful theoretical model to replace the empirical techniques currently employed.

Thus, there is a twofold need for two-phase fluid experiments in space. One is to develop design criteria that can be used for future space system design, without necessarily understanding completely the physical mechanism taking place, i.e., empirical design correlations. The other is to carry out fundamental experiments to provide a better understanding of the physics of the processes for future analytical work.

Although there are several classifications in boiling [2], we'll skip these and begin by considering in detail the two-phase flow pattern which occurs in a heated vertical duct, Figure 4. Fluid is pumped upward through the duct. The duct is uniformly heated along its length, and as fluid is pumped upward it changes phases from pure liquid to pure vapor.

On the left of the figure the temperature variation along the tube length is plotted. Both the wall temperature of the duct and the bulk temperature of the fluid in the duct are plotted. The visual flow patterns which occur are listed on the right-hand side of the figure. The fluid enters as a pure liquid, and heating takes place initially by standard convective heat transfer. Thus, single-phase flow initially takes place in the entrance region. Water is considered in our discussion, but all fluids will behave similarly. As the thermal boundary layer builds up on the duct wall and the temperature exceeds the saturation temperature of the fluid, bubbles begin to form at specific nuclei on the surface. These bubbles will grow, but once they grow outside the thermal layer, they collapse because the bulk fluid temperature outside the thermal layer is below the saturation temperature of the fluid--the dashed line in the figure. This form of boiling is called subcooled nucleate boiling because the bulk fluid temperature is below the saturation temperature. It is also referred to as surface or local boiling because the bubbles exist only in the location of the surface and not within the fluid stream; i.e., they collapse once outside the thermal layer required to make them grow. However, as the flow continues upwards and energy is

continuously added, the bulk temperature of the liquid
reaches the saturation temperature of the fluid. Now the
bubbles will continue to grow even outside the thermal
boundary layer. The flow takes on a bubbly or frothy flow
pattern.

As the fluid moves upward and energy is continuously
added, nucleate boiling continues to take place on the heated
duct surface; however, the bubbles become sufficiently large
that they now coalesce and form large slugs or a frothy
mixture of vapor. This pattern is called the slug, churn,
or froth flow pattern.

Soon the vapor generation becomes so large, and the
vapor flow so fast that it forces the liquid to the walls of
the duct and the vapor flows up the center of the duct as a
continuous core. This is called the annular flow pattern.
Further downstream an exchange of energy between the vapor
and the liquid layer takes place through droplets being torn
from the surface of the liquid and then reentrained into the
layer downstream. This is called the spray or liquid dis-
perse pattern, or sometimes the annular mist region because
the liquid annulus exists with mist in the vapor core.

Eventually the liquid layer will dry out, which is
called the point of dry-out or burn-out. The wall tempera-
ture jumps drastically when the liquid layer dries out
because a very effective mechanism of cooling exists as long
as liquid covers the surface. Once this breaks down, the
heat transfer coefficient to the pure vapor is comparatively
low and the wall temperature rises rapidly. The flow pattern
then becomes a mist with droplets in the entrained vapor, and,
finally, all liquid evaporates and single-phase vapor flow
occurs.

All of the previously described flow patterns are visual
definitions of the flow process. The difficulty with pre-
dicting flow and heat transfer in these various flow pattern
regimes is that associated with the different flow patterns
are different mechanisms of pressure drops and heat transfer.
Convective heat transfer to a pure liquid or vapor is the
mechanism which occurs in the single-phase regime; however,
we will not discuss this mechanism. Rather, consider the
nucleate boiling process which occurs on the walls in the
subcooled boiling and slug flow regimes. Nucleate boiling
heat transfer is a very efficient heat transfer mechanism.
The bubbles growing, collapsing, and being detached from the
surface create a very high transport of energy next to the
wall. Arguments still exist, however, as to the exact
mechanism by which the bubbles enhance the heat transfer.
The contribution due to latent heat of evaporation as

45

compared to that due to augmented turbulence effects is not clearly defined. Although a few other factors are involved, we know that the bubbles growing and collapsing are responsible for the very high heat transfer rates obtained.

Nucleate boiling continues on the wall through the slug flow regime. The mechanism of nucleate boiling heat transfer has been well studied, and the influence of a number of variables documented [2,3]. Equations governing the bubble dynamics have been written, and how gravity enters into the particular growth rate and transient forces acting on the bubbles can be estimated. Near the wall the bubble growth is basically due to thermal effects; i.e., it depends upon the rate at which energy is transported to the liquid-vapor interface to evaporate the liquid. The bubble growth is, thus, pretty much independent of any gravity forces during this stage of growth. This has been partially confirmed by drop tower and flight tests, at least for boiling in a large pool of liquid. Natural convection occurs in large pools rather than forced convection, as illustrated in Figure 4.

The characteristics of pool boiling heat transfer have been outlined by Siegel [3] as shown in Figure 5. In the figure heat flux is plotted versus temperature difference between the wall and the saturation temperature of the fluid. The curve is essentially independent of gravity, although very small gravity effects have been observed in drop tower tests or flight tests. These are generally negligible for design purposes. Thus, gravity is not expected to have a pronounced effect on the mechanism of nucleate boiling heat transfer near the wall.

Gravity will, however, influence the size of bubbles which are torn off the wall by other forces. The bubble departure from the wall is dependent upon four basic forces; one is the surface tension force which tends to hold the bubble on the wall; another is the viscous forces which in the forced flow case tend to drag the bubble off the wall--in a pool boiling experiment they tend to hold the bubble on the wall; the buoyancy or gravity force which lifts the bubble off the wall; and the inertia force which is a function of how fast the bubble grows--if it grows very rapidly, it causes the liquid to have a certain amount of inertia, and this inertia can force the bubble away from the wall. The competing forces of gravity and of inertia are basically the forces influencing the size at which the bubble is torn off the wall. Certain types of bubbles are strongly dependent upon gravity and for low gravity these bubbles will become very large before they are lifted off the wall. Consequently, slugs and churn flow will probably occur quicker at low gravity.

The effect of gravity on isolated bubbles in a fluid has also been studied. We know obviously that bubbles will rise faster under high gravity. Once again, however, there will be competing forces which are not fully understood. For example, the drag versus gravity effects. Utilizing experiments in space, the influence of drag forces can be isolated from gravity.

In the nucleate boiling regime, we expect that the sub-cooled transfer mechanism is not strongly influenced by gravity. However, the transition from nucleate boiling to slug flow will probably occur quicker because it is dependent upon the rate the bubbles rise and coalesce with one another and form slugs.

Since the bubbles cannot escape as fast at low gravity, the occurrence of slug flow is enhanced. There are also competing forces in the transition from slug to annular flow. This transition is dependent on a force balance between liquid flowing down the wall by gravity and vapor dragging the fluid up the wall. Hence, the important dry-out or burn-out conditions will be strongly influenced by gravity. Thus, there is a lot to be learned about the physics of two-phase flow and heat transfer by carrying out an experiment in space.

In the annular flow region the mechanism of heat transfer is not nucleate boiling. Rather it occurs by conduction or convection through the thin liquid layer and evaporation at the interface. Again, this is a very effective mechanism for transferring heat, but all present design correlations are based on experimental results under earth's gravity.

A second complicated problem is that although we can approximately calculate pressure drop and heat transfer in the various flow regions described above, we need to know under what conditions these regions occur in order to employ the appropriate design criteria. To date, the conditions under which these regions exist are not very well defined. Experiments have been carried out using air and water mixtures. In general the liquid flow rate is held constant and vapor flow rate is increased systematically. Figure 6 illustrates a flow regime map measured by Griffith [4], whereas the dashed lines are regime boundaries recommended by Kazlov [5]. The flow regimes are bubbly flow, slug and froth flow, and mist annular flow as simulated using air-liquid mixtures. The gravity dependence of the flow regimes is based on dimensional analysis and has not been confirmed with experiments at sustained low gravity.

This influence of gravity may be even more significant for horizontal flows because now the fluid can stratify, as illustrated in Figure 7. Increasing vapor flow with the liquid flow constant results in the different flow patterns illustrated in the figure. These particular flow conditions may vanish altogether in a reduced gravity environment and, in fact, there is evidence supporting this from flight experiments conducted by General Dynamics [1].

Current techniques available to predict the flow regime are thus in the form of flow regime maps, Figure 6. Flow regime maps are based on earth gravity controlled experiments. It should be noted that the lines on the maps are really broad bands representing transitions between the different flow regimes. The empirical results obtained under earth's gravity where g is introduced by dimensional reasoning indicate that as gravity becomes very low, slug and froth flow may not occur, and that annular flow will be the dominant flow regime. Thus, we expect that slug and froth flow might not exist in space. However, we need to verify this.

The purpose of the Spacelab experiment is to do three things directed toward this goal. First, investigate two-phase flow patterns under reduced gravity using the water-air mixture experiment. A schematic of the proposed test apparatus is shown in Figure 8. Air and water are circulated through the system. The quality or the mixture of air-water is controlled. Photographs of the test section will be made and at the same time pressure drops across the test section will be measured. The data will establish a flow regime map under reduced gravity conditions with corresponding pressure drop correlations.

The test section is also equipped with an electrical resistance heater in order to allow a flow boiling experiment to be carried out; Freon 11 will be used. Again, high-speed photographs will be taken of the test section to determine flow patterns. Measurements of the temperature gradient and pressure drop along the duct will also be made. Thus, quality change can be measured, and heat transfer calculated. This will provide information on two-phase flow and heat transfer under low-gravity conditions. More details of the experimental program are given in Reference 6.

48

REFERENCES

1. Bradshaw, R. D. and King, C. D.: Conceptual Design for Spacelab Two-Phase Flow Experiment, NASA CR-135327, December 1977.

2. Frost, Walter (ed.): Heat Transfer at Low Temperatures, New York: Plenum Press, 1975.

3. Siegel, Robert, Effects of Reduced Gravity on Heat Transfer, Hartnett, James P., and Jr. Irvine, Thomas F. (ed.): Advances in Heat Transfer, Vol. 4, New York: Academic Press, 1967.

4. Griffith, P., and Wallis G.: Two-Phase Slug Flow, Journal of Heat Transfer, 83C(3), 307-320 (1961).

5. Kazlov, B. K.: Forms of Flow of Gas-Liquid Mixtures and Their Stability Limits in Vertical Tubes, Zh. Tekh. Fiz, 24(12, 2285-2288 (1954), Translation RJ-418, Assoc. Tech. Service, East Orange, New Jersey.

6. North, B. F., and Hill, M. E.: Conceptual Design of Two-Phase Fluid Mechanics and Heat Transfer Facility for Spacelab, NASA CR-159810, June 1980.

TWO-PHASE FLUID MECHANICS AND HEAT TRANSFER
FACILITY FOR SPACELAB

GENERAL DYNAMICS CONVAIR DIVISION

B. F. NORTH

NATIONAL AERONAUTICS AND SPACE ADMINISTRATION
LEWIS RESEARCH CENTER

E. PAT SYMONS

LEAD SCIENTIST FOR TWO-PHASE FLOW PATTERNS,
PRESSURE DROP AND FLOW BOILING

UNIVERSITY OF TENNESSEE SPACE INSTITUTE

WALTER FROST

FIGURE 1   LABORATORY EXPERIMENT FOR SPACELAB PROGRAM.

ɹ

OTHER PROJECTS AND LEAD SCIENTIST

- ## LIQUID REORIENTATION

  T.E. BOWMAN
  FLORIDA INSTITUTE OF TECHNOLOGY

- ## POOL BOILING

  J.E. LEINHARD
  UNIVERSITY OF KENTUCKY

- ## BUBBLE DYNAMICS

  TOM LABUS
  NASA LEWIS RESEARCH CENTER

FIGURE 2 OTHER PROJECTS AND LEAD SCIENTIST.

- ● DESIGN AND PERFORMANCE OF SPACE TRANSPORTATION SYSTEMS

  - ● PROPULSION

  - ● AUTOMATED SPACECRAFT

  - ● POWER GENERATION

  - ● EXPERIMENTAL SUPPORT (SPACELAB AND SPACE STATION)

  - ● ENVIRONMENTAL CONTROL/LIFE SUPPORT SYSTEMS (EC/LSS)

- ● ADVANCE FUNDAMENTAL UNDERSTANDING OF TWO-PHASE FLOW AND BOILING HEAT TRANSFER

FIGURE 3   NEED FOR EXPERIMENT
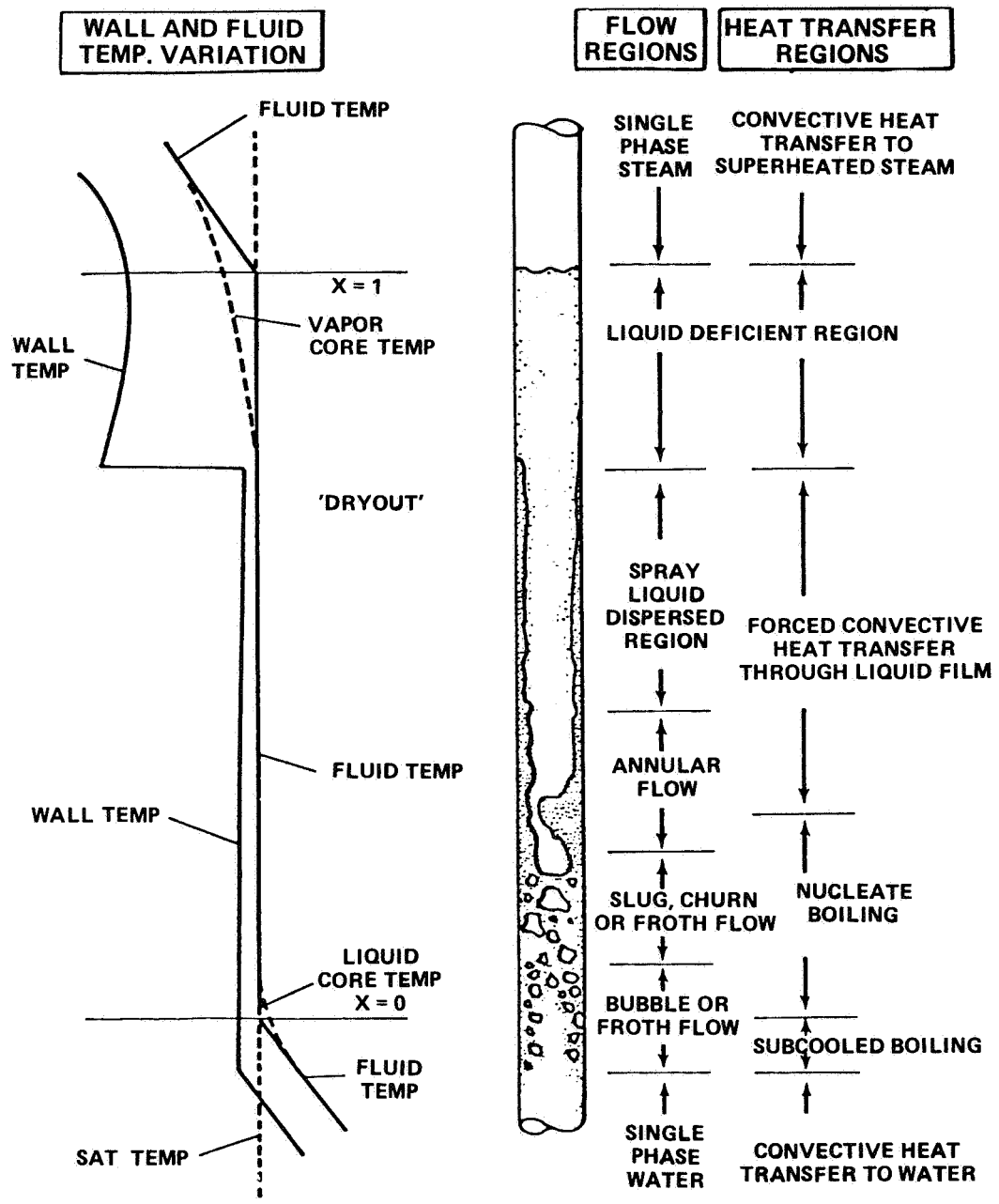
FIGURE 4   CHARACTERISTICS OF FORCED CONVECTION TWO-PHASE HEAT TRANSFER.

Sphere diameter, inch	Fraction of Earth gravity, g/g_e
1/2	0.01-0.03
1	0.01-0.03
1	0.20
1	0.33
1	0.60
1/2	1
1	1

HEAT FLUX, Q/A, BTU/(HR) (SQ FT)

TEMPERATURE DIFFERENCE, $T_W - T_{SAT}$, °F
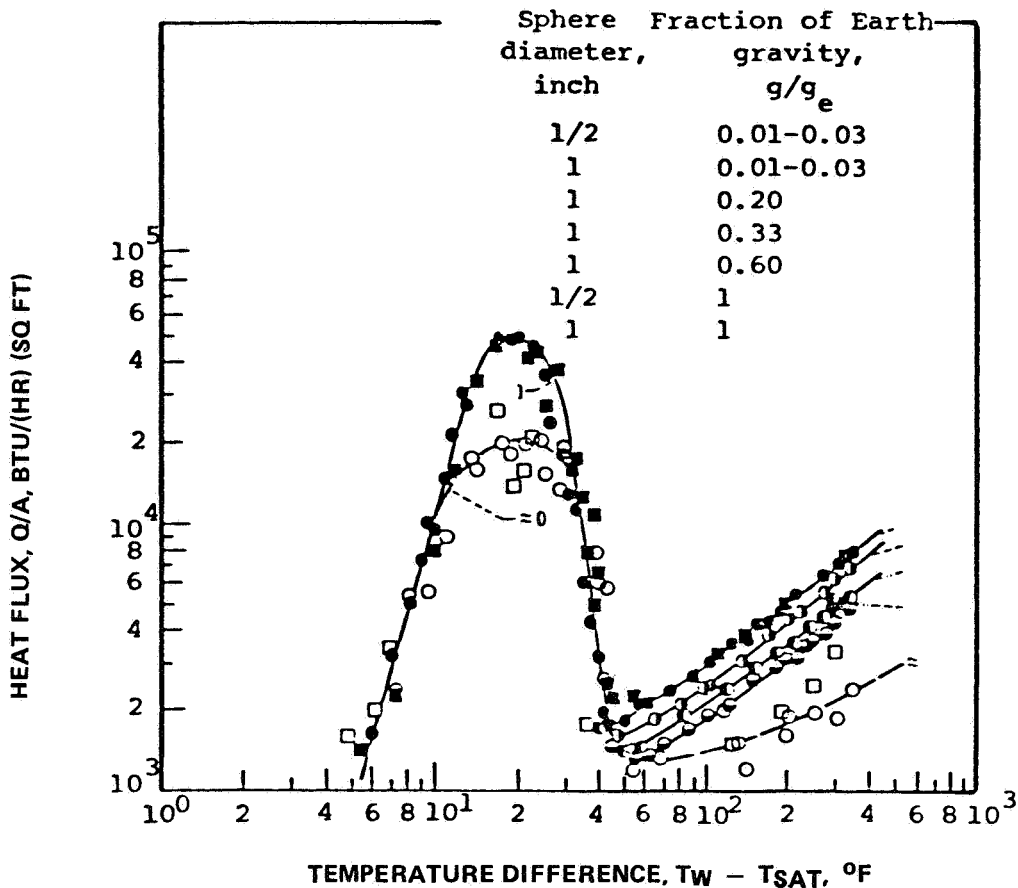
1. FOR NUCLEATE BOILING, BOTH ANALYSIS AND EXPERIMENT INDICATE THAT THE RELATION BETWEEN TEMPERATURE DIFFERENCE ($T_W - T_{SAT}$) AND WALL HEAT FLUX IS INSENSITIVE TO GRAVITY.

2. THE PEAK NUCLEATE BOILING (CRITICAL) HEAT FLUX WAS FOUND EXPERI-MENTALLY TO VARY REASONABLY WELL AS $G^{1/4}$, WHICH IS IN AGREEMENT WITH THEORY.

3. THE RELATION BETWEEN $T_W - T_{SAT}$ AND WALL HEAT FLUX IN THE TRANSI-TION REGION BETWEEN NUCLEATE AND FILM BOILING APPEARS FROM LIMITED DATA TO BE INSENSITIVE TO GRAVITY REDUCTIONS.

4. THE MINIMUM HEAT FLUX VALUE WHERE TRANSITION BOILING CHANGES TO FILM BOILING DEPENDS ON $G^{1/4}$.

5. IN LAMINAR FILM BOILING THE HEAT—TRANSFER COEFFICIENT DEPENDS ON $G^{1/4}$. FOR A TURBULENT VAPOR FILM THE EXPONENT INCREASES AND MAY BE AS LARGE AS 2/5 TO 1/2.

FIGURE 5   CHARACTERISTIC OF POOL BOILING HEAT TRANSFER [3].
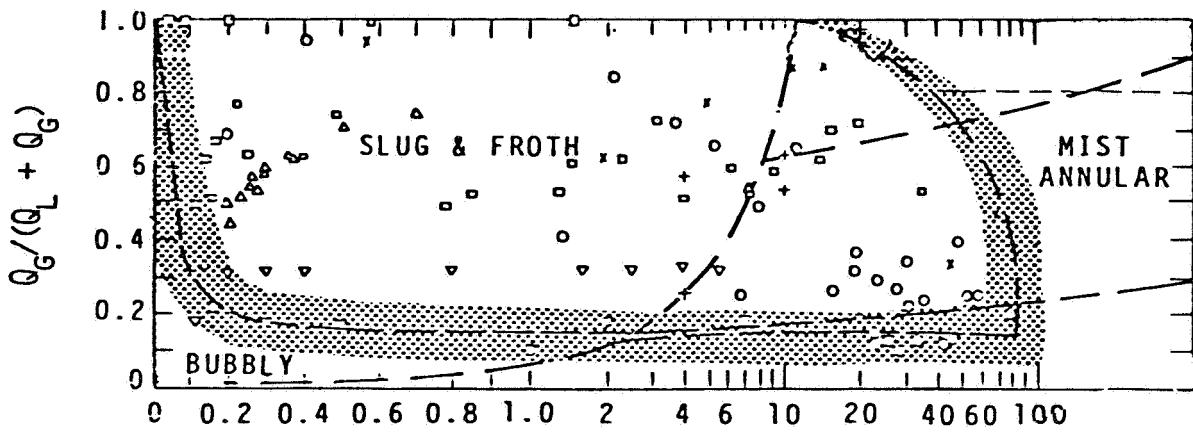
$$FR = \frac{[(Q_L + Q_G)/A_p]^2}{gD_p}$$

Q_G	SUPERFICIAL GAS FLOW
Q_L	SUPERFICIAL LIQUID FLOW
A_p	CROSS SECTIONAL PIPE AREA
D_p	PIPE DIAMETER
g	GRAVITY

FIGURE 6 FLOW MAP FOR A VERTICAL DUCT AIR-WATER MIXTURE [4]; DASHED LINES ARE BY KAZLOV [5].
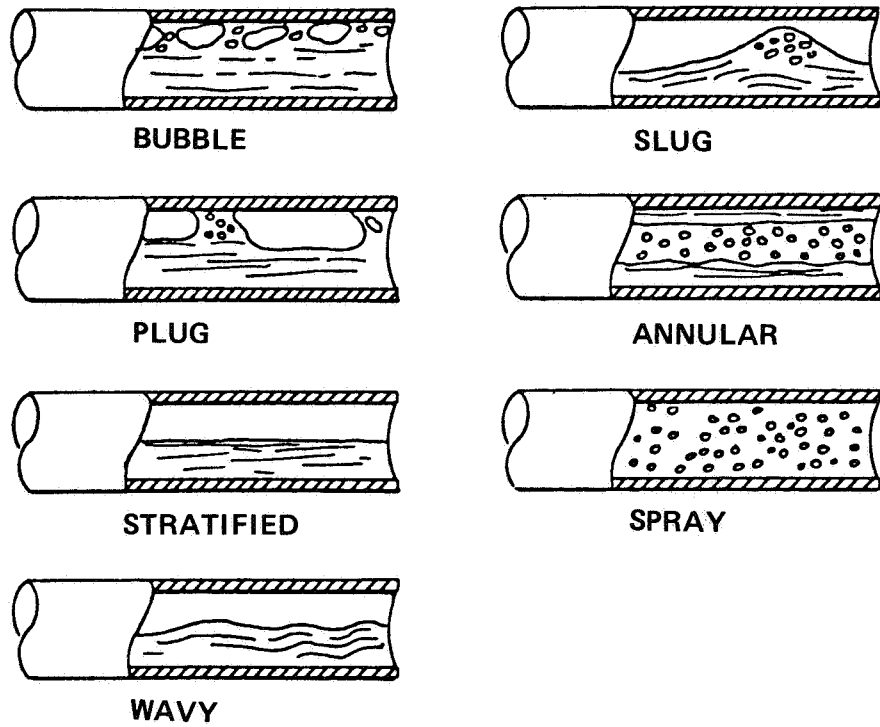
FIGURE 7 FLOW PATTERNS IN HORIZONTAL TUBES
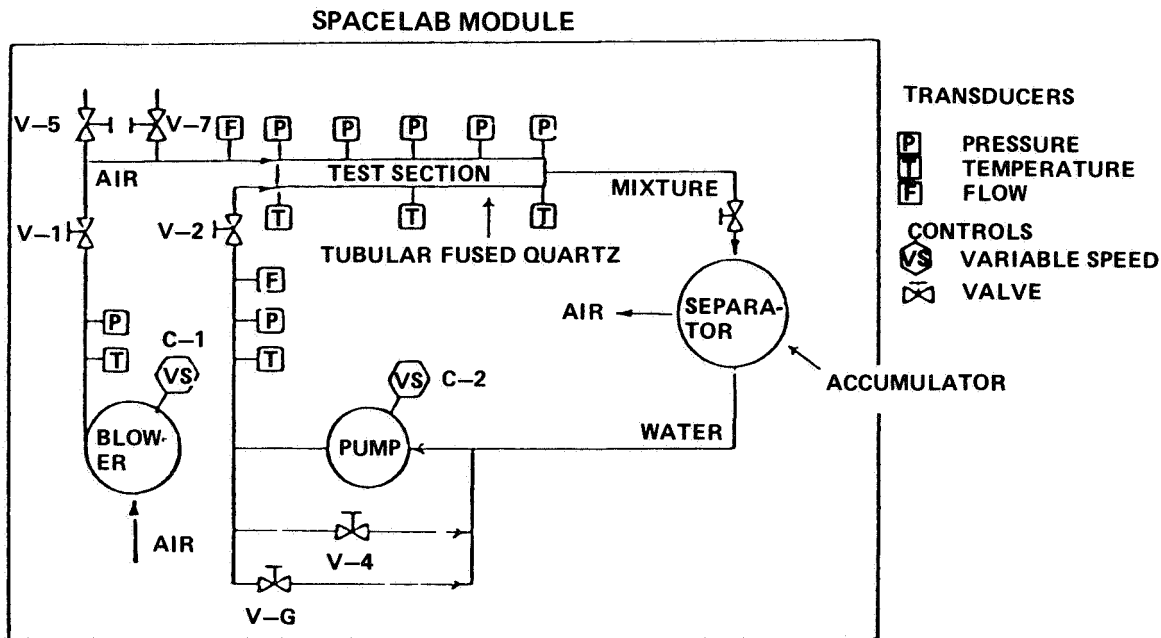
FIGURE 8a FLOW PATTERN AND PRESSURE DROP EXPERIMENT FLOW SCHEMATIC
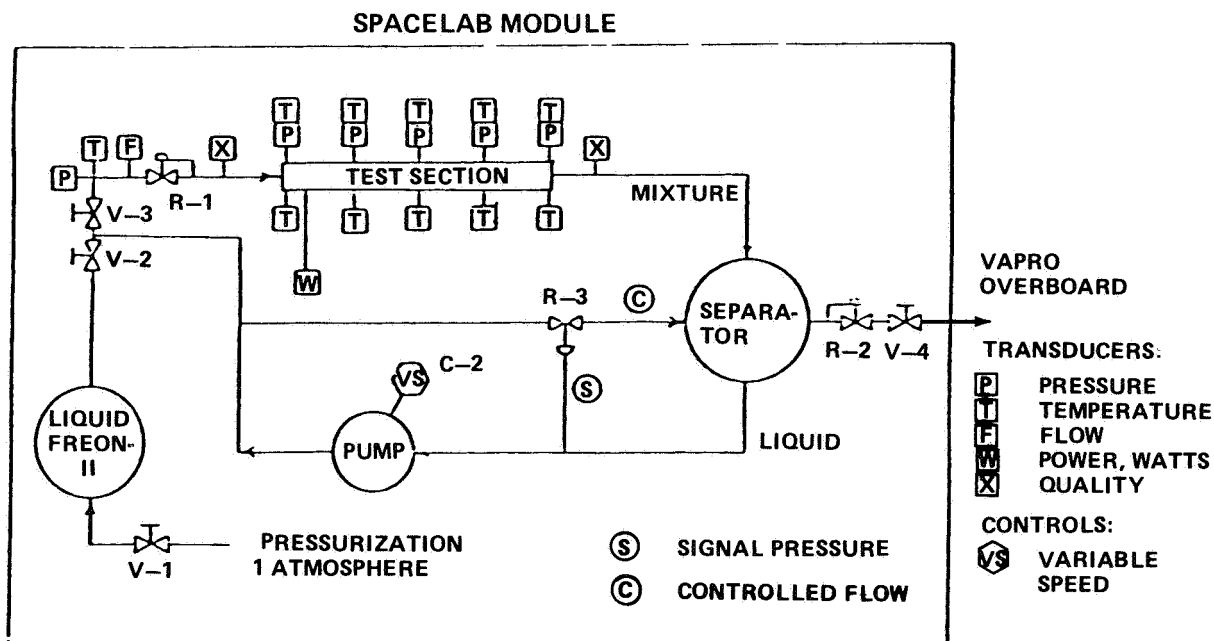
FIGURE 8b SCHEMATIC, FLOW BOILING EXPERIMENT, LIQUID RECYCLE CONCEPT [1]

FIGURE 8 SCHEMATIC OF PROPOSED SPACECRAFT EXPERIMENT

TRIBOLOGY EXPERIMENT

by
William A. Wall
NASA/George C. Marshall Space Flight Center

The purpose of the Tribological Experiments in Zero Gravity (TEZG), Figure 1, is to examine the interaction of liquid lubricants and surfaces under static and dynamic conditions in a low-gravity environment. Three functional objectives are planned: (1) Fluid Wetting and Spreading Experiments (FWS); (2) Journal Bearing Experiments (JB); and (3) means to accurately measure and record the low-gravity environment during experimentation. The scientific objective of the fluid wetting and spreading portion of the TEZG experiment is to study fluid-surface interactions under static conditions. This is to be done by observing the wetting and spreading process of selected commercial lubricants on representative surfaces in a near-zero gravity environment.

The useful life of a machine element is often determined by the slow migration of a liquid lubricant on its surface. This phenomenon is commonly known as wetting and spreading and is controlled by the minute interfacial forces of the three material phases; namely, the solid surface of the machine element, the layer of the liquid lubricant, and the surrounding air. When a static state prevails, the boundary of the lubricant coverage is stationary; then the situation can be characterized by the contact angle together with the surface tension of the lubricant. However, during a wetting and spreading process, the contact angle theoretically reduces to zero, and the rate at which the front of the lubricant advances can no longer be completely described by the static properties. Accurate observation of the wetting and spreading process in an earth environment is not possible because earth gravity is many orders of magnitude larger than the surface forces and would thus dominate the fluid motion. The prolonged zero-g condition during a Spacelab mission provides a unique opportunity to acquire quantitative knowledge of the wetting and spreading phenomenon.

Since FWS concerns both a fluid and a surface, it is of interest to include in the experiment several fluid-surface combinations. The present plan calls for grouping numerous surface coupons into an assembly. Various fluids will be brought to the surface through a small centrally located duct. An automated dispensing mechanism permits the process to start simultaneously on all coupons of the assembly. Also, a

58

photographic record will readily depict any significant differences in the wetting and spreading rates.

The scientific objective of the journal bearing (JB) portion of the TEZG experiment is to study hydrodynamic films in journal bearings operating in zero gravity and the stability of the dynamic bearing system under these conditions. Efforts will be made to control the development of the fluid film by use of experimental bearing configurations. Under dynamic conditions, such as in a simple journal bearing, the formation of hydrodynamic films is affected by low gravity. Because the ability of a journal bearing to develop a hydrodynamic, load-supporting film is responsible for the universal use of such bearing systems, these fluid surface reactions are very important. The film thickness developed in such a bearing is a function of the surface speed N, the lubricant viscosity u, and an inverse function of the load W

$$h = f \ \frac{Nu}{W} \ .$$

In near-zero gravity, the load W approaches zero and the bearing system should go unstable. Data on the development of instability under low-gravity conditions will be of great interest to scientists in the fields of bearings and lubrication. Since, in theory, a nonloaded rotating journal is not stable, it is planned to investigate the possibility of using experimental bearing configurations to control the development and location of the hydrodynamic film. Results of these tests should be of great interest to hydrodynamicists as the development of these data is impossible except under low-gravity conditions. It is believed that the information obtained during these experiments will provide a wealth of data on the development of hydrodynamic films and journal bearing stability under no-load conditions.

To verify the accelerations under which these experiments are subjected, a 3-axis, low-gravity accelerometer will be located in the TEZG experiments operations drawer adjacent to the experiments during operation. This accelerometer system has a threshold of 1×10^{-4} g's and a maximum output of 31×10^{-3} g's. It is desired that the TEZG experiments be run in an environment of less than 1×10^{-3} g's for a successful experiment.

TRIBOLOGY EXPERIMENT 2-DRAWER CONCEPT

Location: Spacelab Rack 7

3—AXIS LOW "G" PACKAGE

JOURNAL BEARING EXP SHOWN

ELECTRONIC CONTROLS

STROBE LIGHT PACKAGE

EXPERIMENT OPERATIONS CHAMBER

INSIDE CONTROL STATION

10.468

CAMERA

REMOVABLE COVER

FRONT PNL CONTROL STATION

JOURNAL BEARING

FLUID WETTING & SPREADING 4 REQD

TEMPORARY COVER STORAGE AREA

38.20

24.00
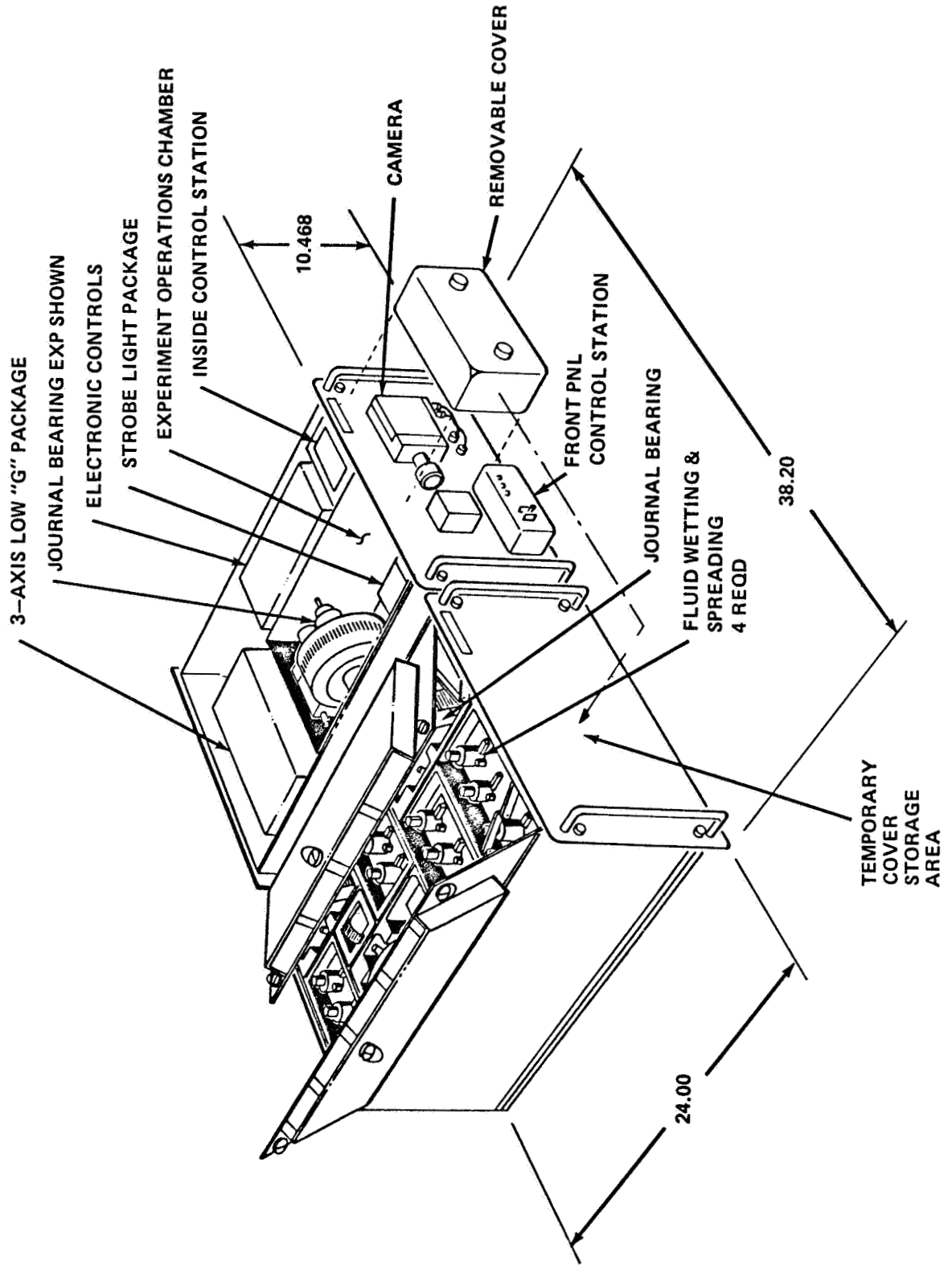
Figure 1. Tribology Experiment Assembly

60

III. EFFECTS OF SPACECRAFT DYNAMICS ON EXPERIMENTS

SUSCEPTIBILITY OF MATERIALS PROCESSING EXPERIMENTS

TO LOW-LEVEL ACCELERATIONS

by
Robert J. Naumann
NASA/George C. Marshall Space Flight Center

Recognizing that it is impractical to maintain an actual zero-gravity environment in an orbiting vehicle,[1] the question is frequently asked, how much residual acceleration can an experiment tolerate? This is not a simple question to answer for the reasons that, (1) there are a multitude of different types of low-level disturbances, and (2) there are a multitude of types of experiments that have varying degrees of susceptibility to each type of disturbance.

In order to attempt to answer this question, it is necessary first to enumerate the types of disturbances expected. These may be classified into four categories: (1) steady low-level accelerations, (2) compensated transient accelerations, (3) uncompensated transient accelerations, and (4) rotations. The origins and effects of the disturbances will be examined briefly in the following paragraphs.

By steady low-level accelerations, we mean accelerations on the order of 10^{-5} g and smaller that are relatively constant for durations of tens of minutes or longer. These arise from aerodynamic drag, Keplerian effects, and slow vehicle rotations. Accelerations arising from aerodynamic drag, of course, depend on vehicle altitude, orientation, and atmospheric density which has a day-night variation and depends to a lesser degree on solar activity. This force is constant in direction for a vehicle in earth-fixed orientation. For a vehicle in an inertial orientation this force rotates in the orbital plane with the orbital period, resulting in a nearly zero time average over one orbital period.

Keplerian forces originate because every particle in the spacecraft has its own individual orbit. These orbits in general have slightly different periods and would result in oscillations of the particles coupled with a drift along the orbital path, unless they are constrained. The magnitude of

---

1. This could only be accomplished by the heroic measure of actually flying the vehicle around the experiment in question.

the constraining force required is on the order of 10^{-7} g per meter of displacement from the center of mass of the vehicle. The direction of these forces generally oscillates with a period of twice the orbital period.

Low-level, nearly steady accelerations are also produced by slow vehicle rotations such as those produced by the rotation required to maintain earth-fixed orientation, those produced by gravity gradient torques in a free-drift mode with altitude control thrusters shut off, or those produced by the barbecue roll sometimes required for thermal control. The magnitude of this acceleration ranges from 10^{-7} g per meter displacement from the center of mass in the case of one revolution per orbit, to approximately 10^{-6} g per meter for the other types of rotation. In all cases the direction of this force is along the radius vector from the vehicle center of mass to the experiment in question.

Grashof numbers can be as much as ~20 for a steady acceleration of 10^{-6} g, assuming a container with characteristic dimensions of 10 cm containing H_2O with a 10° temperature differential. This would result in a flow of ~40 μm/sec. Such flows are sufficient to traverse the container in one-half the orbital period. Therefore, considerable mixing can occur in an experiment even if conditions are chosen to average out low-level accelerations over an orbital period.

By compensated transient accelerations we mean short-duration impulses that do not involve a momentum change to the spacecraft. Such transient accelerations arise from crew activity or internal mechanical vibrations. The important distinction is that such impulses are compensated a short time later by equal and opposite impulses. Even though such impulses may be as high as 10^{-2} g, the flow velocity acts for only a short time and the displacement is small. Furthermore, the random nature of these disturbances further reduces the net displacement. Therefore the fluid transport resulting from g-jitter (as such motion is often referred) is negligible for most cases. However, such transients may be of concern in containerless suspension systems or in experiments with free surfaces such as liquid floating zones.

Uncompensated transient accelerations result from external forces applied to the spacecraft such as thruster firings for attitude control or orbital maneuvers. In Skylab, attitude control was generally accomplished by means of control moment gyros which did not impart external forces to the spacecraft. It was necessary, however, to periodically dump the angular momentum accumulated from the integrated gravity gradient torques by means of cold gas thrusters.

Also, roll maneuvers to execute various earth resource tasks
were accomplished by means of thrusters. In the Apollo-Soyuz
mission, attitude control thrusters fired as a couple which
exerts a torque on the vehicle without a change in linear
momentum. Therefore, no uncompensated transient accelera-
tions were experienced.

Shuttle, on the other hand, uses only downward firing
thrusters for pitch and roll control. This will result in
uncompensated transient accelerations with each attitude
control pulse which has a magnitude of 10^{-4} g. These acceler-
ations can produce fluid velocities as high as 4 mm/sec in
the 10 cm cell described previously. However, since the
duration of these pulses is only 100 milliseconds, the
resultant displacement is on the order of 100 microns for
each thruster firing. Since these thrusters always fire in
the same direction relative to the vehicle, the resultant
displacement will be cumulative. The net result for free
convection is similar to the case of a steady acceleration
with a magnitude equal to the time averaged value of the
thruster accelerations. There may be some difference in the
case of unstable convection in that the critical Rayleigh
number may be exceeded by the higher impulsive accelerations
and not by the lower level steady accelerations.

Vehicle rotations, in addition to producing steady low-
level acceleration described previously, will introduce
rotational flow in a contained fluid. These flows are intro-
duced each time there is a change in angular momentum and
decay by Ekman damping. Damping times depend on the size and
shape of the container, viscosity of the fluid, and change in
angular rate. These times typically range from seconds to
tens of seconds.

The types of material processing experiments being con-
sidered for Shuttle can be grouped into four categories:
(1) contained solidification experiments, (2) quasi-
containerless experiments, (3) containerless experiments, and
(4) fluids experiments.

Contained solidification experiments are characterized
by relatively small dimensions (typically, a centimeter or
less) and high thermal gradients. This will result in
Grashof numbers on the order of unity for 10^{-6} g. Generally,
the emphasis will be on establishing and maintaining a
diffusion-controlled interface. Therefore, it is important
to avoid circulating flows that would disturb this diffusion
layer. Even though the induced flows are low, if the
accelerations act continuously in the same direction for
tens of minutes, displacements on the order of the con-
tainer dimensions can occur. Therefore, a careful analysis

of this effect is necessary and some thought should be given to the possibility of orienting the sample relative to the vehicle so that the flows from sustained low-level unidirectional forces will be minimized. Similar problems could also arise from uncompensated transient accelerations. Orienting the experiment in a thermally stabilizing configuration along the Shuttle + z-axis (up relative to the payload bay) and flying in a gravity gradient mode with the belly in the ram position would minimize flow effects from both aerodynamic drag and uncompensated thruster firings.

Compensated transients arising from internal forces will probably not be significant because of the small net displacements. Rotational changes, however, should be avoided during such experiments to prevent circulating flows.

Quasi-containerless experiments such as floating zones or pedestal melts are characterized by a fluid (usually a melt) supported at one or more points by a solid connected rigidly to the vehicle. Such systems generally have the same dimensions of contained solidification experiments and are subject to the flows described previously. However, the presence of a free surface makes such systems also subject to disturbances from compensated transient accelerations which will cause oscillations of the fluid relative to the support.

Containerless experiments must have a weak suspension system using acoustic, electromagnetic, or electrostatic forces to position the sample. Such a suspension system must be designed to compensate for residual accelerations such as drag, Keplerian effects, vehicle rotations, and various transient accelerations. In such experiments the emphasis is on maintaining the sample position without physical contact with the container walls. Therefore, the low-level steady forces are of less consequence, but the transients become important, especially high-level transients that can arise from internal disturbances, e.g., crew activity.

Generally, the suspension can be characterized as an energy well described by $\psi(x)$. The maximum force that can be exerted by the suspension is given by $-\psi'_{max}(t)$ and the system must be designed such that this is greater in magnitude than the largest expected sustained force. Transient forces greater than $|\psi'_{max}(x)|$ can be tolerated provided the total impulse does not impart sufficient kinetic energy to the sample to enable it to climb out of the potential well. Therefore, it is the impulse, not the peak acceleration, that is of concern to the success of containerless processing experiments.

66

Fluid experiments encompass a wide variety of experiments that are generally characterized by larger dimensions but much lower thermal gradients than encountered in contained solidification experiments. Such experiments include crystal growth from aqueous solution or vapor, electrodeposition, electrophoresis, suspension polymerization, etc. Often the emphasis is on maintaining suspensions of multiphase systems as well as on controlling density-driven convection. In many cases it is desired to observe the nature of convective flows and correlate their behavior with vehicular accelerations and experimental effects.

Such experiments could be seriously affected by low-level steady accelerations, uncompensated transient accelerations, and vehicular rotation, as in the case of the contained solidification experiments. Compensated transients are not expected to be very significant. Although sedimentation of phases with different densities will be slowed by six orders of magnitude from earth-based experiments, it may be desirable to avoid long periods of low-level unidirectional acceleration such as would be produced by atmospheric drag in an earth-fixed orientation.

In summary, there are multiple factors that must be considered in the acceleration environment of a space vehicle whose importance depends on the type of experiment being performed. This is illustrated in the matrix shown in Table I. Some control of these factors may be exercised by the location and orientation of the experiment relative to Shuttle and by the orbit and vehicle attitude chosen for the mission. The effects of the various residual accelerations can have serious consequences to the control of the experiment and must be factored into the design and operation of the apparatus.

TABLE I

	Contained Solidification	Quasi-Containerless Solidification	Containerless Experiments	Fluid Experiments
Low-Level Steady Accelerations	Possibly Serious	Possibly Serious	Unimportant	Possibly Serious
Compensated Transient Accelerations	Relatively Unimportant	Possibly Serious	Possibly Serious	Relatively Unimportant
Uncompensated Transient Accelerations	Possibly Serious	Possibly Serious	Relatively Unimportant	Possibly Serious
Rotation-Induced Flows	Should be Avoided	Should be Avoided	Unimportant	Should be Avoided

CONVECTION IN FLUIDS AT REDUCED GRAVITY

by
Simon Ostrach
Case Western Reserve University
Cleveland, Ohio

At the start of the materials processing in space program it was usually considered that at "zero gravity" there would be no fluid motions due to buoyancy. Since such flows, called natural convection, were considered to be deleterious, there was great enthusiasm for processing materials at "zero gravity." Firstly, I want to say that the gravitational environment in a spacecraft is of the order of 10^{-4} g to 10^{-6} g, and this is not zero! Therefore, I sincerely hope that the term "zero gravity" will be eliminated from our thoughts and publications. It should, more properly, be replaced by micro-gravity, reduced-gravity, or low-gravity. Secondly, it is important to note that natural convection is not always harmful and, therefore, to be avoided. In some situations it may be desirable to have fluid flows in space processes, e.g., to stir the fluid phase for mixing and cooling or to help maintain concentration gradients. In any event, it is important to know the extent and nature of convection in space and the factors on which it depends, in order either to minimize the effects of convection, or to utilize the convection to advantage.

Unfortunately, convection, even in a normal environment, is one of the more complex fluid phenomena, so it is difficult to make specific predictions. The space environment further complicates the situation because there are a variety of nongravity forces that can also induce fluid motion. Such nongravity driving forces which are usually suppressed by gravity include surface or interfacial tension, thermal volume expansions, g-jitter — and that's another term that I'd like to see done away with because I think it leads to some misconceptions — and magnetic and electric fields. Furthermore, gravity-induced convection can still be appreciable even at 10^{-6} g and lower under certain conditions. In order to assess properly the effects of natural convection in a reduced gravity environment, it is essential to comprehend fully what we know about it at the present time. Thus, I will outline for you today some of the key aspects.

Most of the configurations related to materials processing are ones in which the fluid is confined by rigid boundaries. Internal convection problems are considerably

more complex than external ones because the fluid boundary layer and the core are closely coupled. This constitutes the main source of difficulty in predicting the resulting flow and transport. More than one core configuration, that is, more than one flow, is sometimes possible, for a given set of conditions, and which will actually occur for a given set of conditions, cannot be determined a priori. Furthermore, the entire flow is sensitive to configuration geometry and to the imposed thermal boundary conditions.

To add to the complexity it's important to note that there are essentially two basic modes of flow generated by a body force. The first is what I term "conventional convection" (Figure 1). A flow starts immediately. It may be that the flow is sufficiently slow so that there is no heat or mass transfer, but this is not an instability mechanism. This is an immediate flow and yet it has at times been considered to be due to an instability.

The second basic mode is one where the density gradient is parallel to the body force, but opposed to it. This is what I call "unstable convection."

In this situation, we have a fluid in the state of unstable equilibrium and the flow will start only when the density gradient exceeds a certain critical value. In that case there is a transient period, and, finally, a steady flow is established which takes on the form of Bénard cells or transverse or longitudinal vortex rolls, or some combination of them.

Once this is comprehended, you realize what information is needed to assess convection. You have to know both the magnitude and direction of acceleration, and certainly, in some of the early spacecraft flights, only the magnitude was reported--the direction is equally as important. You have to know the geometric configuration, you must know the boundary conditions, and you must know the material properties.

As if all of this were not sufficiently difficult to deal with, both modes of convection, conventional and unstable, can occur simultaneously in a given configuration.

Further complexities arise in material processing because the fluid is not homogeneous and, therefore, we have concentration gradients that can cause density gradients in addition to the temperature gradients. The density gradients due to those two causes can enhance or oppose each other in coupled ways and relatively little work has been done on such problems. In the unstable configuration where you have a temperature and concentration gradient parallel and in

70

different directions, you can have any number of situations. For example, a temperature gradient can be stabilizing and a concentration gradient can be destabilizing. The density gradient, however, can be stable so you have a gravitationally stable situation. There are some gravitationally stable situations like this, that, nevertheless, do lead to very complex flows. These are the kinds of things that one sees in some of the ocean problems where salt fountains and salt fingers occur. Of course, there are some situations where we have gravitationally unstable situations.

Corresponding to the conventional convection, we can have concentration and temperature gradients augmenting each other or retarding each other. Relatively little work has been done on any of this latter type of problem. There has been some work, of an uninteresting type, I think, on these, where similarity solutions are found and the results are quite predictable.

So, for some of these reasons that I have given here, it's necessary to study each problem more or less by itself if you want to obtain detailed information on the transport processes. However, you can get considerable insight into the qualitative nature of the problem from dimensional analysis. The first step in the understanding of these kinds of complex phenomena, therefore, is to obtain the relevant dimensionless parameters. These are best determined from the basic equations and associated boundary conditions.

The parameters that occur for purely natural convection flows are the Grashof number, which equals the product of the density difference, gravity, and the cube of a characteristic dimension divided by the density and the square of the kinematic viscosity. This is a measure of the relative buoyancy to viscous forces. A Rayleigh number appears in the energy equation, and is the product of the Grashof and Prandtl numbers. The latter parameter involves only the thermophysical properties of the fluid. If the density difference is due to temperature gradients alone, then the Grashof number is $\beta g \Delta T d^3 / \nu^2$, where β is the volumetric expansion coefficient. And if the flow is thermally induced, the velocities can be estimated from $U = \sqrt{Gr}(\nu/d)$ for $Gr > 1$ and $U = Gr(\nu/d)$ for $Gr < 1$. If the density gradient is due to concentration gradients, you have a solutal Grashof number and an associated Rayleigh number that looks like

$$Gr_s = \frac{\alpha g \Delta C d^3}{\nu^2} \text{ and } Ra_s = PrGr_s$$

71

In this way an estimate of the conventional natural convection velocities can be obtained.

For the thermally unstable case, the critical Rayleigh number, which is the nondimensional critical density gradient, required for the onset of flow must be determined. Many years ago some of my students and I showed that these critical Rayleigh numbers are very much affected by geometry. I have plotted some of the work that was taken from Edwards and Catton at UCLA, which shows what happens in cylinders of various cross sections (Figure 2). This figure is for a square cross section; it really does not make any difference if it is circular. It can be seen that the configuration is essentially an unbounded horizontal layer, $H/w = 0$; the critical Rayleigh number is 1708, which is a well-known number. However, as you begin to confine the fluid you can raise the critical Rayleigh number up to millions. And if you look at a more general configuration, like a rectangular parallelepiped, in Figure 3 the effect of both aspect ratios can be seen. Again, the critical Rayleigh number can be in the millions. Thus, it is my general feeling that the unstable mode is not going to be a serious one to deal with in a reduced-gravity environment, because the Grashof numbers or the Rayleigh numbers will be six to seven decades smaller than normal; and since most of the problems, in materials processing, at least, are confined problems, the critical Rayleigh numbers will be relatively high.

Now, again, as I pointed out before, both modes are possible in a given configuration, and to illustrate this, we see in Figure 4 a rectangular parallelepiped with one wall hot and one wall cold. Now, if this is oriented at 90 degrees, which means it is in a horizontal position with the hot wall below, you notice that you get no convection until you come to a Rayleigh number of 1708; and then, as you rotate it around to the vertical position with one wall hot and one wall cold, that is $\delta = 0$, you have a steady two-dimensional unicell. If you rotate it all the way around so that it is horizontal with the hot wall above and the cold wall below, the configuration is stably stratified, and, again, you have no convection. But, intermediate to that, you have the two modes interacting and you can have longitudinal rolls, meandering flows, transverse traveling waves, and longitudinal rolls again. So, the situation is fairly complex.

Now, let us go back and look again at some of the detailed kinds of convection and see if we can have buoyancy-induced convection with a background g in a spacecraft. The acceleration of gravity on earth is usually at a constant value of 980 cm/sec^2. A steady and reduced value of acceleration is inherent in most spacecraft because of atmospheric

drag, centrifugal force due to vehicle rotation, gravity gradients, solar wind and solar pressure. Superimposed on this background of a uniform, but weak gravitational field, are temporally variant accelerations that are due to engine burns, attitude control maneuvers and onboard vibrations from machinery or astronaut movement. Some of the steady-state accelerations in several missions are shown in Figure 5. It can be seen that the background accelerations are on the order of 10^{-5} up to 10^{-9}. To give you a feeling as to whether 10^{-6} g or 10^{-7}g is zero, I have computed a Grashof number for rather mundane conditions. Suppose we have a temperature difference of about 10°K at a temperature level of 20°C and a characteristic dimension of 10 cm. At 1-g for a gas, the Grashof numbers would be on the order of 10^6, for liquids on the order of 10^7, and liquid metals on the order of 10^9. If you reduce these by six decades, they still are not zero. I have also computed some representative velocities at 10^{-5} g, and in Fig. 5 you see that for liquids and liquid metals you get velocities of fractions of a millimeter per second and for gases you can get velocities on the order of a half-millimeter/second. Of course, if the conditions are more severe than that, you can get all other kinds of results.

As contrasted to the nonuniformities of the gravitational field, some of which have to be accepted as part of the natural environment in the orbital vehicle, there are transient or time-variant perturbations to the gravity field at a point. The unsteady variations, which are referred to as g-jitter, can arise from spacecraft maneuvers and mechanical vibration. As I said before, I think g-jitter is an improper name, because what we are talking about now are acceleration levels of the spacecraft itself, and that is what provides the driving force for the fluid. During spacecraft maneuvers again, acceleration magnitudes of 10^{-4} g and higher can be encountered. This effect possibly could be overcome if experiments were done during the drift mode. On the other hand, g-jitter caused by mechanical vibrations cannot necessarily be controlled at their sources. Mechanical vibrations that are transmitted to the experiment have the same effect as a time-variant gravity. They can be caused, for example, by astronaut movement, rotating and reciprocating machinery, extravehicular activities, and arm and leg movements.

The earliest study of this phenomenon was done at Lockheed, Huntsville, by means of computer solutions. Numerous instances were considered (see Figure 6): a rectangle which is heated from the side, a rectangle which is heated from below, and a cylinder heated from below. Various modes of jitter were imposed on them, such as sinusoidal and absolute value of the sinusoid and linear periodic (see Figure 7). The greatest effect of this mode was obtained for

73

the saw-tooth g-jitter (linear periodic). In Figure 8 the isotherms for this g-jitter model are shown to be very similar to the isotherms for the model where there is a constant g at the same mean level. The streamline patterns are shown in Figure 9. This was the first indication of these kinds of things, but I do not know how definitive these results are because they were obtained merely from large-scale computer calculations. A few years ago my group started both theoretical and experimental studies of g-jitter. The dimensionless parameters for this problem were found to be as given in Figure 10. The basic configuration considered was a rectangular enclosure which had a hot wall and a cold wall to stabilize it convectively so that there would be no motion other than that due to the g-jitter. The g-jitter was imposed normal to the temperature gradient. The unsteady effects are then determined by L_1/a. Another parameter is the aspect ratio. The next parameter is the volumetric expansion coefficient times the temperature difference, this is the relative imposed temperature difference, and then there is a Reynolds number based on velocity which is $\omega \times$ a dimension.

Now, typical values of the parameters for the given conditions are also shown in Figure 10. Our analysis indicates that if the jitter was of the form $f_x = AF(t)$, where $F(t)$ was a random function, but had a zero time mean, like a sinusoid, in other words, if the imposed acceleration essentially had as much on the plus side as on the negative side, this would correspond to having a fixed experiment in a spacecraft and having nothing that moves it or moves the spacecraft at the same time, it was then found that there would be no motion . . . no significant motion. All that would occur, at most, is a sort of random motion with no net translation of the particles and no influence on the transport. However, if you had a nonzero mean type of acceleration like $f_x = K + AF(t)$, where K is a time mean, then, in fact, you get an equivalent flow like a natural convection flow where K is the essential driving force. There are other aspects of the g-jitter problem that were investigated. In the case just discussed, the g-jitter acts across a temperature gradient, and this corresponds to the conventional convection. If, however, the g-jitter was along the temperature gradient, the unstable mode of convection would be expected. It appears from the work of Greshko and Sani that for that mode, the oscillations of the accelerations tend to stabilize the situation. There are also other issues involved, such as the transient nature of how long does it take for the g-jitter to stabilize.

Experiments on the conventional mode of g-jitter were performed in the Lewis drop tower; the conditions (shown in Figure 11) exceeded the values shown in Figure 10. All of the tests indicated no motions at all. The dimensionless parameters were increased in an attempt to get a motion and it was at that point that the analysis indicated to us that no motion could be obtained with non-zero mean jitter.

We just have run a couple of tests where the jitter has a non-zero mean, and we did pick up some of the oscillatory motion. The results indicate that astronaut movements, like sneezing and coughing, which impose jitter with zero time means would induce, at most, an oscillatory motion which is quite small. There would be no net fluid translation and no net heat transfer change. Spacecraft maneuvers and astronauts walking along the periphery of the spacecraft or violent exercises will lead to non-zero mean jitter, and then motion and transfer at the mean level will be obtained. An interesting sidelight on this was obtained in one of the experiments in which all the bubbles were not removed from the liquid. The bubbles caused a very large streaming motion, which implies that if foreign particles are in the fluid, they could induce rather large scale motions.

Another possible driving force for fluid motions is surface tension. Surface tension on the free surface of a liquid may, under some conditions, considerably affect liquid motion. The presence of an interface between two fluid faces can influence the motion of fluids when either the interface has a finite curvature which is different from the equilibrium curvature, or when an interfacial tension varies from point to point. In both cases, forces appear in the interfacial region that can affect or generate the fluid motions. It has generally been believed, and argued that on earth, this Bond number (Figure 12) is what indicates the relative importance of gravity to surface tension. Computations made on this basis indicate that unless the dimension is very, very small, the surface tension forces are suppressed. This, however, is what I call a static Bond number; in other words, it is one which occurs under isothermal conditions, and I will show shortly that it is not really a relevant one. The relative magnitude of surface tension and buoyancy forces has been considered to be given by the ratio of the Marangoni and Rayleigh numbers. It will be shortly shown that this is not correct either.

It is important to recognize, and this seems to be very much confused, even though a number of years ago Skip Scriven pointed this out, that there are two modes of surface tension-driven flows just as there are two modes of buoyancy-induced flows. If the gradient of concentration or temperature is

along the interface, then you have a flow immediately establishing itself. If the gradient is normal to the interface, you have an instability, just like a Bénard instability, now it is the Marangoni instability (see Figure 12). It is very important that this be understood. Now, the greatest effort has been given to the unstable type of flow, but for materials processing experiments, in fact, the other kind of flow is considerably more important.

I was rather amazed when I was looking at this field that the dimensionless parameters had not been formally derived and so I set out to determine them.

Basically, consider a simple configuration of a rectangular container filled with a fluid with a free surface along which a temperature gradient is imposed. Regular normalization of variables yields the familiar parameters shown in Figure 13. However, this is all in terms of a reference velocity, which is, as yet, unknown. Most of the people who have looked at these kinds of problems used for the reference velocity something like the kinematic viscosity over a length or the thermal diffusivity over a length and this is not the correct one. The correct one is obtained from the free surface boundary conditions. The boundary condition that must be satisfied (Figure 14) is that the shear stress of the wall must be balanced by the surface tension gradient. For the configuration under consideration if the Reynolds number times the square of the aspect ratio is small, we have a viscous-dominated situation, so the characteristic dimension, the proper one, is the height of the fluid layer; then the proper velocity is shown at the top of Figure 14. This is interesting in that it is given in terms of the physically imposed conditions and the thermophysical properties of the fluid, viz., the surface tension gradient, the imposed temperature difference, the viscosity, and an aspect ratio. As a consequence, the important parameter for surface tension-driven flows, is what I call a surface-tension Reynolds number, which is defined in Figure 14.

Now for the other case of a boundary-layer situation, the boundary layer thickness must be used as the reference length and the reference velocity comes out as shown in the lower part of Figure 14. Again, the surface tension Reynolds number is shown thereon. This situation is completely analogous to what happens in natural convection flows and so if you look at the resulting equations shown in Figure 15 for the viscous-dominated situation, you notice that the Marangoni number appears only in the energy equation. Thus, it is not the fundamental parameter that it has been made out to be. It is like a Peclet number, which is important for

76

ⅉ

heat transport. For the boundary layer situation (lower equations) the Marangoni number does not even appear explicitly.

There are other characteristic lengths for other kinds of problems that one has to be careful about, but for this kind of geometry, this is what they come out to be. Also, very interestingly, you notice that the buoyancy effect is given by the parameter shown at the lower left of Figure 15 and it is now a modified Bond number. For the boundary layer case (lower right of Figure 15) it is a modified Bond number of a different kind. Once this was recognized, it turns out that we have done an analysis and we know that we can now look at surface tension flows on earth, because what happens is that the characteristic length is determined by the imposed buoyancy field and you can properly tailor the flow field by heating from above in a stabilizing situation. In this way, surface tension flows in fish tanks were observed for rather large periods of time.

One important result obtained from the determination of the proper dimensionless parameters is that the surface tension Reynolds number in contra-distinction to the conventional Reynolds number does not depend on the dynamics, but depends primarily on the imposed conditions and on the fluids. Thus, the problems can be categorized according to the types of fluids, and the qualitative nature of the flows to be expected in different kinds of fluids can be obtained a priori (see Figure 16).

Brief mention will now be made of other possible types of convection in a reduced-gravity environment (see Figure 17). Those that are dependent on the acceleration field are listed there. Independent of gravity, thermal volume expansions can act as a driving force for convection. After some of these earlier Apollo XIV and XVII heat flow and convection experiments we thought we had some evidence of this type of convection, but I do not think it turned out to be that way. In other words, if you rapidly heat a confined fluid, like a gas, you have rapid local expansions, which, in turn, generate pressure waves. These pressure waves produce a convective motion which can greatly increase heat transfer relative to conduction and can also cause mass and chemical species transport. This provides a mechanism for enhancing or suppressing convective motions at low gravity by controlling the heating rate.

Phase change convection is another type. Shrinkage usually occurs during solidification because the density of the solid is usually higher than that of the liquid and, hence, occupies a small volume. This volume reduction

results in a flow of liquid toward the solidifying interface. Such flows are also generated by non-equimolar reactions that occur in vapor deposition crystal growth. Pressure pulses can also accompany these kinds of flows and, therefore, influence the nature of the material. Relatively little work has been done on this type of convection, and I think it is a rather important one that ought to be considered.

Thermosolutal convection, of course, is one which occurs when we have concentration gradients causing the flow, and I have already talked about that. It is important to understand that electric and magnetic fields induce body forces, just like gravity, so that they can generate convection and phase separation phenomena similar to those in the gravitational field. Whereas, in a gravitational field, convection is generated by density differences, in an electrical field the flow is generated by differences in electrical conductivity and by differences in susceptibility in a magnetic field. The electric conductivity and magnetic susceptibility are temperature dependent, so that temperature differences are usually required to obtain these flows. Again, both conventional and unstable types of convections are possible with these kinds of fields, and, of course, in a given problem, you can have combined or coupled convections due to any one of these.
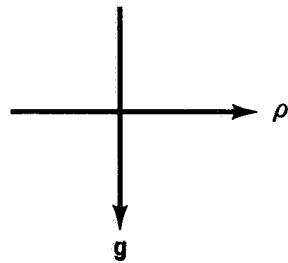
CONVENTIONAL CONVECTION   **UNSTABLE CONVECTION**

INFORMATION NEEDED TO ASSESS CONVECTION
- (A) BOTH MAGNITUDE AND DIRECTION OF ACCELERATIONS
- (B) GEOMETRIC CONFIGURATION
- (C) IMPOSED BOUNDARY CONDITIONS
- (D) MATERIAL PROPERTIES

FIGURE 1

FIGURE 2

FIGURE 3

81
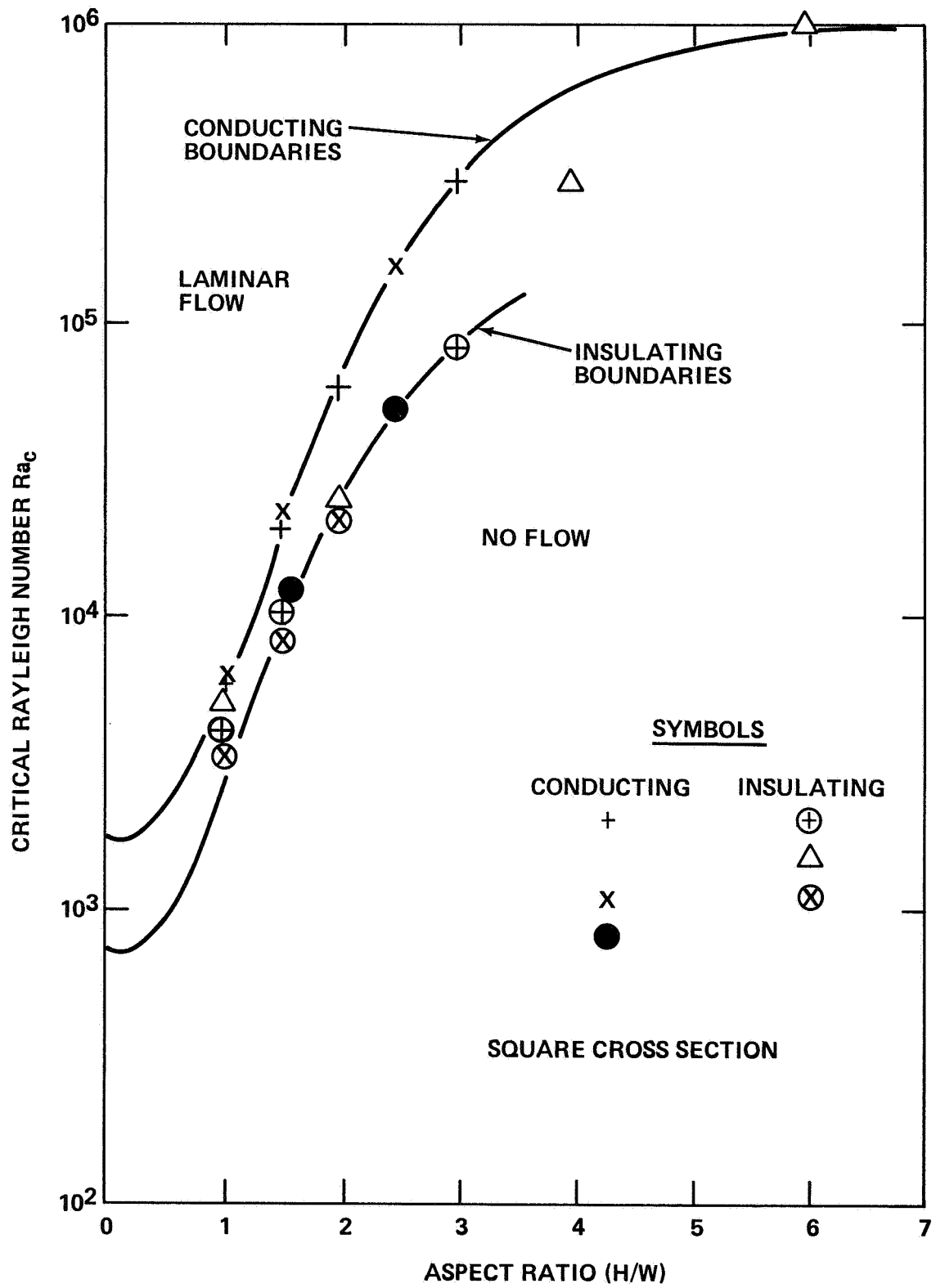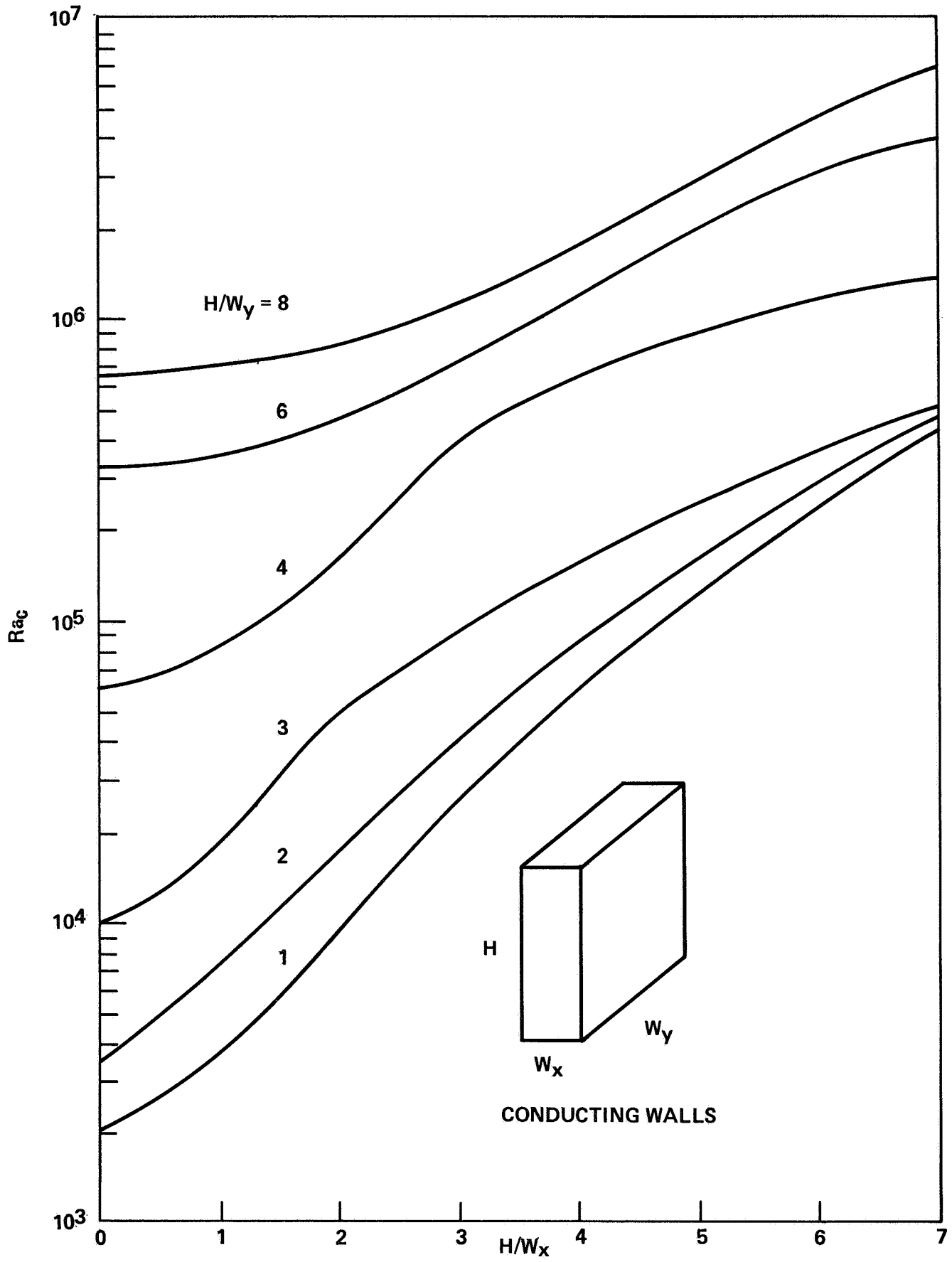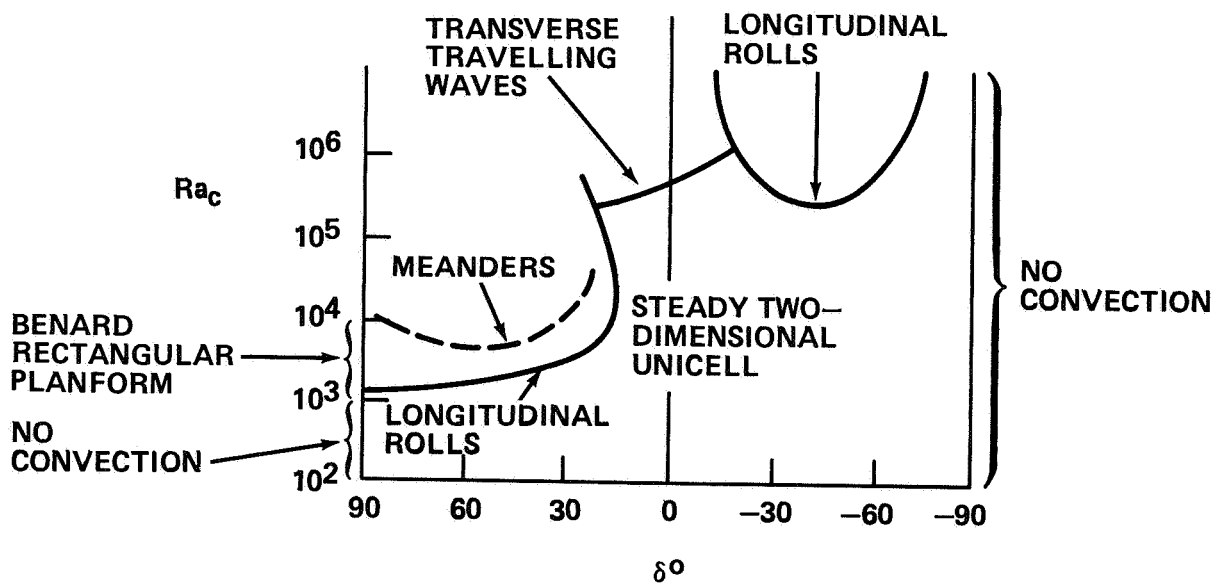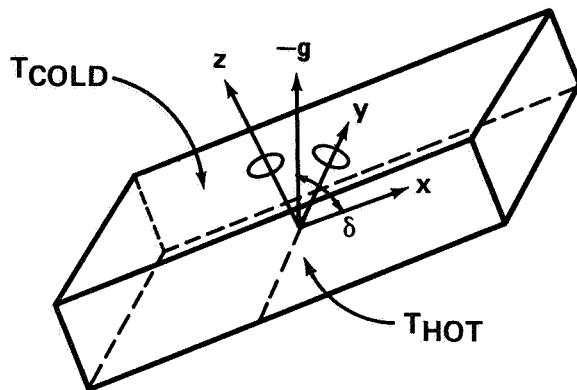
FIGURE 4

STEADY REDUCED–GRAVITY ACCELERATIONS

SOURCE	TYPE OF MISSION		
	LOW–ALTITUDE EARTH ORBIT	LOW–ALTITUDE LUNAR ORBIT	INTERPLANETARY TRAJECTORY
ATMOSPHERIC DRAG	5×10^{-5}g & LOWER	NONE	NONE
CENTRIPETAL FORCE	1×10^{-6}g	3×10^{-7}g	3×10^{-14}g
GRAVITY GRADIENT	3×10^{-9} g/cm	2×10^{-9} g/cm	4×10^{-17} g/cm
VENTING THRUST	ALL 10^{-4}g TO 10^{-6}g, NEGLECTING DRAG		
VEHICLE THRUST	ALL 0.1g TO 6g		

STEADY g–LEVELS IN APOLLO MISSIONS

APOLLO FLIGHT MODE	TYPICAL g–LEVEL
PASSIVE THERMAL CONTROL	3×10^{-6} g
ATTITUDE HOLD IN TRANSLUNAR OR TRANSEARTH ORBIT	7×10^{-8}g
ATTITUDE HOLD IN LUNAR ORBIT	5×10^{-7}g

ONE–g GRASHOF NUMBER $\Delta T = 10^{\circ}K$, $T = 20^{\circ}C$, d = 10cm.

GAS ~ O (10^6)   LIQUID ~ O (10^7)   LIQUID METAL ~ O (10^9)

VELOCITIES AT 10^{-5}g

LIQUID AND LIQUID METALS ~ O (0.13mm/sec.)   GAS ~ O (0.5mm/sec.)

FIGURE 5
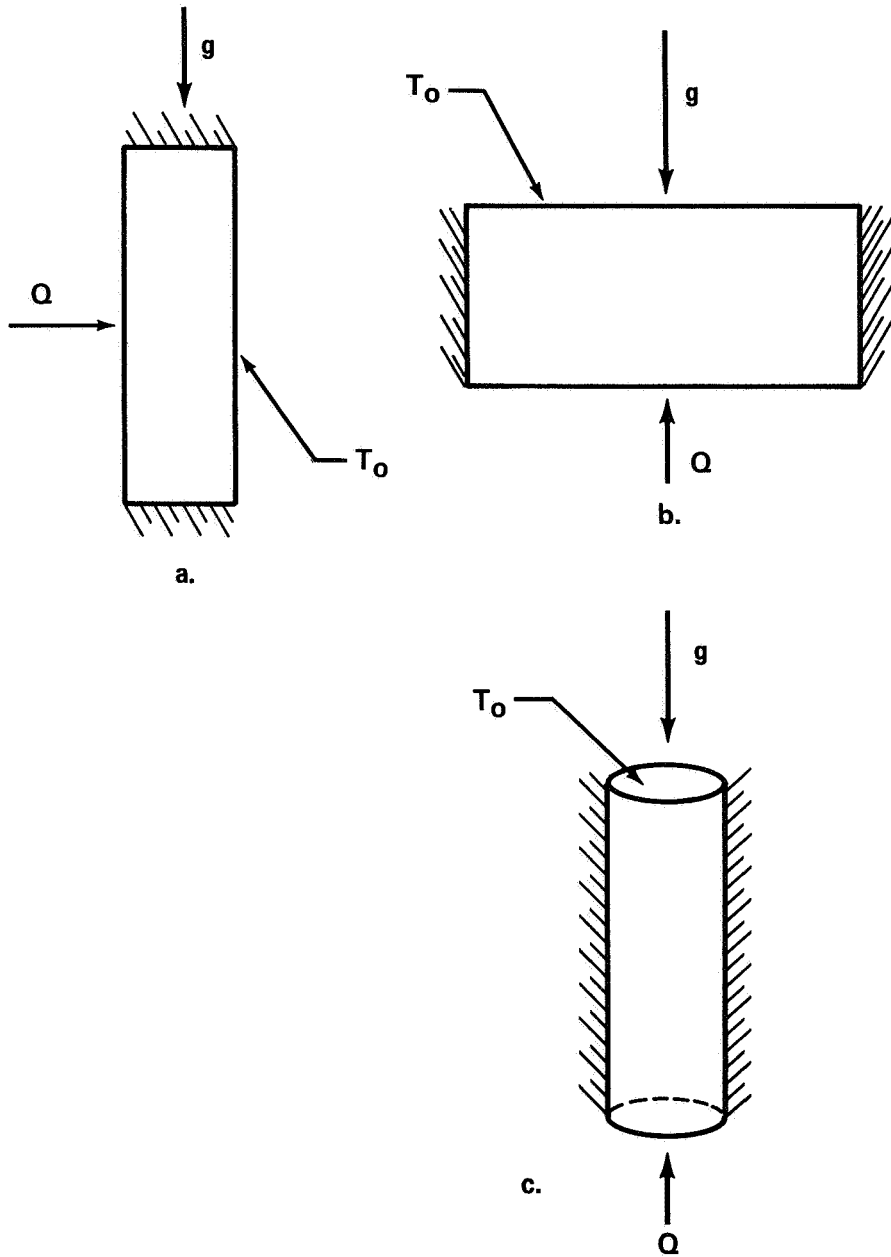
FIG. 6. CONFIGURATIONS USED IN COMPUTER MODELS
OF g-JITTER CONVECTION.
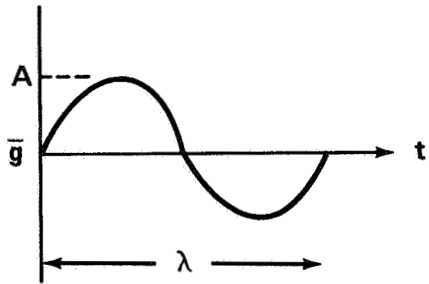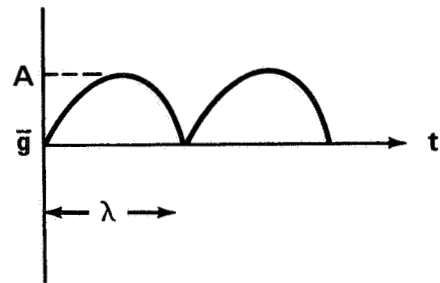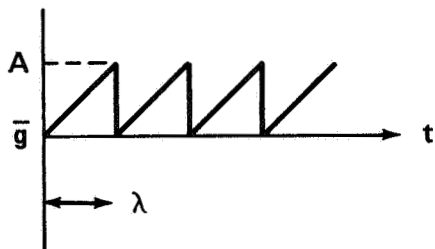
FIG. 7. G-JITTER MODELS USED FOR PARAMETRIC SENSITIVITY STUDY.
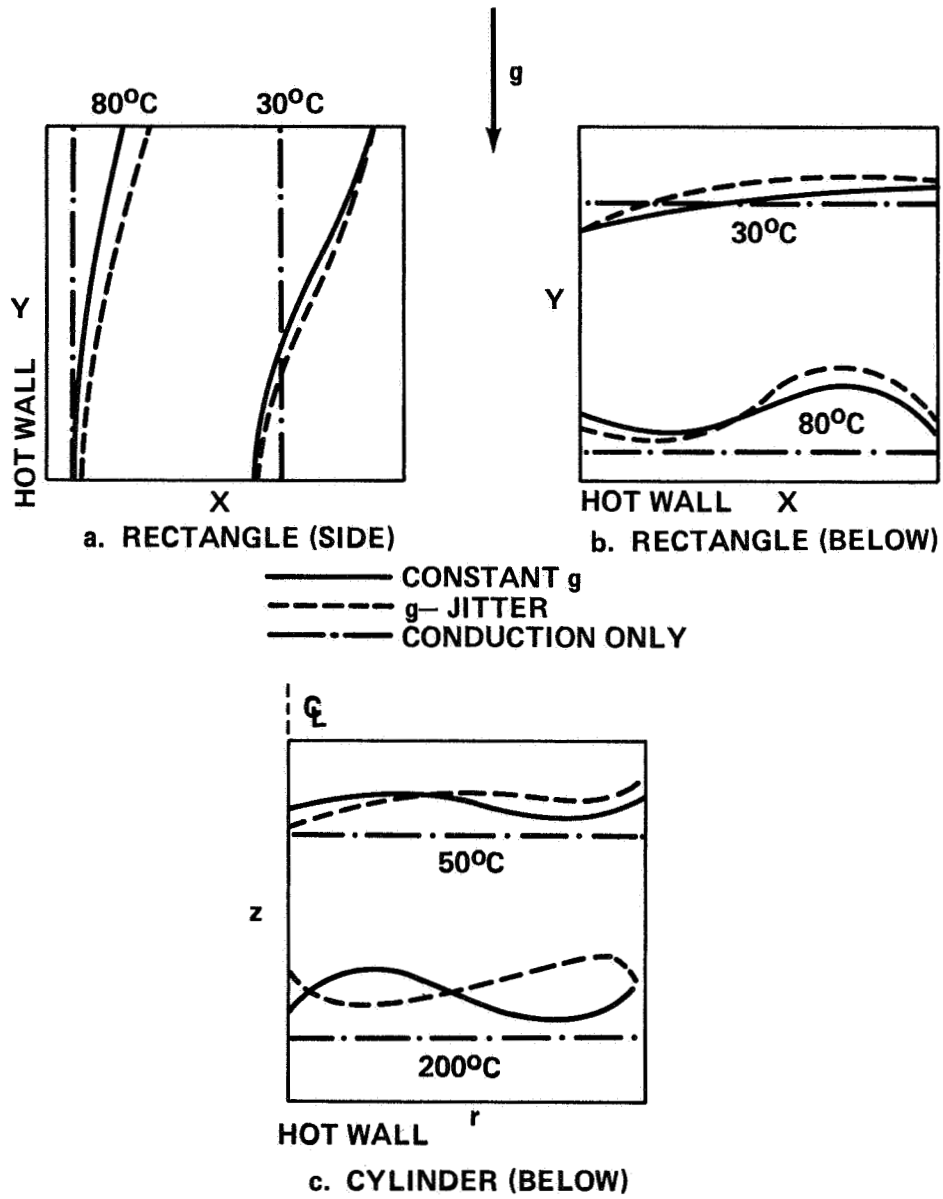
FIG. 8. ISOTHERMS AT t = 3 MINUTES FOR THREE CONFIGURATIONS SHOWING EFFECT OF g-JITTER MODEL.

g

WATER, g = CONSTANT (10^{-3})
RECTANGLE, SIDE HEATING

WATER, g = g (t) MODEL 3
RECTANGLE, SIDE HEATING

a.

MERCURY, g = CONSTANT (10^{-3})
CYLINDER, BELOW HEATING

MERCURY, g = g (t) MODEL 3
CYLINDER, BELOW HEATING

b.
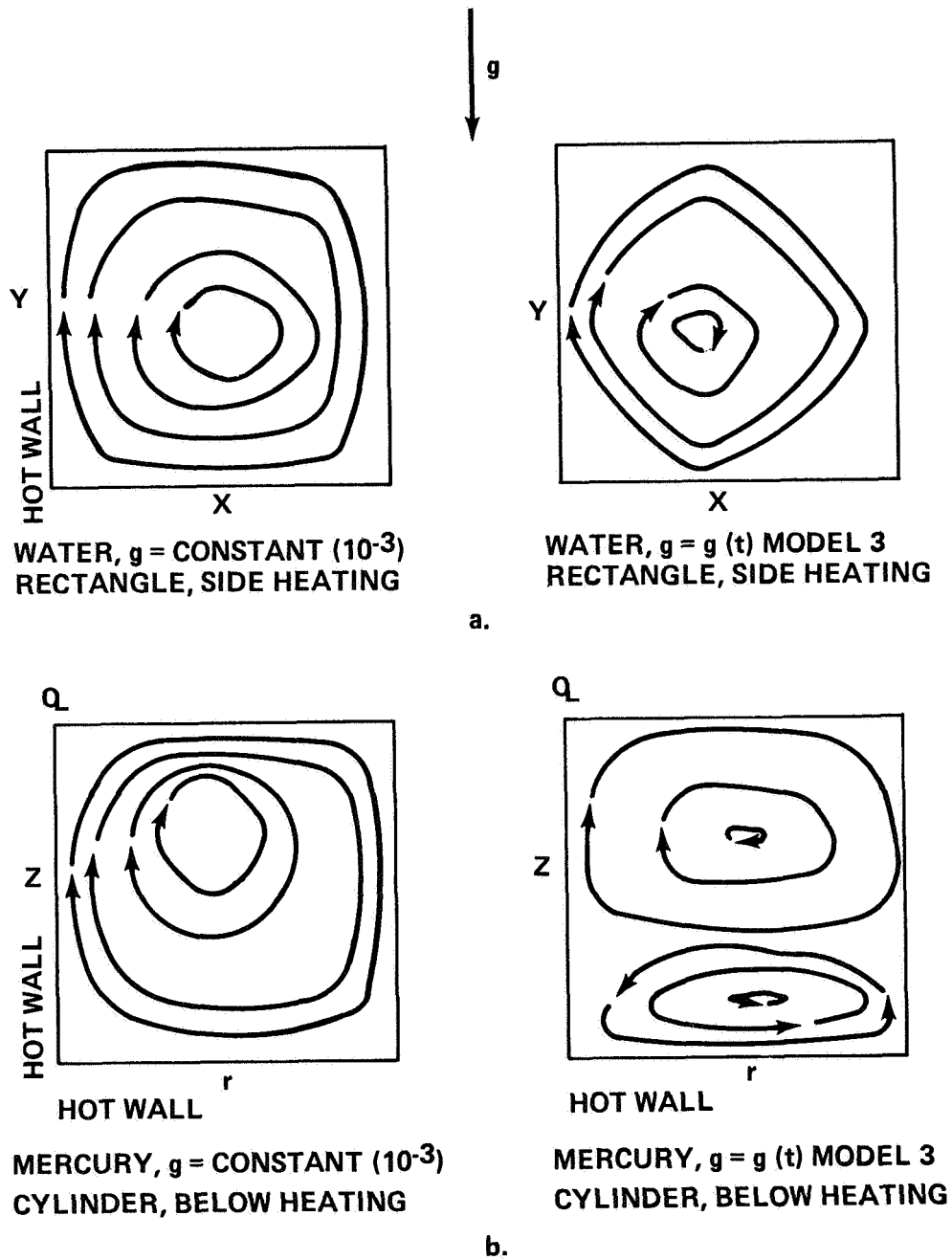
FIG. 9. STREAMLINES AT t = 3 MINUTES SHOWING EFFECTS OF
g - JITTER ON FLOW PATTERNS.

g - JITTER

PARAMETERS: —

$$\frac{L_1}{a} \sim \frac{\text{UNSTEADY}}{\text{INERTIA}} \qquad \frac{L_1}{L_2} \sim \text{ASPECT RATIO}$$

$$\beta\,(\theta_2 - \theta_1) \qquad\qquad \frac{\omega L_1^2}{\nu} = Re \sim \frac{\text{INERTIA}}{\text{VISCOUS}}$$

$$\frac{\nu}{\alpha} = Pr$$

g—JITTER
$\theta_2 > \theta_1$
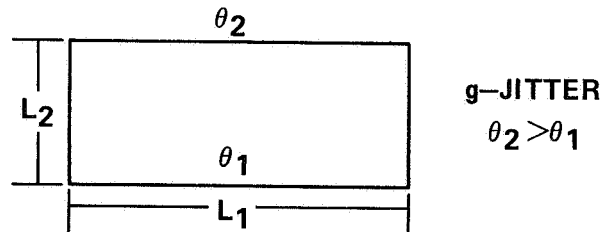
$L_1 = 10\text{cm},\ L_1/L_2 = 5,\ \theta_2 - \theta_1 = 30^{\circ}C \qquad a \approx 0.04\ \text{cm}.$

$\omega/2\pi \approx 0.5\ \text{RAD/SEC.} \qquad A = a\omega^2 \sim 10^{-3} + 10^{-6}g$

$a/L_1 = 4 \times 10^{-3},\ \beta\,(\theta_2 - \theta_1) = 10^{-2}, \quad Re = 4 \times 10^4$

$Pr = 6$

$f_x = AF\ (t)$
       └RANDOM, ZERO TIME MEAN VALUE

$f_x = K + AF\ (t) \qquad \text{NONE} - \text{ZERO MEAN}$
     └TIME MEAN

FIGURE 10

EXPERIMENTS:

$\Delta T = 0^o - 43^oC$ $\qquad\qquad$ $\omega = 10-40$ CPS

a = 0.2 cm $\qquad\qquad\qquad$ $a/L_1 = 0.15$

$\epsilon = \beta \, \Delta T = 0-1.12 \times 10^{-2}$ $\qquad$ Re = 1.27 TO 5.0×10^6

RESULTS:

    ASTRONAUT MOVEMENTS $\sim$ ZERO TIME MEAN

        UNICELLULAR OSCILLATORY RATIO O $(\epsilon a\omega)$

        NO NET FLUID TRANSLATION

        NO HEAT TRANSFER CHANGE

    SPACECRAFT MANEUVERS – NON–ZERO MEAN

        MOTION AND TRANSFER AT MEAN LEVEL

    BUBBLES CAUSED STREAMING

FIGURE 11

	CONVENTIONAL FLOW	UNSTABLE FLOW
SURFACE TENSION	GRADIENT ALONG INTERFACE	GRADIENT NORMAL TO INTERFACE
BUOYANCY	GRADIANT NORMAL TO B. F.	GRADIENT PARALLEL BUT OPPOSITE TO B. F.

BOND NUMBER:

$$Bo = \frac{\rho g d^2}{\sigma} \sim \frac{GRAVITY}{SURFACE\ TENSION}$$

ρ — FLUID DENSITY

g — GRAVITATIONAL ACCELERATION

d — LENGTH

σ — SURFACE TENSION

FIGURE 12

FREE SURFACE
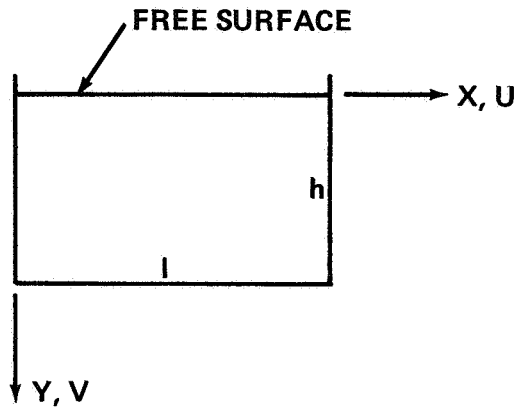
$$x = X/L, \; y = Y/h, \; U = U/U_R, \; v = V/V_R \; (h/L)$$

$$p = P/\rho U_R^2, \; \tau = (T-T_c)/(T_w-T_c)$$

$$u\frac{\partial u}{\partial x} + v\frac{\partial u}{\partial y} = \frac{1}{ReA^2}\left(A^2\frac{\partial^2 u}{\partial x^2} + \frac{\partial^2 u}{\partial y^2}\right) - \frac{\partial p}{\partial x}$$

$$u\frac{\partial v}{\partial x} + v\frac{\partial v}{\partial y} = \frac{1}{ReA^2}\left(A^2\frac{\partial^2 v}{\partial x^2} + \frac{\partial^2 v}{\partial y^2}\right) - \frac{G_r}{Re^2 A}\;\tau - \frac{1}{A^2}\frac{\partial p}{\partial y}$$

$$u\frac{\partial \tau}{\partial x} + v\frac{\partial \tau}{\partial y} = \frac{1}{Pr\,Re\,A^2}\left(A^2\frac{\partial^2 \tau}{\partial x^2} + \frac{\partial^2 \tau}{\partial y^2}\right)$$

REYNOLDS NO. = Re = $U_R L/\upsilon$ ~ INERTIA/VISCOUS

GRASHOF NO. = Gr = βg (Tw—Tc) L $^3/\upsilon(nu)^2$ ~ BUOYANCY/VISCOUS

PRANDTL NO. = Pr = υ/α

ASPECT RATIO = A = h/L

FIGURE 13

$$-\mu \frac{\partial U}{\partial Y} = \frac{\partial \sigma}{\partial X} = \frac{\partial \sigma}{\partial T} \ \frac{\partial T}{\partial X}$$

FOR $ReA^2 < 1$ $\qquad\qquad$ $y = Y/h$

$$U_R = \frac{(\partial\sigma/\partial T) \ (Tw-Tc)}{\mu} \quad \left(\frac{h}{L}\right)$$

$$\frac{h}{L} \ll \sqrt{\frac{\mu\nu}{(\partial\sigma/\partial T) \ (Tw-Tc) \ h}} \equiv \sqrt{\frac{1}{R_\sigma}}$$

FOR $ReA^2 > 1$ $\qquad\qquad$ $y = Y/\delta$ $\qquad\qquad$ $\delta = \dfrac{1}{A \ \sqrt{Re}}$

$$U_R = \left[\frac{(\partial\sigma/\partial T)^2 \ (Tw-Tc)^2 \nu}{\mu^2 \ L}\right]^{1/3}$$

$$\frac{h}{L} \gg \sqrt{\frac{1}{R_\sigma}}$$

FIGURE 14

92

$\lrcorner$

FOR $R_\sigma A^2 \ll 1$

$$O = A^2 \ \frac{\partial^2 u}{\partial x^2} + \frac{\partial^2 u}{\partial y^2} - \frac{\partial p}{\partial x}$$

$$O = A^2 \ \frac{\partial^2 v}{\partial x^2} + \frac{\partial^2 v}{\partial y^2} - \frac{GrA}{R\sigma} \ \tau - \frac{1}{A^2} \left(\frac{\partial p}{\partial y} \right)$$

$$Ma \ A^2 \left(u \frac{\partial \tau}{\partial x} + v \frac{\partial \tau}{\partial y} \right) = A^2 \ \frac{\partial^2 \tau}{\partial x^2} + \frac{\partial^2 \tau}{\partial y^2}$$

FOR $R\sigma A^2 \gg 1$

$$u \ \frac{\partial u}{\partial x} + v \ \frac{\partial u}{\partial y} = \left(\frac{A}{R\sigma} \right)^{2/3} \frac{\partial^2 u}{\partial x^2} + \frac{\partial^2 u}{\partial y^2} - \frac{\partial p}{\partial x}$$

$$u \ \frac{\partial v}{\partial x} + v \ \frac{\partial v}{\partial y} = \left(\frac{A}{R\sigma} \right)^{2/3} \frac{\partial^2 v}{\partial x^2} + \frac{\partial^2 v}{\partial y^2} - \frac{Gr \ A}{R\sigma} \ \tau - \left(\frac{R_\sigma}{A} \right)^{2/3} \frac{\partial p}{\partial y}$$

$$u \ \frac{\partial \tau}{\partial x} + v \ \frac{\partial \tau}{\partial y} = \frac{1}{Pr} \left[\left(\frac{A}{R_\sigma} \right)^{2/3} \ \frac{\partial^2 \tau}{\partial x^2} + \frac{\partial^2 \tau}{\partial y^2} \right]$$

Ma = Marangoni number = $Pr \ R_\sigma$

For $R_\sigma A^2 \ll 1$

$$\frac{Gr \ A}{R\sigma} = \frac{\rho \beta g L^2}{\partial \sigma / \partial T} \equiv \overline{Bo}$$

For $R_\sigma A^2 \gg 1$

$$\frac{Gr \ A^{2/3}}{R\sigma^{5/3}} = \overline{Bo} \left(\frac{A}{R\sigma} \right)^{2/3}$$

FIGURE 15

93

FOR: (Tw—Tc) = 50°C, h = L = 10 cm.

	R_σ	G_r	M_a	$\overline{B}_o$	$\overline{B}_o/R_\sigma^{2/3}$
OILS	$10^{-1} - 10^4$	$10^2 - 10^7$	$10^2 - 10^6$	10^3	10
GLASS	10^{-1}	10	10^2	10^2	—
WATER	10^6	10^8	10^9	—	10^{-2}
LIQUID METALS	$10^5 - 10^6$	$10^8 - 10^{10}$	$10^3 - 10^5$	—	10^{-2}

FIGURE 16

TYPES OF REDUCED–GRAVITY CONVECTION

ACCELERATION FIELD DEPENDENT

THERMAL CONVECTION
SOLUTAL CONVECTION
g – JITTER CONVECTION
THERMOSOLUTAL CONVECTION

INDEPENDENT OF ACCELERATION FIELD

SURFACE TENSION CONVECTION (MARANGONI)
THERMOACOUSTIC CONVECTION
PHASE CHANGE CONVECTION
CONVECTION DUE TO ELECTRIC AND MAGNETIC FIELDS

COMBINED OR COUPLED CONVECTION

FIGURE 17

EFFECTS OF SPACECRAFT MOTIONS ON

FLUIDS EXPERIMENTS

by
Roger F. Gans
Department of Mechanical and Aerospace Engineering
The University of Rochester

ABSTRACT

The equations of motion governing an incompressible fluid contained in an orbiting laboratory are examined to isolate various "fictitious forces" and their relative influence on the fluid. The forces are divided into those arising from the orbital motions and those arising from small local motions of the spacecraft about its center of mass. The latter dominate the nonrotating experiments. Both are important for rotating experiments.

A brief discussion of the onset of time-dependence and violent instability in earth-based rotating and precessing systems is given.

The dynamics of a fluid in an orbiting spacecraft, whether stratified or not, whether contained or not, will be affected by all the motions of the spacecraft. I address contained unstratified fluids below.

Experimental data will be measured in a spacecraft-fixed noninertial frame. Thus measurements must be interpreted to take into account "fictitious forces."

A spacecraft-fixed coordinate system is shown in Figure 1. Three orbital modes, gravity gradient, z-local vertical, and inertial hold, are shown in Figure 2.

Both orbital and local (thruster burns, etc.) frame accelerations are important. Because they have different time scales, I will separate them by making two coordinate transformations.

First, I will transform to the "orbital system," in which the center of mass of the spacecraft (CM) is fixed. This introduces a fictitious acceleration

$$\underline{f} = -\underline{\Omega} \times (\underline{\Omega} \times \underline{R}) - \dot{\underline{\Omega}} \ \underline{R} - 2\underline{\Omega} \times \underline{v} - \underline{a} \tag{1}$$

where $\underline{\Omega}$ is the instantaneous orbital angular velocity, $\underline{R}$ is a position vector originating at the orbital focus, a dot denotes differentiation with respect to time, $\underline{v}$ is the local velocity and $\underline{a}$ is the apparent acceleration of the focus.

The quantity $\dot{\underline{\Omega}} \times \underline{R}$ is the secular deceleration of the orbital motion and is equivalent to the aerodynamic drag deceleration. The quantity $\underline{a}$ is a radial acceleration, and is negligible compared to the gravity gradient forces.

The Coriolis acceleration, $2\underline{\Omega} \times \underline{v}$, exceeds both drag and gravity gradient values if $|\underline{v}|$ is larger than a few mm/sec.

The total apparent acceleration is then approximately

$$-\underline{\Omega} \times (\underline{\Omega} \times R) - \frac{GM_{\oplus}}{R^3} \ R - 2\underline{\Omega} \times \underline{v} + \underline{a}_D; \quad \underline{a}_D = -\dot{\underline{\Omega}} \ \underline{R} \ . \tag{2}$$

If I put $\underline{R} = \underline{R}_0 + \underline{r}$, where $\underline{R}_0$ is the orbital radius of $\underline{r}$ a position vector from the CM, then the equations of HeCM and motion in terms of the velocity $\underline{v}$ measured relative to the orbital system are

$$\frac{D\underline{v}}{Dt} + 2\underline{\Omega} \times \underline{v} + \nabla\{P/\rho - \frac{3}{2} \frac{GM_{\oplus}}{R_0^5} \ (\underline{R}_0 \cdot \underline{r})^2 - \underline{a}_D \cdot \underline{r}\} = \nu \nabla^2 \underline{v} \ ;$$

$$\nabla \cdot \underline{v} = 0 \ . \tag{3}$$

For a spacecraft in a perfect gravity-gradient or a z-local vertical orbit, only the Coriolis force appears. Its magnitude can be estimated in terms of U, T and L, which denote characteristic velocity, time and length scales. Figure 3 shows U, T space for L = 30 cm and Ω^{-1} = 90 min.

To examine disturbances (attitude corrections, etc.) to the perfect orbit, I make a second transformation to a system rotating about the CM at $\omega(t)$, which is changing in magnitude and direction. The inertial velocity $\underline{v}$, the orbital frame velocity $\underline{u}$ and the local velocity $\underline{q}$ are related by

$$\underline{v} = \underline{u} + \underline{\Omega} \times \underline{R}; \quad \underline{u} = \underline{q} + \underline{\omega} \times \underline{r} \ . \tag{4}$$

The pseudoforces associated with this transformation, combined with those from the first transformation, lead to the full equations governing $\underline{q}$:

$$\underline{q}_t + \underline{q} \cdot \nabla \underline{q} + 2(\underline{\Omega} + \underline{\omega}) \times \underline{q} + \nabla \pi = \nu \nabla^2 \underline{q} + (\underline{\Omega} \times \underline{\omega}) \times \underline{r} - \underline{\dot{\omega}} \times \underline{r} + \underline{F};$$

$$\nabla \cdot \underline{q} = 0 . \qquad (5)$$

Here $\underline{F}$ is the perturbation introduced by the experimenter and $(\underline{\Omega} \times \underline{\omega}) \times \underline{r}$ is called the Poincaré force.

For a perfect inertial hold orbit $\underline{\omega} = -\underline{\Omega}$, $\underline{\dot{\omega}} = 0$, and all the effects of rotation not reducible to potential form vanish.

The disturbance term $\underline{\dot{\omega}} \times \underline{r}$ is probably dominated by crew with magnitude ~ 0.1 cm/sec^2 at frequencies near 1 Hz. Corrections to the motions induced are made by firing vernier thrusters at intervals measured in minutes for times less than one second. The power spectrum is presumably dominated by these frequency bands.

The Poincaré force has a similar power spectrum. The disturbance ω can be estimated from $\omega f L = 0.1$ cm/sec^2, where f is the frequency of the disturbances. Thus the Poincaré acceleration is $\sim 10^{-4}$ cm/sec^2 and will generally be negligible.

The experimenter then needs to disturb his system in ways equivalent to an acceleration of 1 cm/sec^2 or greater to perform experiments at frequencies comparable to these. For quasisteady experiments smaller disturbances can be used in conjunction with data averaging. However, account must be taken of "rectified" flows arising from nonlinear interaction in the $\underline{q} \cdot \nabla \underline{q}$ term.

If the experiment rotates, the equations of motion can be deduced by direct substitution. Let $\underline{q} = \underline{w} + \underline{\gamma} \times \underline{r}$ where $\underline{\gamma}$ is the experimental rotation rate and $\underline{w}$ the velocity relative to the experimental container.

For any reasonable rotation rate, the terms $\underline{\omega} \times \underline{\gamma}$ and $\underline{\Omega} \times \underline{\gamma}$ will dominate $\underline{\Omega} \times \underline{\omega}$. Since the direction of $\underline{\omega}$ cannot be controlled, it would be prudent to arrange $\underline{\gamma}$ to be parallel to $\underline{\Omega}$. The remaining Poincaré force, $(\underline{\Omega} \times \underline{\gamma}) \times \underline{r}$ will now dominate the $\underline{\dot{\omega}} \times \underline{r}$ term, and the appropriate approximate equations are

$$\gamma \, \frac{\partial}{\partial \phi_1} \, \underline{w} \; + \; \underline{w} \cdot \nabla \underline{w} \; + \; 2\gamma \times \underline{w} \; + \nabla \pi \; - \; \nu \nabla^2 \underline{w} \; \approx \; (\underline{\omega} \times \underline{\gamma}) \times \, \underline{r} \; + \; \underline{F};$$

$$\nabla \cdot \underline{w} = 0 \, . \qquad (6)$$

Steady precession, which provides a steady Poincaré force, has been examined in some detail [1]. For values of the ratio of precession rate Ω to rotation rate ω ($\Omega/\omega = R_p$) and the Ekman number, $E = \nu/\omega L^2$, where ν, L denote kinematic viscosity and container length scale, small compared to unity, the first effect of precession is to tilt the apparent rotation axis by an amount $O's(R_p)$. For perfect spheres, and cylinders of certain specific aspect ratios, the tilt amplitude is $O's(R_p E^{-\frac{1}{2}})$.

At tilt amplitudes of a few parts in 100, time dependence appears. The nature of the time dependence depends on the container shape. Further increase in R_p leads to violent instability in both spheres and cylinders.

These laboratory examples are at best crude guides to what one might expect in space. No studies have been done for even a simple time-dependent situation, let alone the sort of pitching one might expect in an orbital situation. Such studies would be useful as better guides to space phenomena. Since the disturbances are apparent in a contained incompressible fluid, there is opportunity to study them on earth, where the conditions of relative acceleration can be controlled.

REFERENCES

[1] Busse, F. H.: J. Fluid Mech. 33:739 (1968); Gans, R. F.: J. Fluid Mech. 41:865 (1970); Gans, R. F.: J. Fluid Mech. 45:111 (1971); Malkus, W. V. R.: J. Geophys. Res. 68:2871 (1963); Malkus, W. V. R.: Science, 160:259 (1968); Roberts, P. H., and Stewartson, K.: Proc. Camb. Phil. Soc. 21:279 (1965); Stewartson, K., and Roberts, P. H.: J. Fluid Mech. 17:1 (1963).
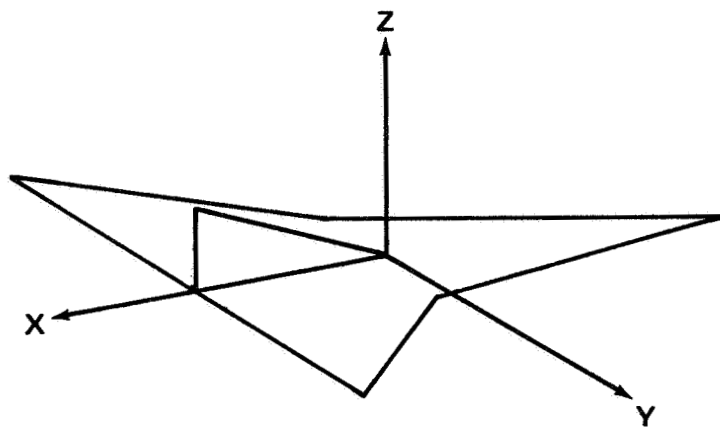
FIGURE 1. CARTOON OF SPACECRAFT SHOWING
SPACECRAFT COORDINATES.

FIGURE 2. ORBITAL MODES.
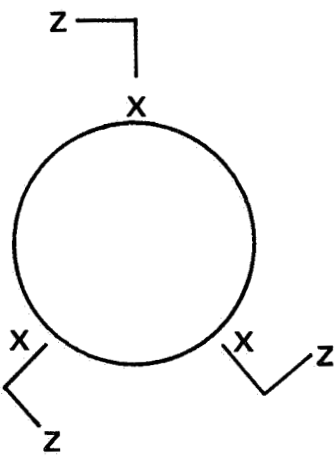
2a. GRAVITY GRADIENT
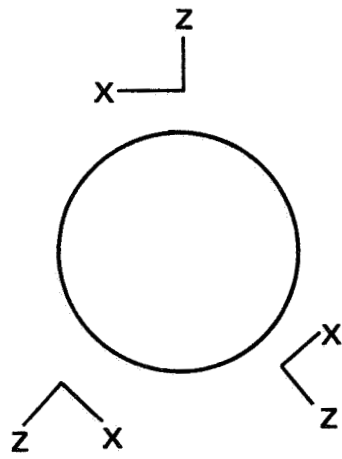
2b. Z—LOCAL VERTICAL
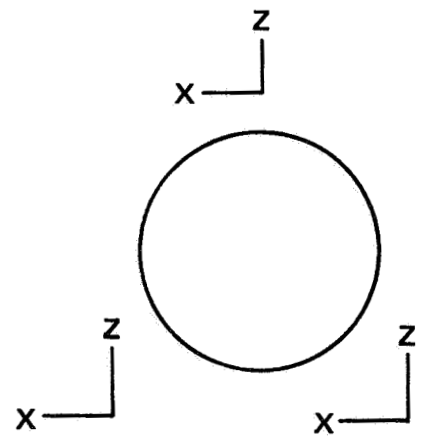
2c. INERTIAL HOLD

FIGURE 3.   PARAMETER SPACE FOR PERFECT 2a AND 2b ORBITS WITH L = .3m AND
Ω^{-1}=90 MIN. COMPETING ACCELERATION TERMS ARE: (1) OSCILLATORY, $\underline{v}$;
(2) INERTIAL, $\underline{v} \cdot \nabla \underline{v}$ AND (3) ROTATIONAL (CORIOLIS), $2\underline{\Omega} \times \underline{v}$. EACH
BALANCES PRESSURE AND VISCOUS FORCES IN ITS LABELLED REGION.
FOR "LARGE" ν THE VISCOUS TERM LEADS TO A STOKES–LIKE FLOW;
FOR "SMALL" ν A BOUNDARY LAYER FLOW WILL OCCUR. THE CRITICAL
VALUE FOR EACH REGION IS GIVEN. IN THE ROTATIONAL REGION νCRIT
= 4×10^{-5} cm^2/sec AND ALL FLOWS WILL BE STOKES–LIKE.

U, mm/sec   U, mm/sec

1.0

0.5

INERTIAL
$\nu_{CRIT} \propto UL$

OSCILLATORY
$\nu_{CRIT} \propto L^2 T^{-1}$

ROTATIONAL
$\nu_{CRIT} \propto \Omega^2 L$

500

1000

T, sec
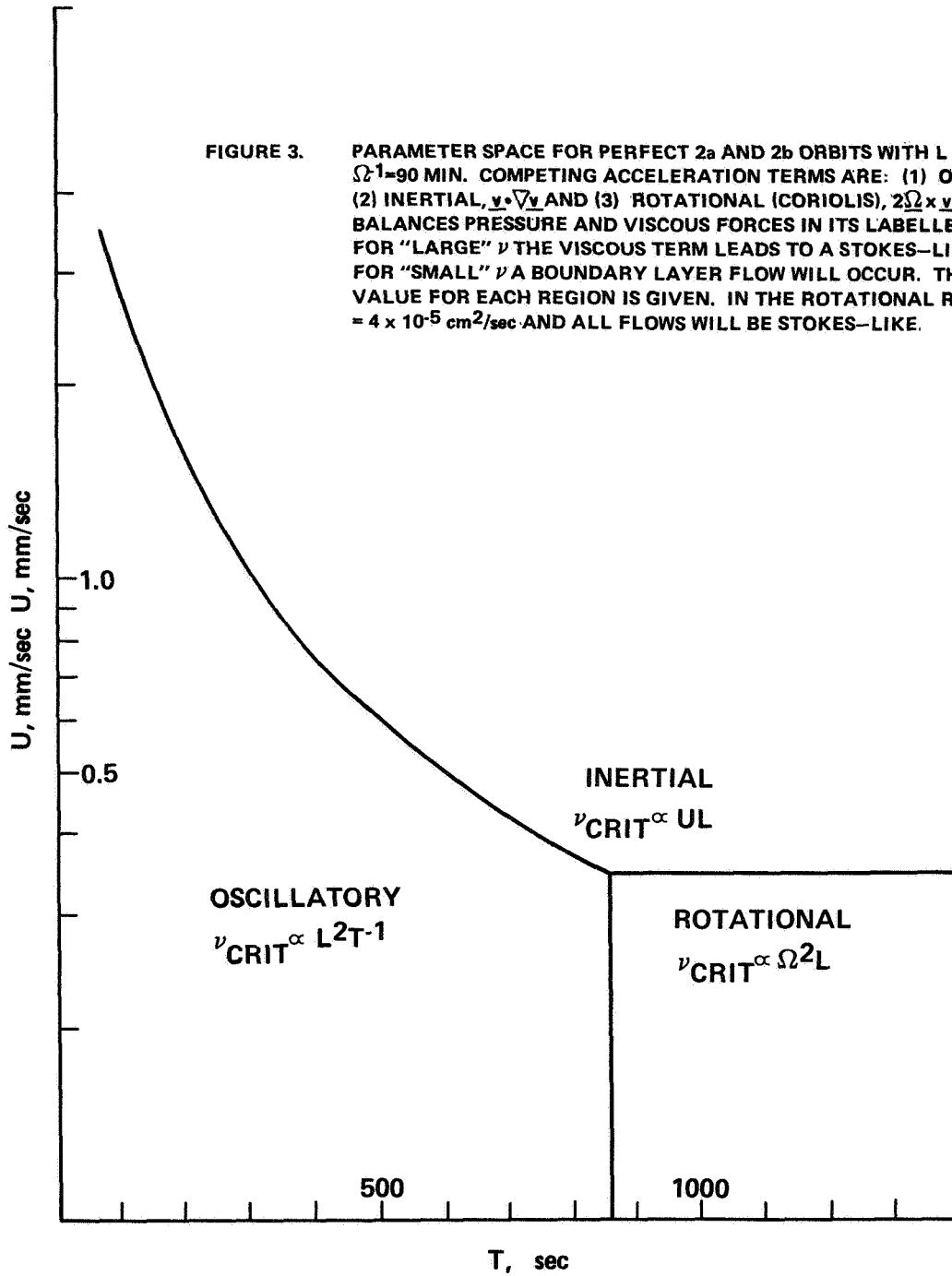
TRANSIENT THERMAL CONVECTION IN MICROGRAVITY

by
Robert F. Dressler
Materials Processing in Space Division
NASA Headquarters
Washington, D. C.

ABSTRACT

The unsteady two-dimensional thermal convection in a
cylinder due to a transient acceleration is first solved for
a step-function excitation. From this, the solution is then
obtained for an arbitrary time-dependent acceleration. The
solutions are valid for sufficiently low Rayleigh numbers
and, therefore, relevant to microgravity fields. As an
example, two graphs are presented for the convection result-
ing from the movement of an astronaut inside the Shuttle.
One graph is for a low value of a^2/ν, the other for an upper
value, where a is the diameter and ν the viscosity. An
approximate solution is then obtained for the three-
dimensional unsteady convection in the interior of a cube,
valid when the Grashof number is sufficiently small. This,
therefore, gives approximate flow velocities for an arbitrary
three-dimensional orientation of the acceleration vector
relative to the hot and cold faces of the cube. The analysis
can also be applied to obtain any other convective flows such
as those caused by g-jitter or variable rotation of the
Shuttle.

The Materials Processing in Space program is using the
weightless environment of space for studies that will require
a fundamental understanding of the response of fluids to
various types of inertial acceleration excitations. Most of
these processes have associated temperature and concentration
gradients (i.e., density gradients) which are necessary to
control the processes. A better understanding of these fluid
effects will assist not only materials processing, but also
help us to specify in advance the g-level constraints which
the program needs to impose on the space mission.

The unsteady two-dimensional thermal convection in a
cylinder with a linear transverse temperature gradient is
first solved for a step-function acceleration based upon the
Navier-Stokes equations. From this basic solution, the
transient flow can then be obtained for an arbitrary time-

dependent acceleration. The solutions are valid for a suffi-
ciently low Rayleigh number, and therefore are relevant to
microgravity fields important to the behavior of fluids in
space.

Figure 1 illustrates the replacement of the convection
model for a square cross-section by a cylinder, with little
error for the maximum velocity, because the maximum velocity
in both cases occurs far from the outer wall. Our basic
step-function solution approaches a steady-state flow for
large time which is identical with the steady solution
obtained by Weinbaum [1] for a cylinder, and almost identical
with the steady solution obtained by Batchelor [2] for a
square cross-section. Our step-function transient is
expressed in terms of the Bessel functions J_0, J_1, J_2, and
J_3.

Figure 2 shows for our step-function transient solution
the velocity distribution (in dimensionless form) versus the
cylinder radius for various values of time. The limiting
profile for infinite time is the steady solution identical
with the Weinbaum [1] steady solution. The figure shows the
effect of the boundary layer moving inward through the flow
with increasing time.

In all the following examples, the direction of the
acceleration vector has been chosen to produce maximum two-
dimensional convection. Figure 3 illustrates an application
of our general analysis to the specific example of a 200 lb
astronaut moving across the Shuttle by pushing against one
wall to start, and braking against the opposite wall to stop.
The $v^B(r,t)$ is our basic step-function solution, and this
inertial problem is solved by the appropriate linear combi-
nation of the basic solution with various phase lags.

All velocities in our solutions are directly propor-
tional to the magnitude of the imposed acceleration and to
the percentage density variation across the cylinder. They
are more complicated functions of the basic parameter a^2/ν,
where a is the cylinder radius and ν is the viscosity.

Figure 4 shows the maximum velocity, which is approxi-
mately located at $r/a = 0.6$ resulting from the astronaut
motion, for two extreme values of a^2/ν at 2500 and at 100,
for water. The former case has a = 5 cm with a half-life for
decay of 170 seconds. The latter case for a = 1 cm has a
half-life of 7 seconds. In order to show specific values, we
have taken a 4% density variation here. θ is the angle
through which a particle rotates in its circular path. In
both cases of a^2/ν, peak velocities are the same at
12 microns/sec, but θ approaches a final value of 0.06° for

the large cylinder. It peaks at 0.28° for the small cylinder, then returns to a smaller value for large t. These quantitative results suggest that the astronaut motion in some cases may not significantly interfere with fluid-crystal experiments in Spacelab.

By contrast, Figure 5 shows peak velocity and angular displacement of the fluid when the Shuttle makes a 90° roll by firing its main thrusters initially for 0.7 seconds, rolling about 90 seconds at 1°/sec, then firing reverse thrusters to stop the roll. The same extreme values of a^2/ν are used, with the same 4% density variation, and assuming the fluid cell to be located one meter from the axis of rotation of the Shuttle. The upper two graphs give peak velocities and the corresponding displacements due to the centrifugal force. For the large a^2/ν, the velocity peaks at 0.17 mm/sec, and in both cases θ reaches a large final value. The velocity for the small a^2/ν has attained almost the steady-state value after the first 20 seconds.

The bottom two graphs show the effect of angular acceleration. Here the excitation consists of two short pulses, but having a much larger magnitude than the centrifugal acceleration. The peak velocities are high at 0.12 mm/sec, and the peak θ values are also high, although θ decreases after 90 seconds to small final values.

These velocities and displacements are all sufficiently large to suggest that a roll-maneuver should not be made during fluid-crystal experiments in Spacelab.

When the direction of the acceleration vector is arbitrary, a three-dimensional motion will in general be produced. Figure 6 shows the acceleration vector resolved into three components. The (0) component will produce no convection unless the critical Rayleigh number is exceeded, and only for strict alignment of density gradients and acceleration, which are unlikely for microgravity excitations. Components (1) and (2) would each separately produce a two-dimensional convection as shown. If the velocity vector fields for these two motions are added together, the sum will not satisfy the nonlinear Navier-Stokes equations because of the cross-product terms in the acceleration. However, if these quadratic terms are small relative to the other terms, the superposition can be considered as an approximate solution. Figure 6 illustrates the symmetric case where the (1) and (2) acceleration components are equal. Calculations of errors around a closed trajectory show that the approximate three-dimensional flow should be accurate when the Grashof number is sufficiently small, as indicated.

Both Batchelor [2] and Weinbaum [1] give upper bounds of about 2000 on the Rayleigh number for which their steady solutions should be accurate. In most of our transient solutions, the velocities are very much lower (usually only a few percent, e.g., for the astronaut-motion example, only 6% for $a^2/\nu = 100$ and 0.25% for $a^2/\nu = 2500$) than the corresponding steady flow; therefore, the range of Rayleigh number for validity can usually be greatly increased. An analogous increase should also be possible for the Grashof number since this was calculated for steady flows.

REFERENCES

1. Weinbaum, S.: J. Fluid Mech. 18:409-437 (1964).

2. Batchelor, G. K.: Quarterly Appl. Math, 12:209 (1954).

TRANSIENT THERMAL CONVECTION

COLD · HOT · MAX. V · ϵ g

HOT · a · v · ϵ g

2–D STEADY FLOW
4 P.D.E. 'S

MASS
MOM Ω
MOM θ
ENERGY
} NAVIER–STOKES

STEADY SOLUTION ONLY

[BATCHELOR 1954
[WEINBAUM 1964
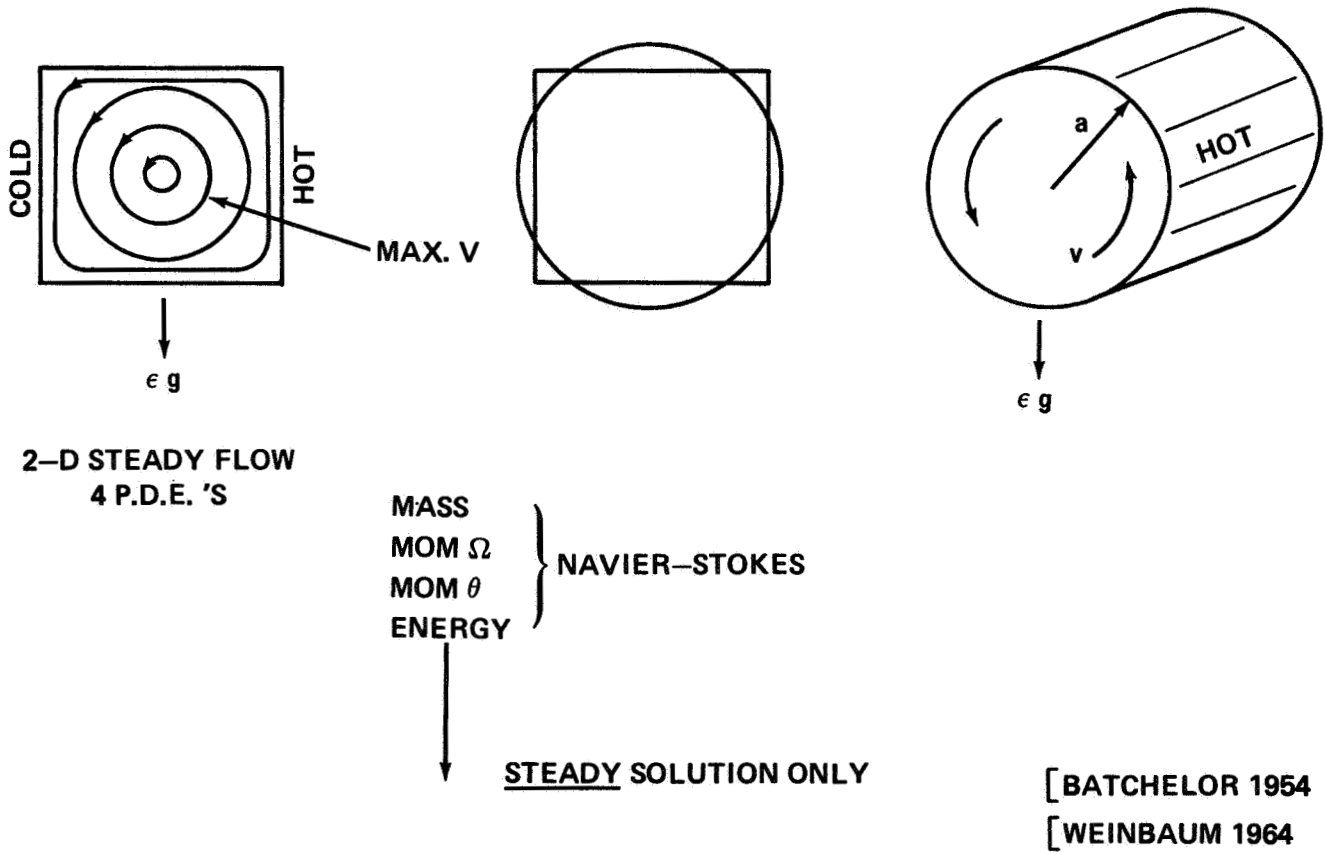
FIGURE 1

CONVECTIVE VELOCITY FOR
STEP—FUNCTION
ACCELERATION
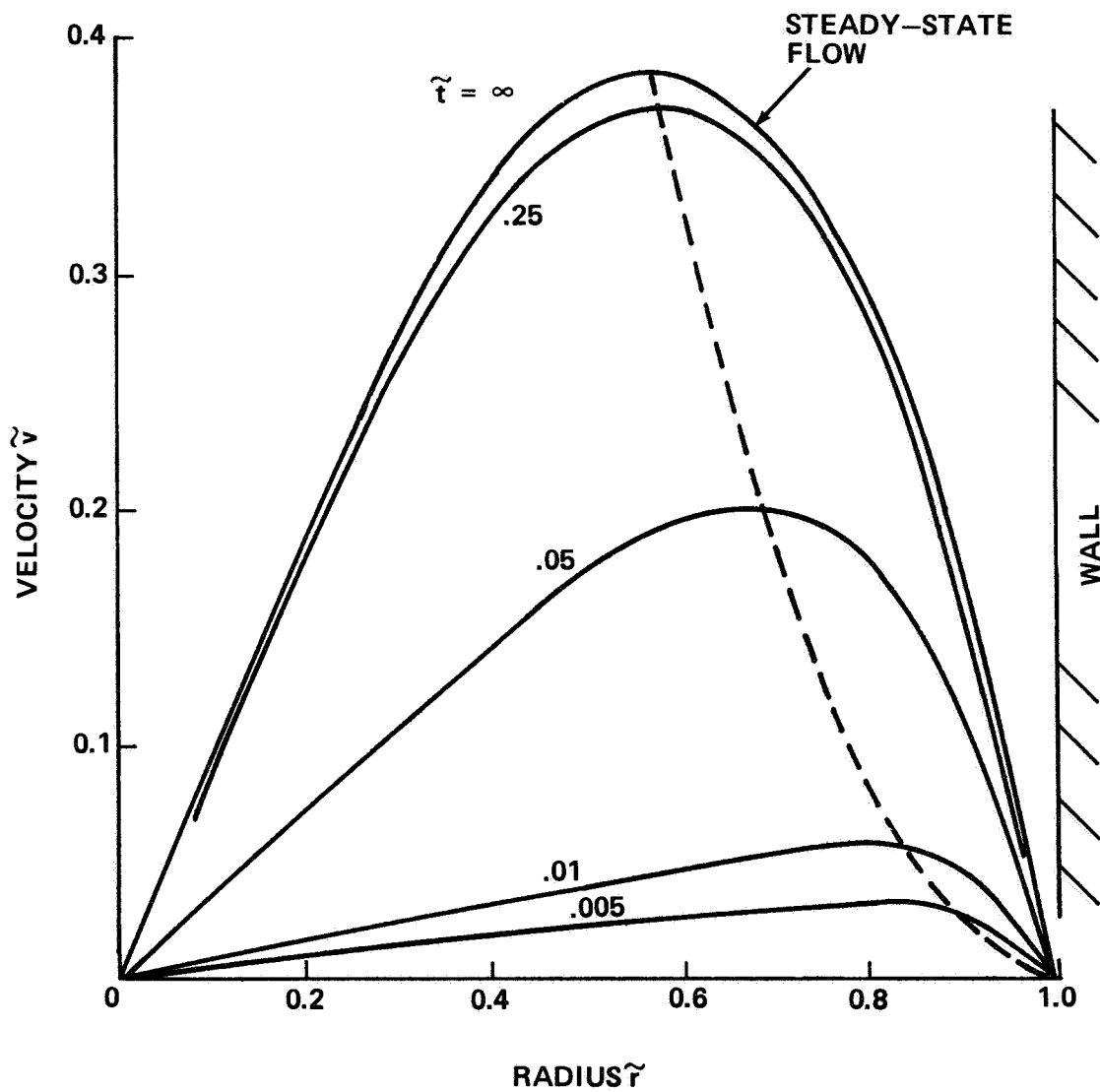
FIGURE 2

EXAMPLE: ASTRONAUT MOVES IN SHUTTLE

$$v(r,t) = \sum_{1}^{4} c_i v_i^B(r, t - \tau_i)$$

FIGURE 3

4% Δρ

WATER

$\frac{r}{a} = .6$

v = 12μ/SEC

θ NO BRAKE

θ = .06°

LARGE $a^2/\nu = \dfrac{5^2}{.01} = 2500$
D = 10 CM
t½ = 170 SECS

t SECS.

5

v = 12 μ/SEC

θ = .28°

SMALL $a^2/\nu = \dfrac{1^2}{.01} = 100$
D = 2 CM
t ½ = 7 SECS

10

20 t SECS

v = −3 μ/SEC
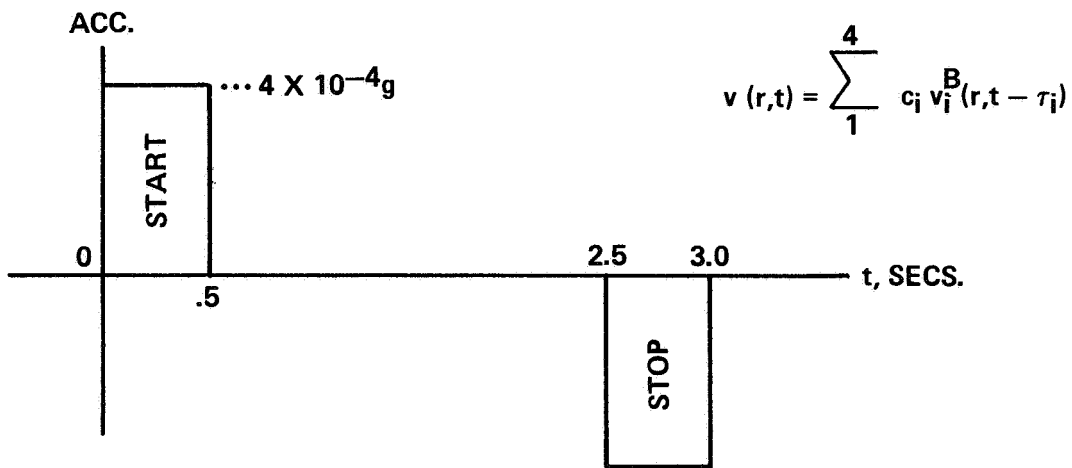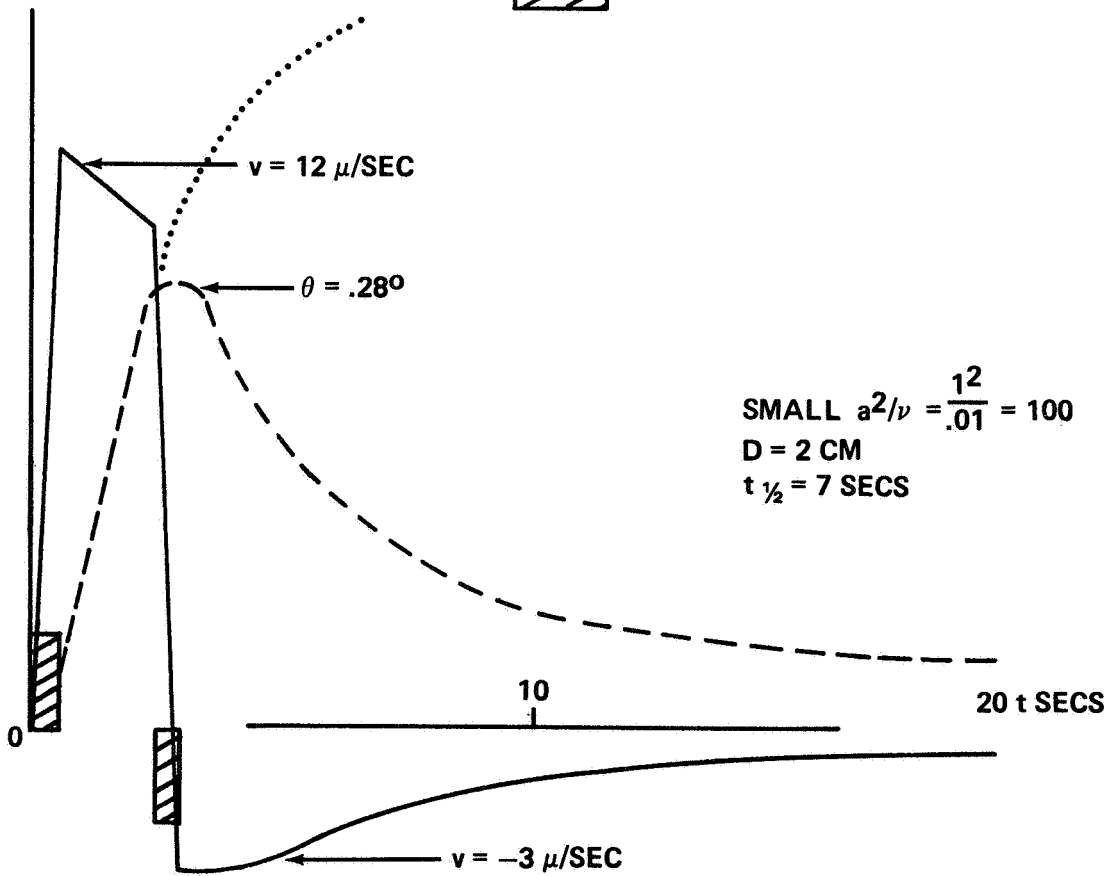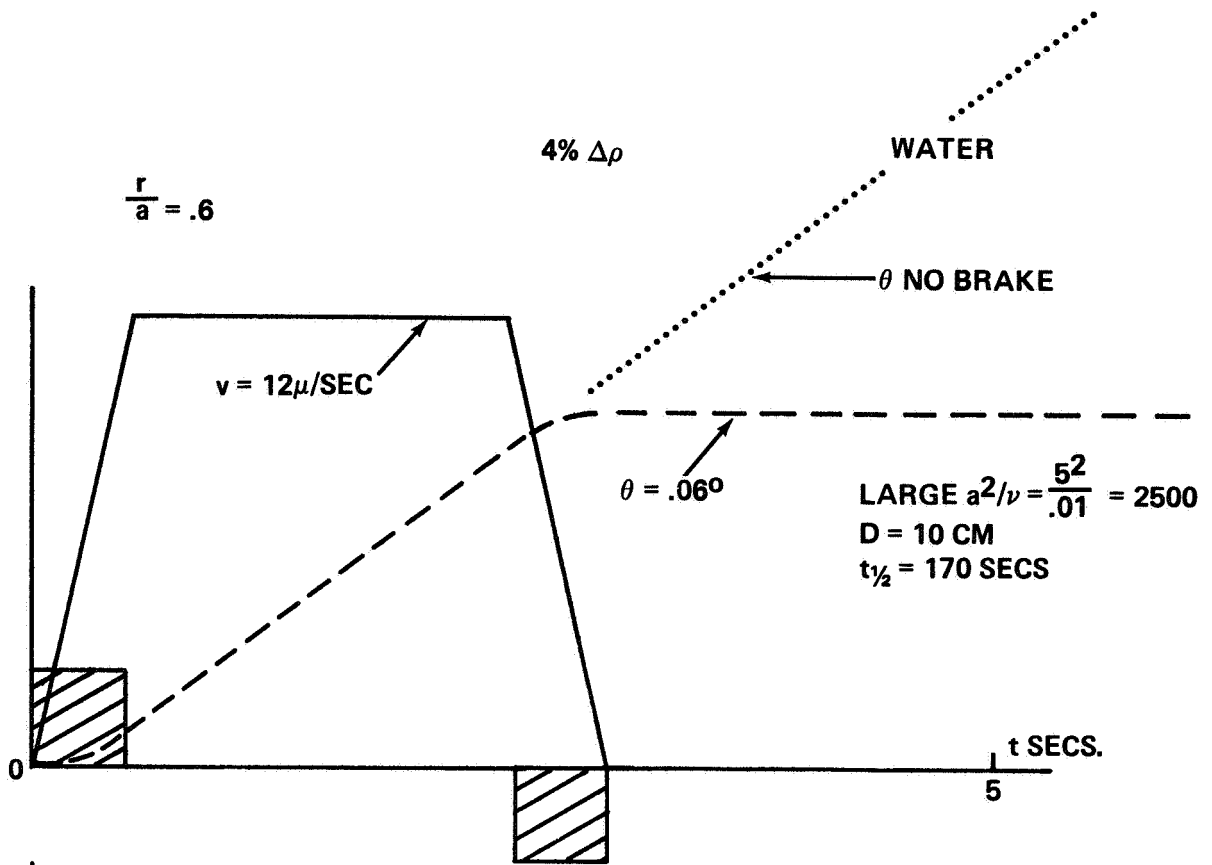
MAX. VELOCITY AND ROTATIONAL DISPLACEMENT θ
FOR ASTRONAUT MOTION
FIGURE 4

110

TRANSIENT THERMAL CONVECTION

$$\dot{\omega} = 1.4^{\circ}/\text{sec}^2$$

90° ROLL $\omega = 1^{\circ}/\text{sec}$
$a = 5$ cm $a^2/\nu = 2500$
$t_{1/2} = 170$ sec

$r = 1$m   4% $\Delta\rho$
$a = 1$ cm, $a^2/\nu = 100$
$t_{1/2} = 7$ sec

$\boxed{\omega \times \omega \times r}$

acc.

$\downarrow 3 \times 10^{-5}g$

0.7   90.   SEC

ν
θ .17 mm/sec

θ

13°

90   SEC

ν
θ

.014 mm/sec

10°

θ

90   SEC

$\boxed{\dot{\omega} \times r}$

acc.

$2.3 \times 10^{-3}g$

90
0.7   SEC

ν
θ .12 mm/sec

14°

θ

0.7   90   SEC

ν
θ .12 mm/sec

θ

6°

90

0.7   SEC

FIGURE 5

111

APPROX. 3-D FLOW SOLUTION

$$\bar{\nu}_{3D} \doteq \bar{\nu}_1 + \bar{\nu}_2$$

ACCURACY IN N–S EQUATIONS:

$$\text{AVER.} \left| \text{ERROR} \right| \leqslant 15\%$$
$$\text{WHEN}$$

$$\therefore \left| \nu_{3D} \right| \leqslant \sqrt{2} \left| \nu_{1,2} \right|$$

$$N_{GR} = \frac{Eg \; \frac{\Delta\rho}{\rho} \; a^3}{\nu^2} < 280$$

FIGURE 6

112
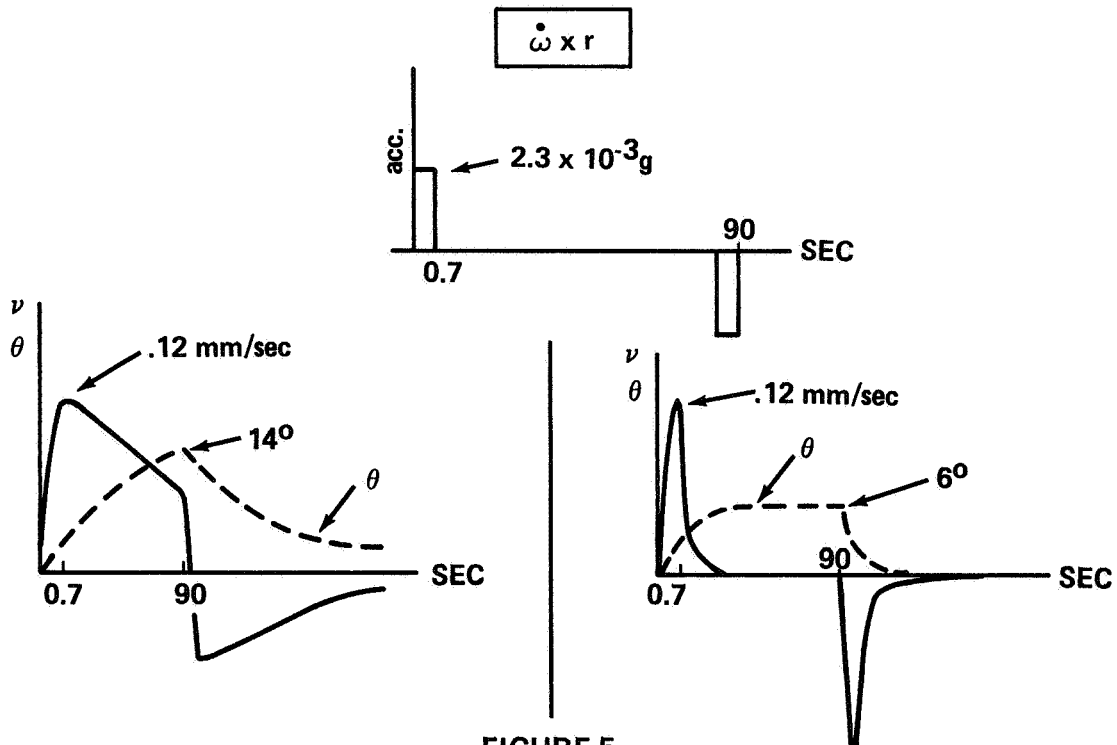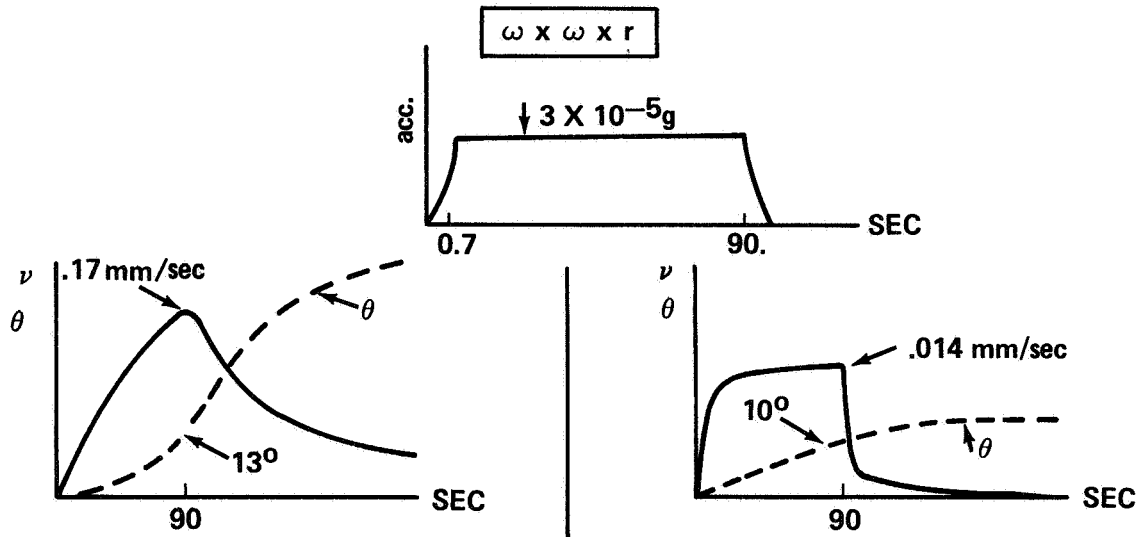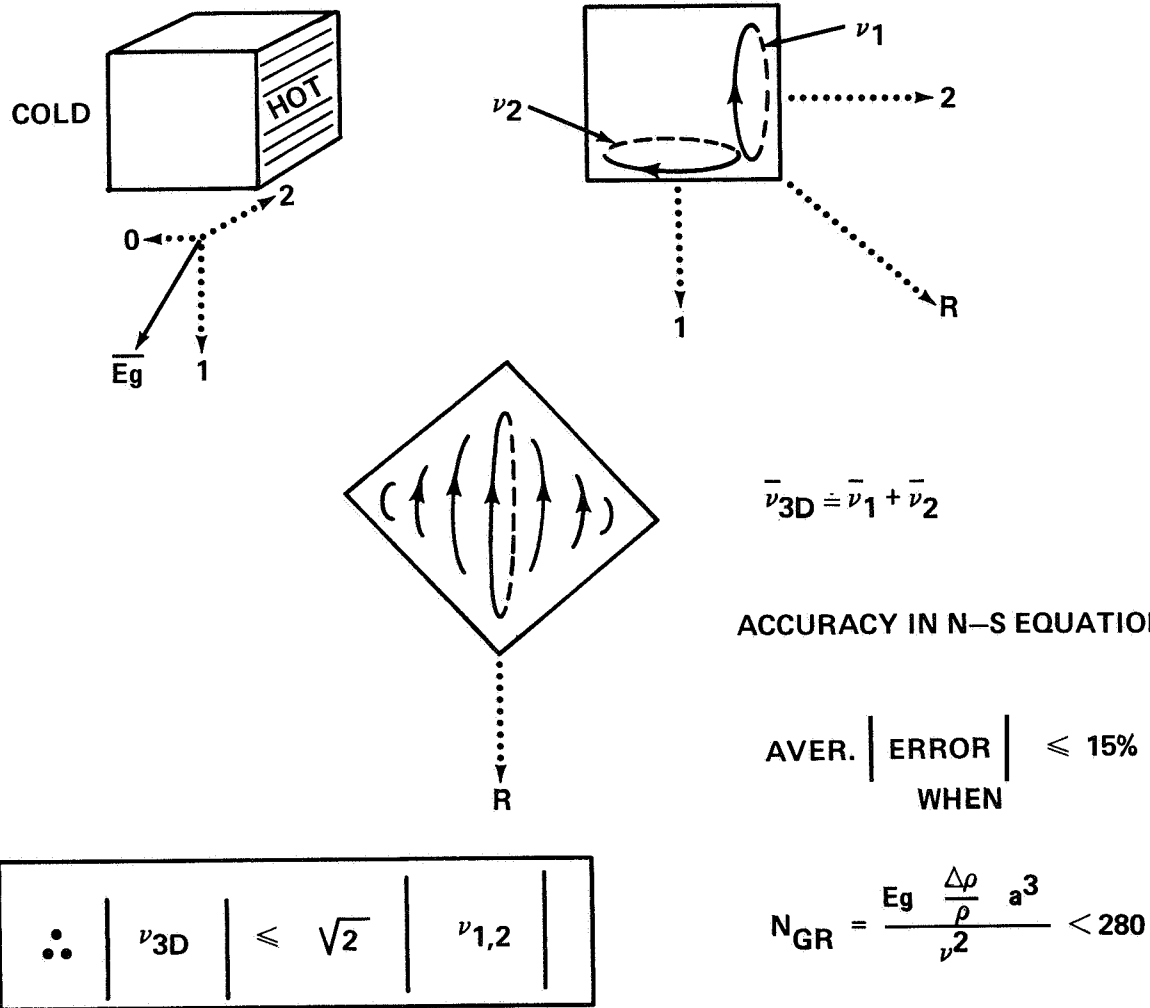
IV. SPACECRAFT DYNAMIC ENVIRONMENT

SPACECRAFT DYNAMIC ENVIRONMENTS

by
George H. Fichtl
NASA/George C. Marshall Spafe Flight Center

It is useful to present a brief summary of the dynamic
environment that is anticipated to occur during the Shuttle
Orbiter missions. The dynamic environment of planned Shuttle
missions has been examined in a relatively detailed manner
for the Spacelab Missions 1, 2, and 3. Accordingly, the
comments that follow relate to these missions, especially the
Spacelab 3 Mission since it is the first operational flight
of Spacelab and is a materials processing, low-gravity
emphasis mission. However, the ideas presented can be carried
over to other missions. Zero-gravity conditions in Earth
orbit cannot be obtained in the Shuttle Orbiter, at least on
the first three Spacelab missions. However, through careful
planning, the dynamic environment and its effects on experi-
ments can be minimized. Furthermore, although the dynamic
environment of the Shuttle Orbiter is to a large degree
stochastic, it is possible to predict characteristics of this
environment so that scientists and technologists can plan
their experiments and mission managers can plan missions with
a view toward minimizing the effects of spacecraft dynamics
on experiments. Characteristics of the dynamic environment
that might be predicted include typical and "worst case"
values of vehicle acceleration for the anticipated accelera-
tion sources, typical number of acceleration events, duration
times of discrete acceleration events, bandwidth of
acceleration time history, etc.

The dynamic environment that will occur during a Shuttle
Orbiter mission can range over many orders of magnitude (for
example, 10^{-7} g to 10^{-3} g on the Spacelab 3 Mission) and will
be characterized by a frequency bandwidth ranging from $1/T$
(T is the orbit period) to approximately 10 Hz for rigid body
accelerations, and from approximately 0.01 Hz to audio fre-
quencies for the accelerations associated with flexible body
dynamics, and vibration and acoustic sources. Extensive
information is available on the former relative to providing
scientists and technologists with information about space-
craft dynamics. This is especially true for Spacelab
Missions 1, 2, and 3. A unified summary of the latter in the
context of experiment planning and performance is not avail-
able. The discussion that follows is directed toward space-
craft dynamics as related to rigid body dynamics.

115

Table 1 provides a brief summary of the major sources of rigid body accelerations and associated values that are expected to occur during the Spacelab 3 Mission. The aerodynamic drag and gravity gradient forces create a quasi-steady acceleration with characteristic time scale on the order of the orbit period. Superimposed on this quasi-steady acceleration environment are short-period disturbances with time scales on the order of a few seconds or less. The most important of these disturbances are the accelerations associated with the vernier control system thrusters and crew activity. Water dumps, flash evaporators, and venting of experiment gases and liquids will create accelerations in the 10^{-7} g to 10^{-6} g range and thus are small (although not necessarily unimportant) compared to the accelerations created by the vernier control system and crew activity. The accelerations associated with crew motions were predicted from force measurement data acquired from the Skylab missions [1]. Crew activity has acceleration levels with bandwidth ranging from approximately 0.3 Hz to about 2 Hz.

Vernier control system thrusters are used to maintain Orbiter attitude. The duration of a vernier control system thruster firing event ranges from 0.08 sec upwards to 0.5 sec and depends on the attitude deadband setting. Typically the larger the selected attitude deadband, the larger the vernier control system thruster firing event time. Thus, at the minimum attitude deadband of 0.10 the typical vernier control system thruster firing time is 0.08 sec. As the attitude deadband is increased, the thruster event firing time will increase. The thruster firing rate depends on the vehicle attitude and the attitude deadband setting. For a given attitude deadband setting, the minimum number of thruster firings will occur for the gravity gradient flight mode. To minimize the thruster firing rate on the Spacelab 3 Mission, a gravity gradient flight mode will be used with the Orbiter tail toward the Earth with the wings essentially in the orbit plane. On the Spacelab 3 Mission, attitude deadband setting will be determined by pallet experiment pointing requirements and fluid flow effects that result from spacecraft accelerations associated with thruster firings. Spacelab 3 Mission flight simulations, wherein the effects of random crew motion are included, predict 25 to 80 thruster firings per orbit for a 1° deadband and 90 to 350 firings per orbit for a 0.1° deadband, depending on the crew activity level, so that deadband setting can have a pronounced effect on vernier thruster firing rate. The associated number of vernier thruster firings per orbit to maintain an inertially fixed attitude will be significantly larger than those noted above.

The number of acceleration disturbances per orbit associated with crew motion is at least a factor of ten greater than that associated with the vernier thruster firings. However, the spacecraft accelerations associated with crew motions do not on average (in time) impart net momentum to the fluids, while thruster firings do impart momentum on average. The former is a result of conservation of momentum. The reason for the latter situation results from the thruster geometry depicted in Figure 1. When the vernier thrusters are fired to produce roll, pitch, and yaw motions, both a net torque and a net force occur. The net torques can average to zero over a sufficiently long period of time, while the net forces associated with thruster firings to induce roll and pitch modes of motion will not average to zero no matter how long the averaging period. This is a direct result of the fact that vernier thruster firings associated with pitch and roll motions always result in a rectilinear acceleration vector directed out of the Shuttle Orbiter bay. Net thruster forces associated with yaw motions will average to zero when averaged over a sufficiently long period of time.

As noted above, additional accelerations can occur as a result of vibrations and acoustic fields resulting from the operation of machinery, etc. A prediction of these environments has of yet not been made. However, current constraints on acoustic and vibration levels require that the Spacelab 3 Mission experiment developers design equipment so that acoustic and vibration levels of experimental apparatus do not exceed the specified levels in the Spacelab Payload Accommodation Handbook [2].

The Spacelab 3 Mission timeline has been planned so as to exclude major vehicle maneuvers. The technical motivation for this constraint on maneuvers results from the pronounced fluid flows that can occur in a contained fluid when the container walls suddenly undergo a change in rotation. If the Orbiter is set into rotation impulsively with angular radian rotation rate $\Delta\Omega$, then a fluid in a container of characteristic size r will experience a flow adjacent to the container walls with typical initial velocity $r\Delta\Omega$. This wall boundary flow will be transmitted into the interior fluid via viscous diffusion of vorticity and Ekman boundary layer effects. For a major maneuver with $\Delta\Omega = 2\pi/120$ rad sec^{-1} and a fluid container with r = 10 cm the initial flow adjacent to the container wall, for an impulsive initiation of the maneuver, is approximately 0.3 cm sec^{-1}.

The requirement for constraining the Orbiter attitude to one in which the wings are essentially in the orbit plane arises from the requirement to preclude the occurrence of precessional modes of fluid motion in the spherical

convection experiments in the Geophysical Fluid Flow Cell (GFFC) [3] as a result of precession of the GFFC angular velocity vector about the orbit angular velocity vector. Constraining the attitude of the Shuttle Orbiter so the wings remain in the orbit plane results in the GFFC angular velocity vector being parallel to the orbit angular velocity vector. This precludes the occurrence of precessional fluid motions in the GFFC.

REFERENCES

1. Conway, Bruce, A., and Hendricks, T. C.: Summary of Skylab Crew/Vehicle Disturbance Experiment T-013, NASA TN-D8128, March 1976.

2. Spacelab Payload Accommodation Handbook, SLP/2104, National Aeronautics and Space Administration and European Space Agency, June 30, 1977.

3. Hart, John E.: Studies of Earth Simulation Experiments, NASA CR-2753, October 1976.
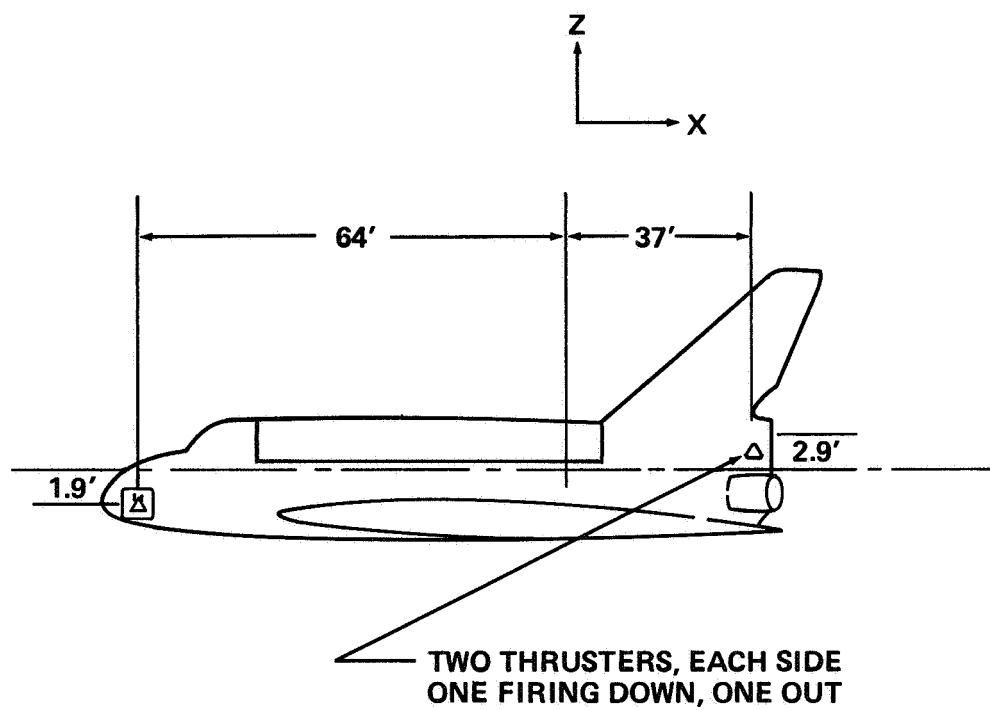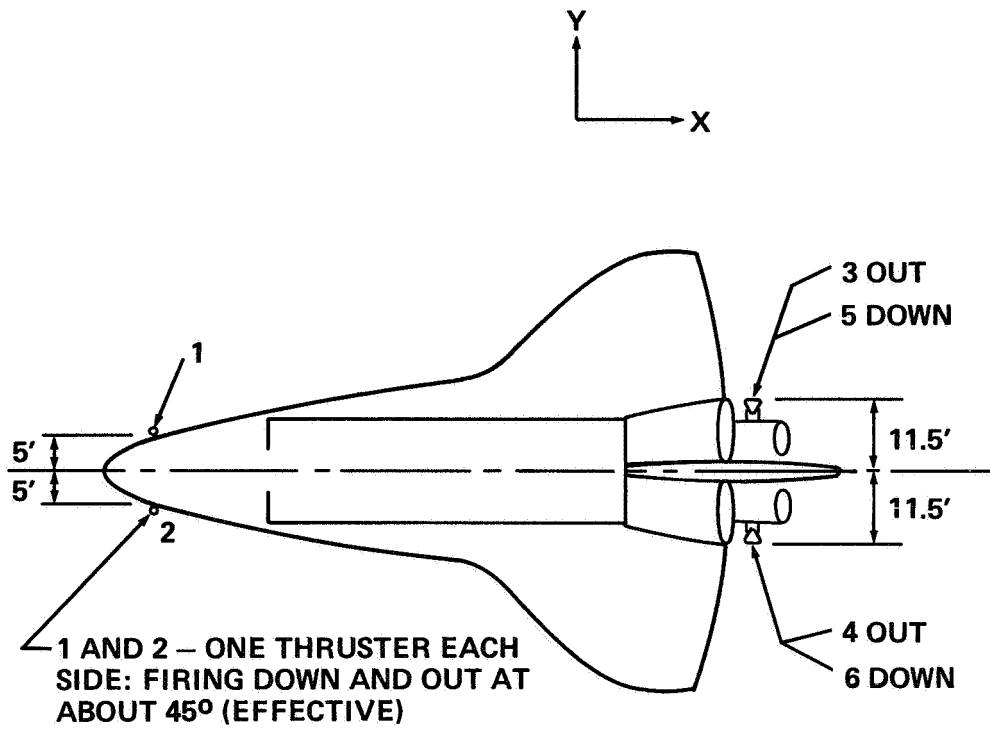
FIGURE 1. VERNIER CONTROL SYSTEM THRUSTER LOCATIONS ON THE SHUTTLE ORBITER

TABLE 1

ACCELERATION G-LEVELS AND SOURCES*

Source	Disturbance Level	Comments
Aerodynamic Drag	$10^{-9}g - 10^{-8}g$	Quasi-steady
Gravity Gradient Force	$10^{-7}g - 10^{-6}g$	
Left, Right Flash Evaporators	$2 \times 10^{-6}g$	Dirac Delta Function-like Disturbances
Both Flash Evaporators	$1 \times 10^{-7}g$	
Water Dump	$4 \times 10^{-6}g$	
Vernier Thrusters	$5 \times 10^{-5}g - 5 \times 10^{-4}g$	
Crew Motion (nominal)	$10^{-4}g$	Frequency Bandwidth 0.3 to 2 Hz
Crew Motion (vigorous)	$10^{-3}g$	

*The values in this table are appropriate for Spacelab 3 Mission.

ORBITAL ENVIRONMENT DYNAMICS

by
Robert E. Smith
NASA/George C. Marshall Space Flight Center

Very little was known about the upper atmosphere prior to the advent of satellites. During the tracking of the earlier satellites, it was found that the upper atmosphere was not static but had several variations. Figure 1 shows that the atmosphere has a diurnal variation which also varies with height, from a factor of three at the lower altitudes to a factor of seven at the higher. Figure 2, which is a picture of the atmospheric density, shows that the maximum density occurs at about 1400 LST, while the minimum density occurs slightly before 0400 LST. This maximum density bulge follows the sun, so that it is about 2 hours behind the sun and at the same latitude; therefore, if the maximum density is in the northern hemisphere, then the minimum nighttime density would be in the southern hemisphere. In the real atmosphere the ratio of the daytime maximum to the nighttime minimum density is somewhat a function of solar activity, but the atmospheric models, for simplicity, used a constant 20% difference between the two values. In the models the constituents are assumed to be in diffusive equilibrium above about 100 km and all mass densities have been tied to temperature, so that when the temperature at any altitude is known, then there is one density associated with that temperature, no matter where it occurs on the globe. The temperature and density also are dependent upon the level of solar activity and sunspot cycles. Figure 3 shows that the temperature of the exosphere varies from around 600°K to on the order of 2,000°K. In the models all temperatures and densities go to a single value around 90 to 100 km. At orbital altitudes the models are fairly representative of the real atmosphere; however, below 180 km, care should be taken in their use because the models aren't very representative of the real atmosphere. Variations occur there that are not modeled very well because this is a region where there are not too many measurements. Single values of temperature, pressure, and density at 90 to 100 km are used and the models built up from those.

The upper atmosphere density also has radical changes associated with geomagnetic activity. Figure 4 shows that the higher the altitude, the more the effect of the geomagnetic disturbance. The a_p index is a measure of the magnetic activity of a solar storm. In the models the

response of the upper atmosphere to a magnetic disturbance, a density increase, is usually global; however, the atmosphere itself really responds with a large density increase in the auroral zone where the energy from the magnetic disturbance is dumped and then a series of waves propagates toward the equator. The time delay between a magnetic storm and the atmosphere response is very short at the auroral zones; however, it takes about 6-1/2 hours for the density waves to propagate to the equator. This effect is very short-lived, and a spacecraft sees it as a spike in density.

Figure 5 shows that at 600 km there is about two orders of magnitude difference in the density between high solar activity and sunspot minimum.

Some seasonal effects have been found, but they are very minor compared to the rest. Changes in atmospheric density were correlated with the 2,800 MHz, 10.7 cm, solar flux measured at Ottowa, Canada, and also with the geomagnetic activity index, although neither of these really affects the upper atmosphere. It is the ultraviolet solar radiation that does cause the observed changes. Figure 6 shows that these indicators are fairly representative of the EUV input and the temperature changes which have been observed.

Recent studies have shown different compositions than those portrayed by the older models, while the total mass densities have stayed the same. If the constituents of the upper atmosphere are important in your application the newer, models should be used.

122

DIURNAL DENSITY VARIATION

THE MAGNITUDE OF THE VARIATION IS INDICATED BY THE VALUES OF TYPICAL MAX TO MIN RATIOS NOTED UNDER EACH PEAK. THE PHASE IS INDEPENDENT OF ALTITUDE.
(AFTER JA CCHIA.)

Fig. 1

123
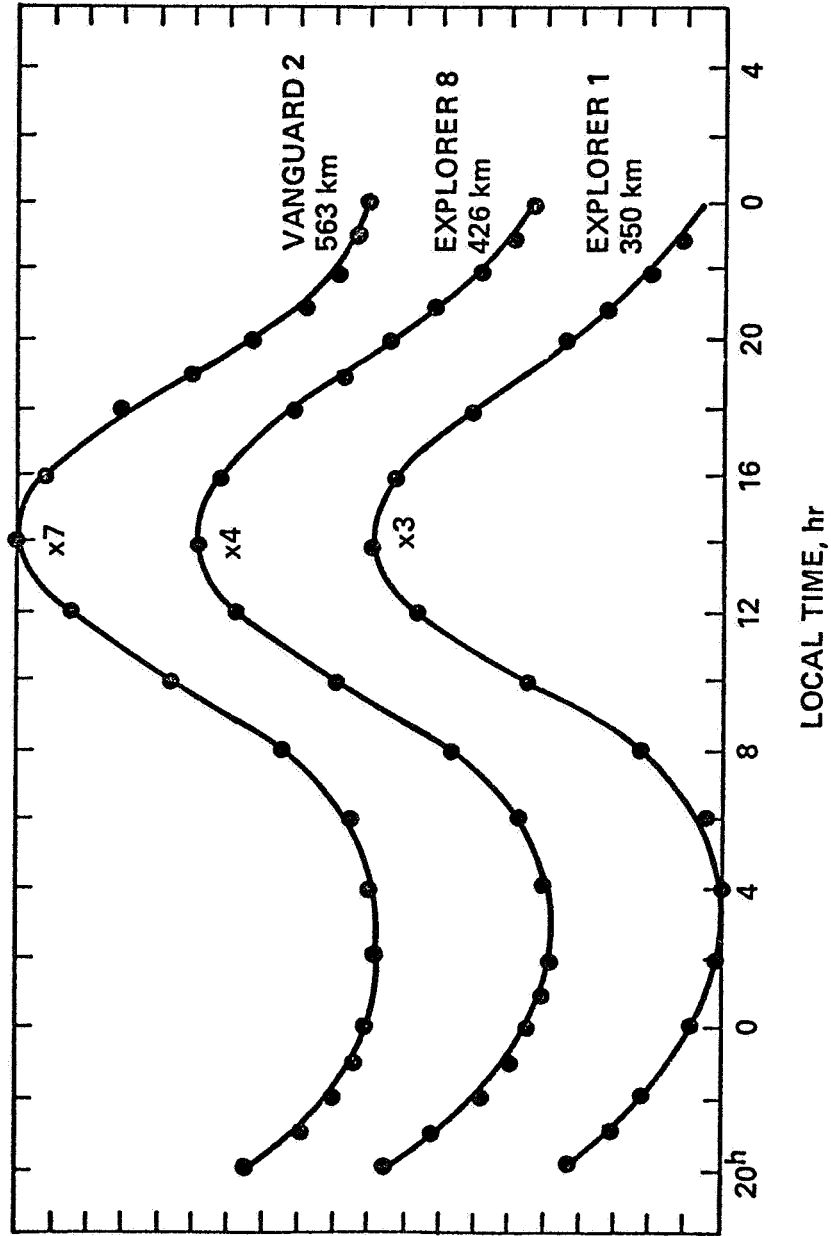
TEMPERATURE DISTRIBUTION ABOVE THE THERMOPAUSE WHEN $T_0 = 1000°$ K.

HOURS OF LOCAL TIME, COUNTED FROM MIDNIGHT, ARE MARKED ON THE EQUATOR.

(AITOFF'S EQUAL-AREA PROJECTION.)

Fig. 2

124
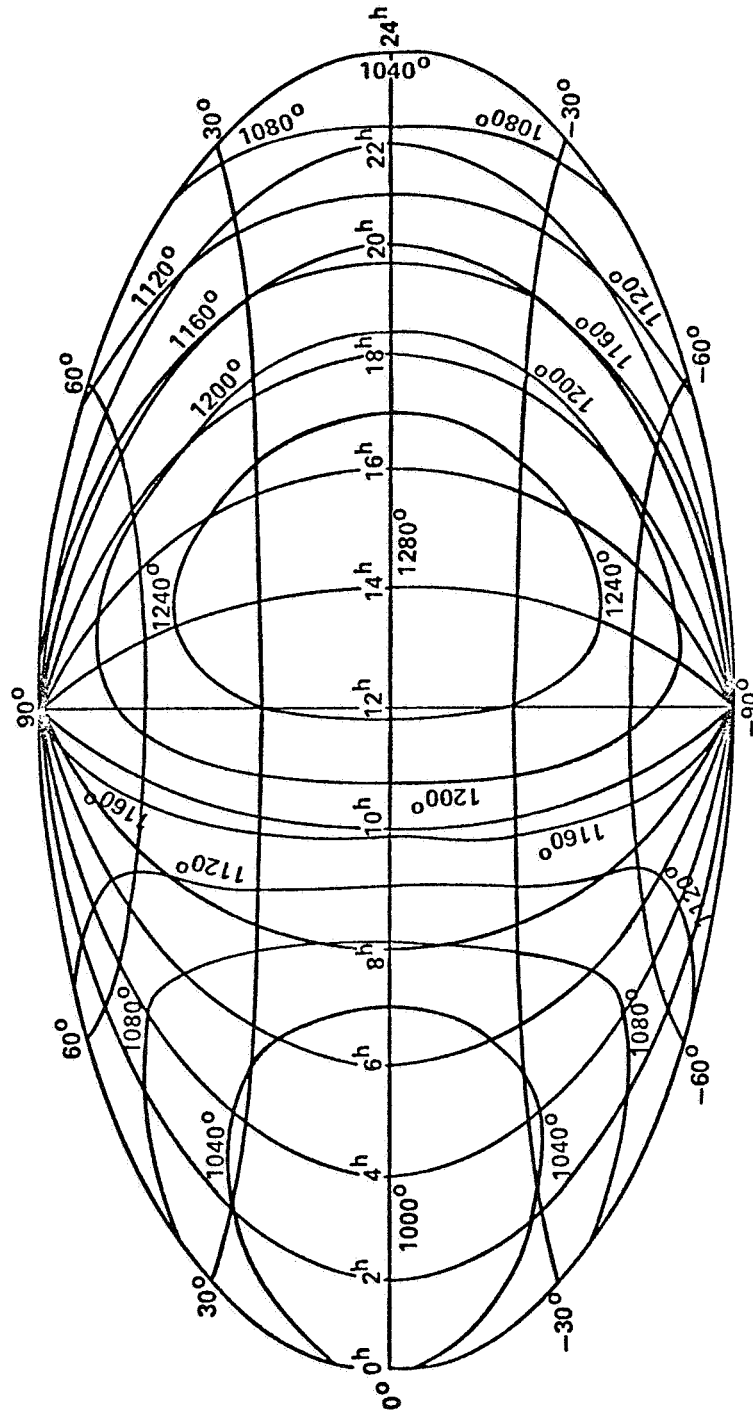
EXTREMES OF TEMPERATURE VARIATION OVER THE 11-YEAR SOLAR CYCLE
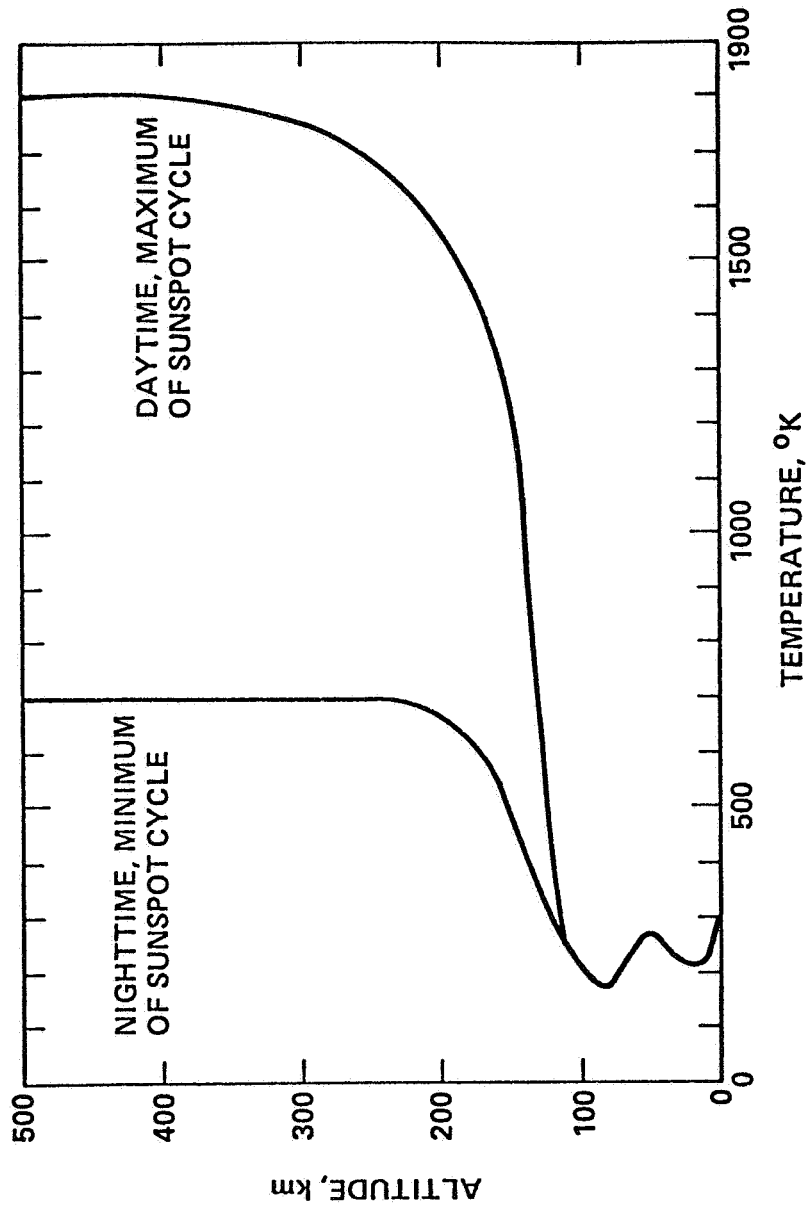
Fig. 3

ENHANCEMENT OF UPPER ATMOSPHERIC DENSITY DURING A GEOMAGNETIC STORM.
DATA DEDUCED FROM SIMULTANEOUS OBSERVATIONS OF DRAG ON THE INDICATED
SATELLITES. THE MAGNETIC INDEX ap IS A MEASURE OF THE MAGNETIC DISTURBANCE,
ZERO BEING QUIET TIMES AND 400 BEING A VERY INTENSE STORM. (AFTER JACCHIA.)

Fig. 4

126
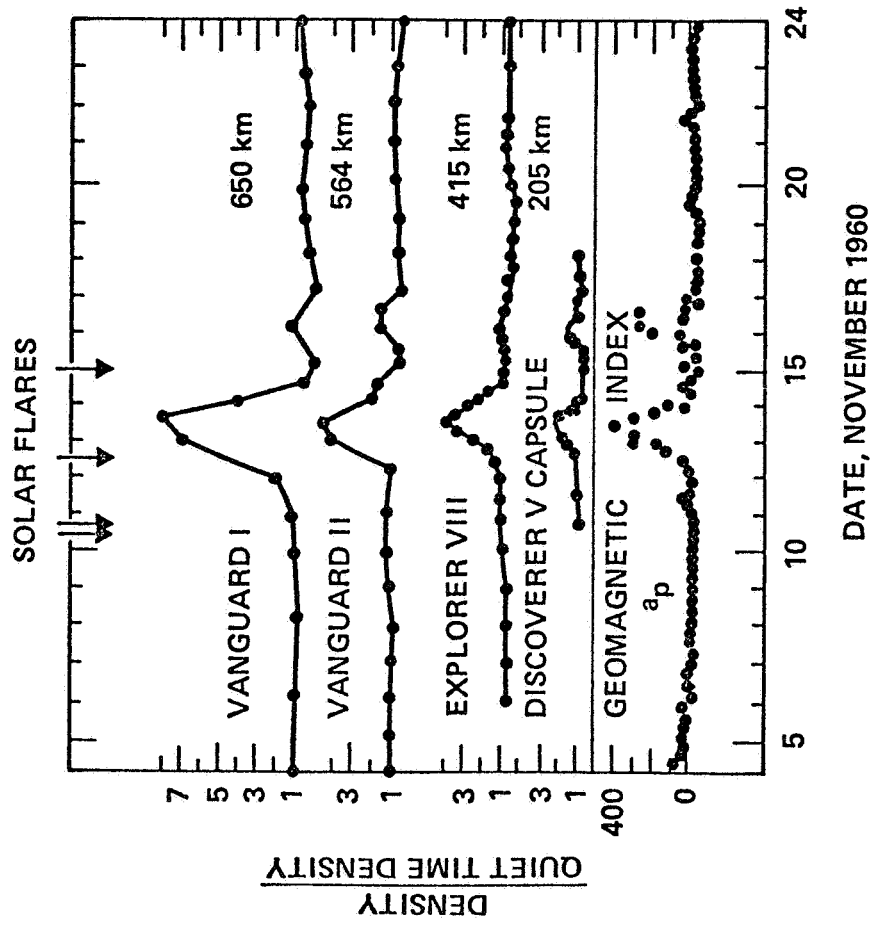
DAY AND NIGHT DENSITY PROFILES IN THE UPPER ATMOSPHERE AT SUNSPOT
MINIMUM AND AT A TIME OF EXCEPTIONALLY HIGH SOLAR ACTIVITY

Fig. 5

127
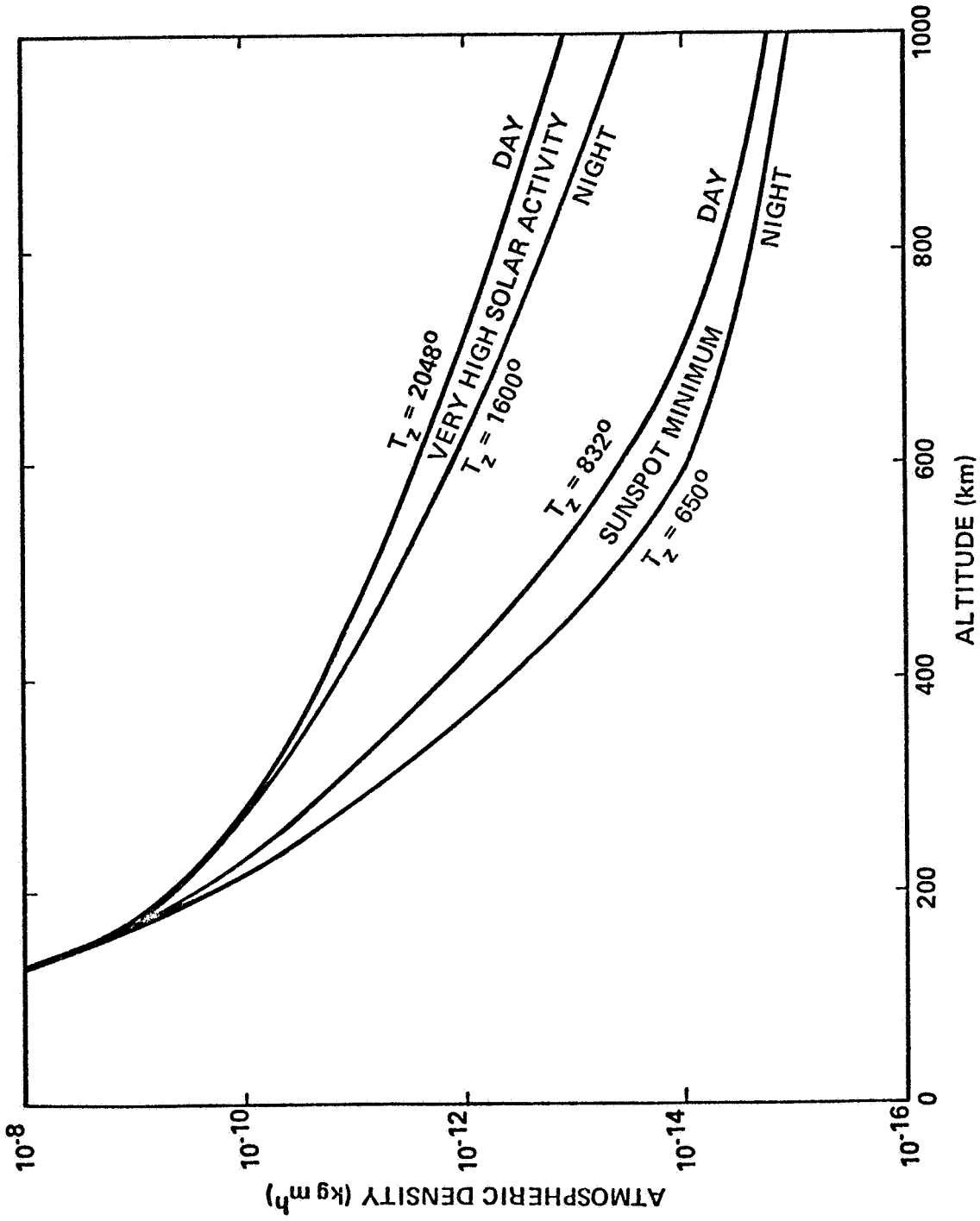
COMPARISON OF THE EUV FLUX WITH THE EXOSPHERIC TEMPERATURE, THE 2800 Mc/sec SOLAR FLUX. AND THE GEOMAGNETIC INDEX ΣK_p.
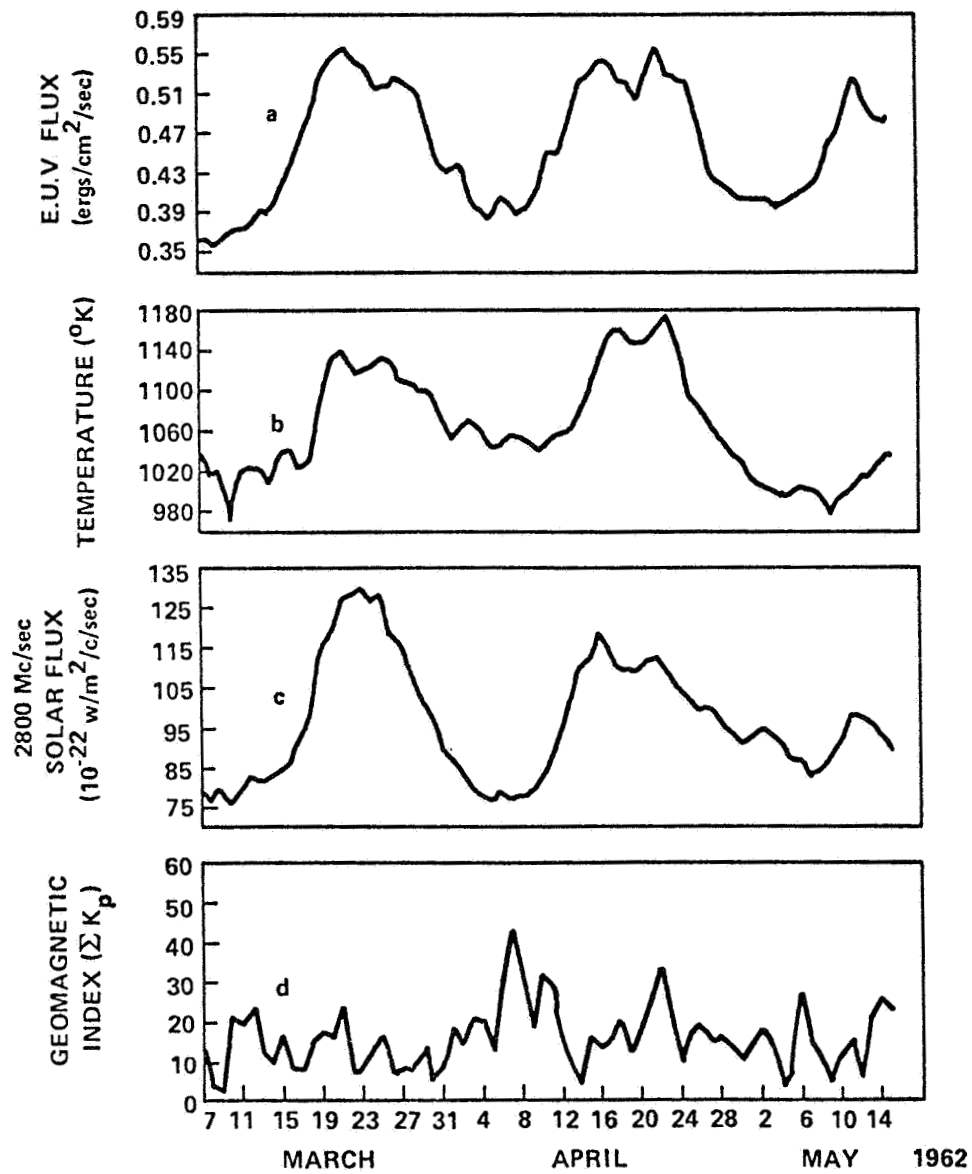
Fig. 6

CONTRIBUTIONS OF ORBITAL MECHANICS TO

CONDUCTING EXPERIMENTS IN SPACE

by
Larry D. Mullins
NASA/George C. Marshall Space Flight Center

ABSTRACT

Orbital Mechanics as a discipline is principally concerned with solving the set of equations (1) for analyzing the motion of a satellite under various conditions. This activity on the surface may not seem crucial to conducting experiments in space, but it provides insights into the way in which forces may influence these experiments. More directly, for experiments concerned with external "targets," it provides predictions of the satellite's position and velocity versus time, enabling extensive preflight planning and resulting in optimum use of on-orbit time.

Orbital Mechanics applied to artificial earth satellite motions is concerned primarily with analyzing the motion of a point mass under the influence of forces acting on it. Even though an earth satellite such as the Space Shuttle may be an extended body, it is treated in orbital mechanics as though it were a point mass. The satellite's position and velocity or state vector is commonly described by a set of six orbital elements. For a pure two-body motion (inverse square radial force) all of the elements remain constant in time except the mean anomaly, which increases at a uniform rate. Additional (perturbing) forces cause the orbital elements to change in time. This change in time is described by the Lagrange Planetary Equations. These are written in equations (1) in terms of perturbing forces S,T,N along radial, tangential and normal directions, respectively, as illustrated in Figure 1. The main problem of orbital mechanics is to describe accurately the forces acting on the satellite (Figure 1) and then to integrate the set of equations (1). The integrals of equations (1) describe the orbital elements as a function of time. This task, in itself, may appear on the surface to be only indirectly related to the conduction of experiments in space.

129

$$\dot{a} = 2 \sqrt{\frac{a^3}{\mu(1-e^2)}} \left[S \ e \ \sin f + \frac{a(1-e^2)}{r} \ T \right]$$

$$\dot{e} = \sqrt{\frac{a(1-e^2)}{\mu}} \ [S \ \sin f + T(\cos E + \cos f)]$$

$$\frac{di}{dt} = \frac{1}{\sqrt{\mu a(1-e^2)}} \ N \ r \ \cos(\omega + f)$$

$$\dot{\Omega} = \frac{1}{\sin i \ \sqrt{\mu a(1-e^2)}} \ N \ r \ \sin(\omega + f) \qquad\qquad (1)$$

$$\dot{\omega} = -\dot{\Omega} \ \cos i - \frac{1}{e} \sqrt{\frac{a(1-e^2)}{\mu}}$$

$$\left\{ S \ \cos f - T \left[1 + \frac{r}{a(1-e^2)} \right] \sin f \right\}$$

$$\dot{M} = n - \frac{2}{\sqrt{\mu a}} \ S \ r - \dot{\omega} \ \sqrt{1-e^2} - \dot{\Omega} \ \sqrt{1-e^2} \ \cos i$$

Orbital Mechanics, however, can offer insights into planning and analyzing experiments in space by providing estimates of the forces acting on the satellite (and experiment) and describing how those forces affect the orbit of the satellite. Many experiments are conducted in space primarily because of the (nearly) force-free environment. To be precise, the nearly force-free environment is due not to the absence of forces on the satellite but to the balancing of oppositely directed forces; principally, the balancing of the inwardly directed gravitational force and the outwardly directed centrifugal force. To further clarify the problem one must know if the experiment is rigidly attached to the spacecraft, in which case it experiences the same forces (and accelerations) as the center of mass of the spacecraft. If the experiment is suspended freely from the spacecraft (as, for example, a cloud experiment), the most important aspect is the relative acceleration between the spacecraft center of mass and the suspended experiment.

There are four principal types of perturbing forces acting on an earth satellite. They are (1) gravitational forces, (2) atmospheric drag forces, (3) solar radiation pressure, and (4) electromagnetic (Lorentz) forces. These forces affect the spacecraft and its contents differently.

The Gravitational Force

The gravitational force acts alike on both the spacecraft and the experiment inside, thus producing no relative acceleration between them except possibly for small gravity gradient effects. The sources of perturbing gravitational forces are the distant celestial bodies (sun, moon and planets) and the nonspherical mass distribution in the earth. For close earth satellites the latter is by far the largest. The forces produced by the celestial bodies can be ignored in all but the most sensitive of experiments. The gravitational force produced by the earth can be written as the gradient of a potential function

$$\vec{F} = - \vec{\nabla} V = - \left[\hat{r} \, \frac{\partial V}{\partial r} + \hat{\delta} \, \frac{1}{r} \, \frac{\partial V}{\partial \delta} + \hat{\phi} \, \frac{1}{r \cos \delta} \, \frac{\partial V}{\partial \phi} \right] . \qquad (2)$$

This can be written in terms of $\hat{S}$, $\hat{T}$, and $\hat{N}$ by the relations

$$\hat{r} = \hat{S} \; ; \; \hat{\delta} = \cos \theta \, \hat{T} + \sin \theta \, \hat{N} \; ; \; \hat{\phi} = \sin \theta \, \hat{T} - \cos \theta \, \hat{N}, \qquad (3)$$

as illustrated in Figure 2, where

$$\sin \theta = \frac{\tan \delta}{\sin u \, \tan i} \; ; \; \cos \theta = \tan \delta \, \cot u . \qquad (4)$$

The potential function, V, is written as

$$V = \frac{-\mu}{r} \left[1 - \sum_{n=2}^{\infty} J_m (\frac{\rho}{r})^n P_n (\sin \delta) + \sum_{n=2}^{\infty} \sum_{m=1}^{n} (\frac{\rho}{r})^n P_n^m (\sin \delta) \right.$$

$$\left. \{ S_{n,m} \sin m\phi + C_{n,m} \cos m\phi \} \right] . \qquad (5)$$

The coefficients J_n (zonal harmonics) and $S_{n,m}$ and $C_{n,m}$ (Tesseral harmonics) can be found to high order in various publications, e.g., the Smithsonian Standard Earth (III)

131

(SAO Special Report 353). The values of the first few coefficients are

$$J_2 = 1.0826 \text{x} 10^{-3}; \quad J_3 = -2.546 \text{x} 10^{-6}; \quad J_4 = -1.649 \text{x} 10^{-6}$$

$$C_{2.2} = 1.57 \text{x} 10^{-6}; \quad S_{2.2} = -.897 \text{x} 10^{-6}; \tag{6}$$

$$\mu = 3.987012 \text{x} 10^{14} \ m^3/s^2$$

Equations (2) through (6) can be used to calculate the magnitude of perturbing gravitational forces (those not balanced by centrifugal forces) on the satellite. Gravity gradient effects are those produced due to the magnitude of the gravitational force being slightly different at different locations in the satellite.

The principal effects of the gravity perturbations on the orbit plane are caused by the first zonal harmonic J_2. It causes a secular regression of the line-of-nodes amounting to about 5°/day and short period oscillations in the semi-major axis of amplitude up to 7 or 8 kilometers. The J_3 zonal harmonic causes a long period oscillation in the eccentricity of near circular orbits.

The Atmospheric Drag Force

The atmospheric drag force is a nonconservative force acting generally in a direction opposite the velocity vector. This force takes energy out of the satellite orbit, causing the orbit gradually to decay. The magnitude is given by

$$D = \frac{1}{2} \rho v^2 \frac{C_D A}{M} \ (m/s^2) \tag{7}$$

where

ρ = atmospheric density (kg/m^3)

v = satellite velocity (m/s)

C_D = coefficient of drag
    (dimensionless number with a value near 2)

A = cross-sectional area of satellite (m^2)

M = mass of satellite (kg)

J

The direction of this force, for near circular orbits, can be taken as being in the $-\hat{T}$ direction. The magnitude of the force decreases strongly (exponentially) with increasing altitude because the atmospheric density varies this way.

Unlike gravity, atmospheric drag exerts a force only on those surfaces exposed to the atmosphere. Thus, it would exert a force on a satellite but not on a freely suspended experiment inside, producing a relative acceleration between them of the magnitude given in equation (7). This would cause the freely suspended experiment or sample to drift relative to the spacecraft until it contacted some restraining surface such as a wall. The magnitude of the drag accelerations on a shuttle can vary from as much as 10^{-4} m/s^2 for a very low altitude orbit, say about 250 km, to as little as 10^{-7} m/s^2 for a very high altitude orbit, say about 600 km.

Solar Radiation Pressure

This force is due to sunlight falling on the satellite and, like the atmospheric drag force, it acts only on those surfaces to which it is exposed, thus producing relative accelerations between spacecraft and freely suspended objects inside. Its direction is taken to be opposite that of the solar vector and it exhibits the unique behavior of "switching off and on" when the satellite enters and exits the earth's shadow. Its magnitude is given by

$$\left|\frac{\vec{F}}{m}\right| = \frac{(1+\beta)E_p}{c}\left(\frac{A}{m}\right) \tag{8}$$

where

β = the reflectivity ($0 \le \beta \le 1$)

c = speed of light ($\sim 3 \times 10^8$ m/s)

A = area of satellite presented to the sun (m^2)

m = mass of satellite (kg)

E_p = "solar constant" ($\sim 1.4 \times 10^3 \frac{\text{joules}}{\text{m}^2\text{-sec}}$)

For the Space Shuttle (A/m) is on the order of 10^{-3} m^2/kg, making this acceleration on the order of 10^{-8} m/s^2. The direction (illustrated in Figure 3) is taken to be opposite the solar vector which in the $\hat{S},\hat{T},\hat{N}$ coordinate system is

133

$$-\hat{R}_{*_{S,T,N}} = (u)_z (i)_x (\Omega)_z \begin{pmatrix} -\cos \delta_* \cos \alpha_* \\ -\cos \delta_* \sin \alpha_* \\ -\sin \delta_* \end{pmatrix} \qquad (9)$$

where $(\Omega)_z$ is a rotation about the z-axis through the angle Ω, etc.

Electromagnetic Force

The Lorentz force is that acting on a charged particle moving in a magnetic field. Satellites can and do build up charges on their surfaces, and the earth about which they are orbiting possesses a magnetic field; thus they experience the Lorentz force. The magnitude and direction of the resulting acceleration is

$$\vec{a} = \frac{q}{m} (\vec{v} \times \vec{B}) \qquad (10)$$

where

q = net charge on satellite

m = mass of satellite

$\vec{v}$ = velocity vector of satellite

$\vec{B}$ = geomagnetic field

The major difficulty in calculating this force is knowing what charge is built up on the satellite. In any case this acceleration is very small. One source has estimated that it is no larger than 10^{-9} m/s^2 in a maximum case.

134

FIGURE 1   ORTHOGONAL DIRECTIONS AT THE SATELLITE POSITION:
S—RADIAL, T—TANGENTIAL, N—NORMAL

$$\hat{\delta} = \cos\theta\,\hat{T} + \sin\theta\,\hat{N}$$

$$\hat{\phi} = \cos\theta\,\hat{N} + \sin\theta\,\hat{T}$$

$$\hat{r} = \hat{S}$$

$$\cos\theta = \tan\delta\,\cot u$$

$$\sin\theta = \frac{\cot i\,\tan\delta}{\sin u}$$

FIGURE 2 RELATIONSHIP BETWEEN $\hat{r}, \hat{\phi}, \hat{\delta}$ AND $\hat{S}, \hat{T}, \hat{N}$

135

j
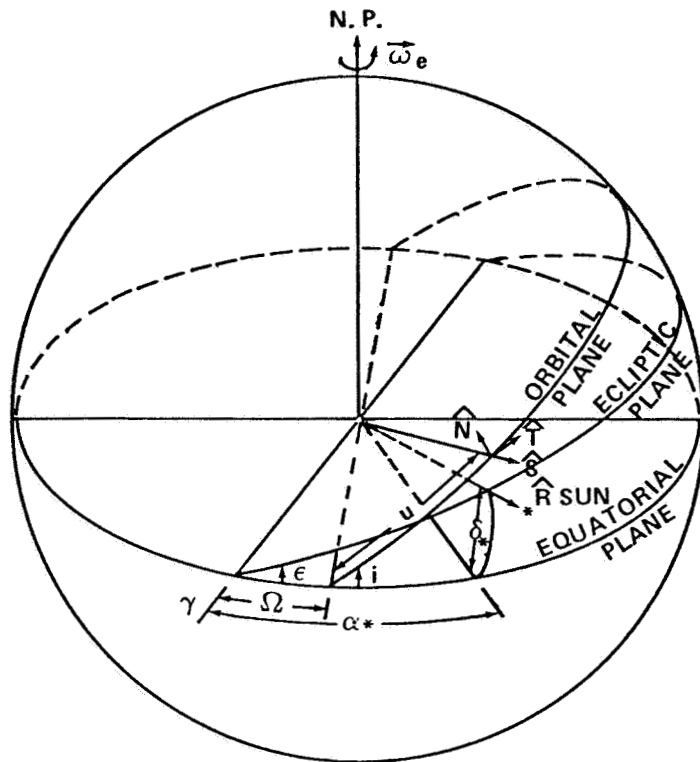
$$
\begin{pmatrix} R_{*S} \\ R_{*T} \\ R_{*N} \end{pmatrix} = (u)_z \; (i)_x \; (\Omega)_z \begin{pmatrix} \cos \delta_* \cos \alpha_* \\ \cos \delta_* \sin \alpha_* \\ \sin \delta_* \end{pmatrix}
$$

FIGURE 3   RELATIONSHIP OF SOLAR VECTOR TO $\hat{S}, \hat{T}, \hat{N}$
COORDINATE SYSTEM

DYNAMIC BEHAVIOR OF PARTICLES

IN SPACECRAFT

by
Barton S. Perrine
NASA/George C. Marshall Space Flight Center

INTRODUCTION

This presentation is concerned with the behavior of particles relative to a spacecraft frame of reference. The discussion was based on work performed by the author in the late 1960's as described in NASA TM X-53643 [1].

With the advent of sophisticated scientific space missions, the need to understand the behavior of the motion of particles relative to a spacecraft frame of reference has become of paramount importance. Intuitively, it seems that there would be no problem caused by the extremely small differential forces acting on the spacecraft arising from crew motion, vernier thrusters, small variations in venting thrusts, solar pressure and drag decelerations. However, as Figure 1 shows, these forces, typical of those acting on a spacecraft of differing configuration and orientation, can cause large separation distances in a relatively short period of time. For this particular figure, the difference in the drag deceleration between the two bodies was 0.312×10^{-6} m/sec^2. The technical motivation for the need to understand free particle behavior arises from the fact that one may require free particles to remain in a specified volume of space within the spacecraft. Movement of the particles outside of this volume could result in adverse experimental conditions, like for example the particle leaving a field of view, or striking an experiment boundary. Specific possible applications of this knowledge can be cited relative to the Drop Dynamics Module scheduled to fly on Spacelab Mission 3 in 1984, Materials Processing in Space containerless processing experiments, certain kinds of relativity experiments, as well as others. We shall not attempt to present a completed or exhaustive theory of particle motion in space, but rather we shall outline the kinds of theoretical considerations that we must make relative to the definition of experiments.

137

DERIVATION OF THE EQUATIONS OF MOTION

Let the spacecraft be in a circular orbit of radius, R, and angular velocity, $\bar{\omega}$ (Figure 2). Set up a two-dimensional coordinate system in this spacecraft with the positive y-axis pointing outward along the radius vector and the x-axis in the opposite direction of the inertial velocity vector. Let the position vector in this coordinate system to a second body be $\bar{r}$. If $\bar{R}$ is the radius vector from the center of the earth to the origin of the relative rotating coordinate system, then the differential equation of motion for the center of mass of the second body can be written:

$$\ddot{\bar{r}} = \bar{a} - 2\bar{\omega}\text{x} \, \dot{\bar{r}} + \bar{g} - \bar{\omega}\text{x} \, [\bar{\omega}\text{x}(\bar{r} + \bar{R})]$$

where $\bar{a}$ is the sum of all the differential accelerations between the two bodies due to aerodynamics, vernier thruster firings, venting of gases, crew motion, etc., $-2\omega\text{x}\dot{\bar{r}}$ is the Coriolis acceleration, $\bar{g}$ is the gravitational acceleration, and the last term is the centrifugal acceleration. The last two terms can be combined in the following manner:

$$\bar{g} = - \frac{\mu(\bar{r} + \bar{R})}{|\bar{r} + \bar{R}|^3}$$

according to the inverse square gravitational law, where μ is the gravitational constant for the earth. Since $\omega^2 = \mu/R^3$,

$$\bar{g} = \frac{-\omega^2(\bar{r} + \bar{R})R^3}{|\bar{r} + \bar{R}|^3}$$

Since $\bar{\omega}$ is perpendicular to $(\bar{r} + \bar{R})$,

$$\bar{\omega}\text{x} \, [\bar{\omega}\text{x}(\bar{r} + \bar{R})] = -\omega^2(\bar{r} + \bar{R})$$

and

$$\bar{g} - \bar{\omega}\text{x}[\bar{\omega} + (\bar{r} + \bar{R})] = \omega^2(\bar{r} + \bar{R})\left(1 - \frac{R^3}{|\bar{r} + \bar{R}|^3}\right)$$

The term $|\bar{r} + \bar{R}|$ can be approximated by $R + y$ with an error of only about x^2/R, where x and y are the components of $\bar{r}$ in Figure 2. Therefore,

$$\bar{g} - \bar{\omega}x[\bar{\omega}x(\bar{r} + \bar{R})] = \omega^2(\bar{r} + \bar{R})\left[1 - \frac{R^3}{(R + y)^3}\right]$$

$$= \omega^2(\bar{r} + \bar{R})\left[1 - \frac{1}{(1 + \frac{y}{R})^3}\right]$$

Expanding the second term in the brackets by the binomial expansion yields

$$\bar{g} - \bar{\omega}x[\bar{\omega}x(\bar{r} + \bar{R})] = \omega^2(\bar{r} + \bar{R})\left[1 - \left(1 - 3\frac{y}{R} + \ldots\right)\right]$$

$$\approx 3\omega^2 y \frac{(\bar{r} + \bar{R})}{R}$$

where $\bar{r} + \bar{R}/R$ may be approximated by the unit vector in the y-direction, $\hat{j}$,

$$\ddot{\bar{r}} = \bar{a} - 2\bar{\omega}x\,\dot{\bar{r}} + 3\omega^2 y\hat{j}$$

Separating this acceleration into x and y components yields

$$\ddot{x} = a_x + 2\omega\dot{y}$$

$$\ddot{y} = a_y - 2\omega\dot{x} + 3\omega^2 y$$

For this report, it will be assumed that the difference in drag deceleration acts on the spacecraft in the positive x-direction and is a constant, D. The Rand Corporation investigated the equations for a drag which is dependent on altitude [2]. However, this assumption is justified for very nearly circular orbits in a spherically symmetric atmosphere (with no diurnal bulge). The governing differential equations therefore become

139

$$\ddot{x} = D + 2\omega\dot{y} \tag{1}$$

$$\ddot{y} = -2\omega\dot{x} + 3\omega^2\dot{y} \tag{2}$$

These equations may be solved analytically as shown in Reference 1 to give x, y, $\dot{x}$, and $\dot{y}$ as functions of time.

$$x = x_o + c_o t - \frac{3}{2} D t^2 - 2b_o \sin \omega t + 2a_o(1-\cos \omega t) \tag{3}$$

$$y = \frac{2c_o}{3\omega} - \frac{2D}{\omega} t - b_o \cos \omega t + a_o \sin \omega t \tag{4}$$

$$\dot{x} = c_o - 3Dt - 2\omega b_o \cos \omega t + 2\omega a_o \sin \omega t \tag{5}$$

$$\dot{y} = - \frac{2D}{\omega} + \omega b_o \sin \omega t + \omega a_o \cos \omega t \tag{6}$$

where

$$a_o = \frac{1}{\omega}\left(\dot{y}_o + \frac{2d}{\omega}\right)$$

$$b_o = 3y_o - 2\frac{\dot{x}_o}{\omega}$$

$$c_o = 6\omega y_o - 3\dot{x}_o$$

and x_o, y_o, $\dot{x}_o$, and $\dot{y}_o$ are the conditions of position and velocity at time $= 0$.

These equations may be used to describe the motion of any body in a near-circular orbit which remains fairly close (i.e., much less than the radius of the orbit) to the origin of the rotating relative coordinate system. Also, these equations are not restricted to describing the motion of only one body. By having a separate set of equations as (3) through (6) for each body, the motion of multiple bodies in low eccentricity orbits can be described. By subtracting their coordinates, the motion of all of the bodies can be described relative to one of them. This is a possible method of removing the restriction that the spacecraft be exactly in a circular orbit.

BEHAVIOR OF FREE BODY

In the following discussion, the body located at the origin of the relative coordinate system will be called the reference body and the other body the experiment body.

The equations of motion developed in the previous section predict the experiment body to follow a trajectory relative to the reference body similar to that shown in Figure 3. In this particular example, the motion of the experiment body is initiated at the position x = 30 m, y = 4 m, with a positive $\dot{x}$ and $\dot{y}$ such that its orbital energy is greater than that of the reference body. Superimposed onto an oscillation in the vertical and horizontal direction, the experiment body first experiences a drift to the right and then a drift to the left. The oscillation in the vertical direction results as it moves between apogee and perigee. The oscillation in the horizontal direction is due to the fact that the perigee and apogee velocities are different. The drift to the right is caused by the semi-major axis of the conic of the experiment body being initially greater than that of the reference body and thus having a longer period.

CONCLUSIONS

Significant spatial excursions of particles in space can occur relative to the spacecraft frame of reference as a result of drag deceleration of the vehicle. These vehicle excursions tend to be large as time increases. Thus, if the particle is required to remain in a specified volume, constraints may be required. Thus, for example, in levitation experiments it may be extremely difficult to turn off the forces of constraint which keep the particles in a specified region. This means experiments which are sensitive to disturbances may be very difficult to perform if perturbation forces are required to be absent. A case in point are the drop dynamics experiments currently planned for Spacelab Mission 3. In these experiments an acoustic positioner is used to keep liquid drops in a field of view as well as for excitation of the droplets into oscillatory and rotational modes. However, after the droplets are excited via the acoustic field, it would be highly desirable in certain of the experiments to turn off the acoustic field in order to study the transition from one state of droplet motion to another. However, the acoustic field at the level of 10^{-4} g is required to keep the droplet in the field of view to cancel

the effects of spacecraft motion resulting from crew activity, drag deceleration, etc.

In the analysis herein, it has been assumed that aerodynamic drag on the particle is absent. However, aerodynamic drag will in most cases be present in the form of a Stokes-type of drag, given by

$$D_s = 6\pi\rho\nu aV$$

where ρ is the density of the gas within which the particle resides, ν is kinematic viscosity of this gas, a is the radius of the particle, and V is the velocity of the particle relative to the gas. If m denotes the mass of the particle and ρ_p the associated mass density, then we can rewrite the above as

$$D_s = m \frac{V}{\tau}$$

where τ is a viscous time scale

$$\tau = \frac{4}{18} \frac{\rho_p a^2}{\rho\nu}$$

which provides a measure as to how long it takes for the particle to react to the effects of viscosity. Thus, if τ is sufficiently large, viscous drag is unimportant, while if τ is sufficiently small, viscous drag is important. Thus, we may conclude that viscous drag will be unimportant for cases in which particle mass density and radius are sufficiently large or in which gas density and kinematic viscosity are sufficiently small, with the reverse being true at the opposite extremes.

The analysis herein has also neglected the effects of crew motion, venting of gases, and thruster firings. These effects can be included via specification in a_x in the governing equations.

REFERENCES

1. Perrine, B. S.: A Method of Soft Tether Stationkeeping, NASA TM X-53643, 1967.

2. Schechter, H. B., and Cole, J. D.: An Approximate Solution to the Relative Motion of Two Close Satellites in the Presence of Drag and Oblateness, The Rand Corporation, RM-4481-PR, August 1965.
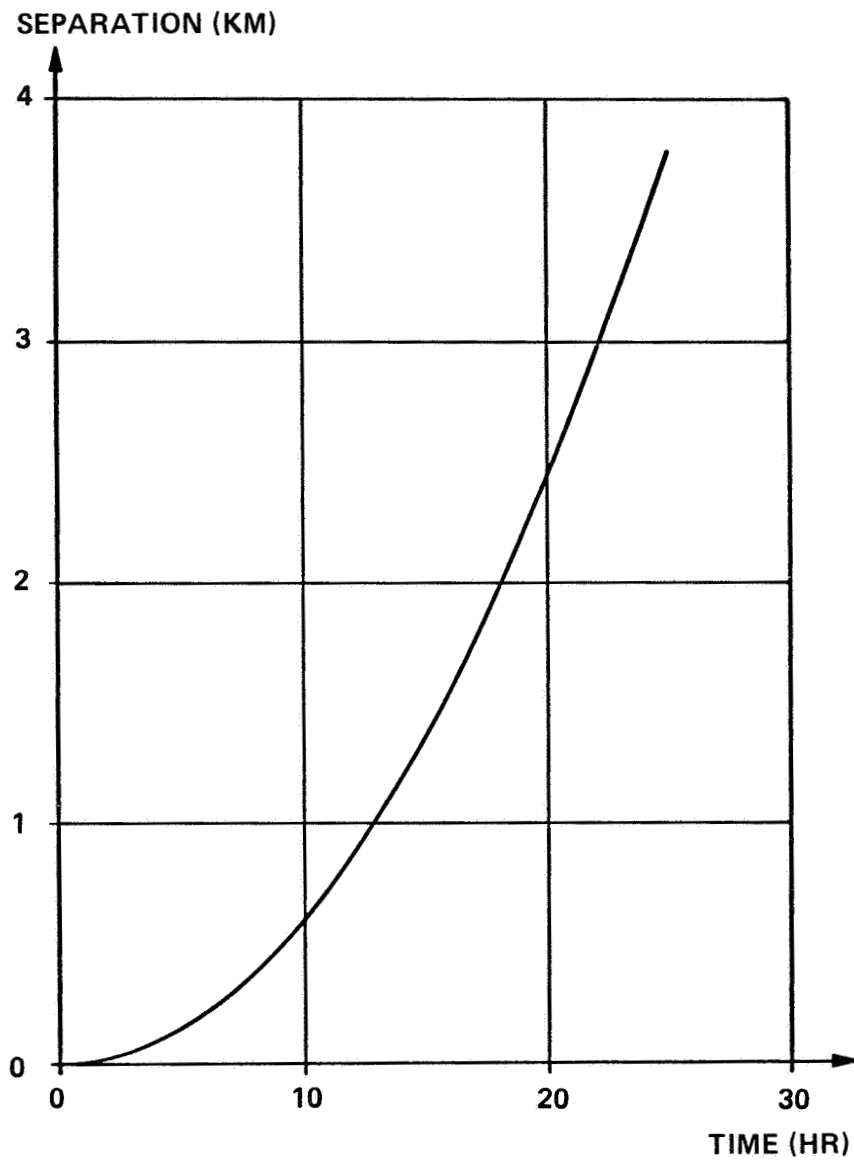
FIG. 1. TYPICAL SEPARATION GROWTH BETWEEN A SPACECRAFT AND A PARTICLE IN LOW EARTH ORBIT.

144
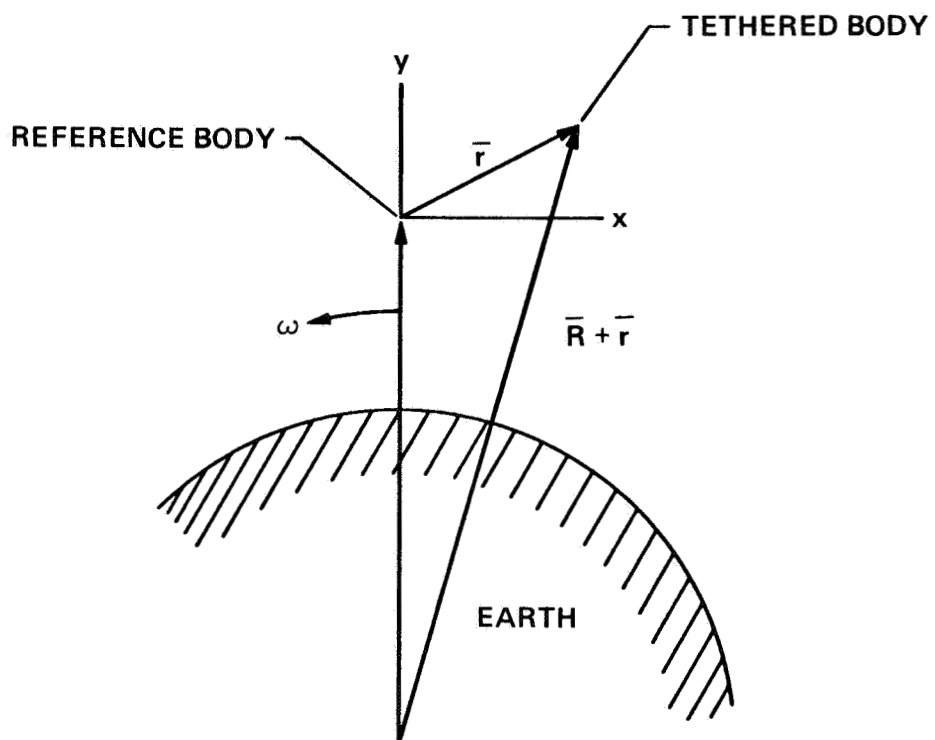
FIG. 2. RELATIVE COORDINATE SYSTEM
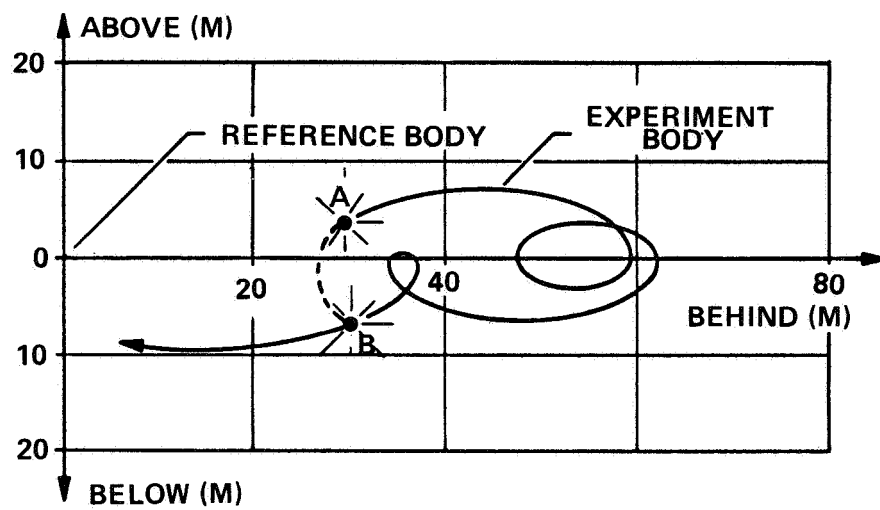
FIG. 3. TYPICAL TRAJECTORY IN THE RELATIVE COORDINATE SYSTEM

DESIGN OF THE SPACE SHUTTLE DIGITAL AUTOPILOT

AND RESULTING DYNAMIC ENVIRONMENT

by
Stanley Fay
The Charles Stark Draper Laboratory, Inc.

This compilation progesses through the development of the Space Shuttle phase plane controller from fundamental considerations, and it provides quantitative insight regarding the nature of the dynamic environment aboard the Shuttle.

Figure 1 is a tutorial preliminary to the development of Euler's Equations. It introduces a vector torque as a time derivative of the angular momentum vector and then describes the necessary use of the Law of Coriolis to take the derivative.

Figure 2 is a compact derivation of Euler's Equations.

Figure 3 displays the assumptions used to simplify Euler's Equations for design of the Shuttle digital autopilot.

Figure 4 displays further assumptions used in the DAP (digital autopilot) and presents a basic block diagram of the control loop.

Figure 5 starts the basic development of the phase-plane controller of the DAP. It introduces the control variable U as torque per unit moment of inertia and demonstrates how phase-plane state drifts to the right for positive angular rate and drifts to the left for negative angular rate.

Figure 6 derives the parabolic trajectory on the phase plane for the constant thrust of the attitude control jets. Figure 6 also demonstrates that one particular trajectory (dotted) is desired in order to achieve zero error in attitude position and attitude rate.

Figure 7 introduces the concept of "switch lines" to dictate when to coast and when to reverse fire in order to ultimately approach zero error.

Figure 8 introduces the concept of "deadband" and limit cycling, and how to slant the deadband switch lines in order to attenuate the limit cycle rate.

Figure 9 shows how using parabolic deadband switch lines enable us to achieve the smallest limit cycle in <u>one</u> pass.

Figure 10 and Figure 11 derive a common "one side of deadband" limit cycling which results from experiencing a constant torque disturbance. (Note that the <u>larger</u> the torque disturbance, the <u>smaller</u> the amplitude of limit cycle.)

Figure 12 displays some numerical values of Shuttle limit cycle amplitude and period for various torque disturbances, T_d.

Figure 13 presents an array of pertinent Shuttle facts.

Figure 14 is a comparison of attitude stabilization accuracy of various systems.

Figure 15 and Figure 16 are a derivation of the type and level of disturbance to be experienced aboard the Shuttle as a result of the firing of a single vernier jet for one minimum impulse.

Figure 17 displays drag deceleration as a function of altitude.

Figure 18 displays various accelerative g-levels due to various disturbance sources.

EULER'S EQUATIONS

$F = ma$

$*F = \dfrac{d}{dt}(mv)$

$\quad = \dot{m}v + m\dot{v}$

$\quad = 0 + ma$

$*T = \dfrac{d}{dt}(J\Omega)$

$T = \dot{J}\Omega + J\dot{\Omega}$

$T = 0 + J\alpha$

$*T = \dfrac{d}{dt}H$
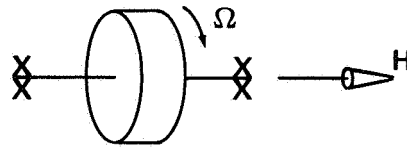
3–DIMENSIONAL SPACE
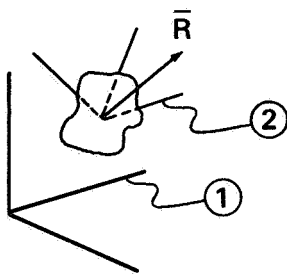
$\bar{T} = \dfrac{d}{dt}\bar{H}$, DERIVATIVE WRT INERTIAL SPACE

$p_1\bar{R} = p_2\bar{R} + \bar{\omega}_{12} \times \bar{R}$, LAW OF CORIOLIS
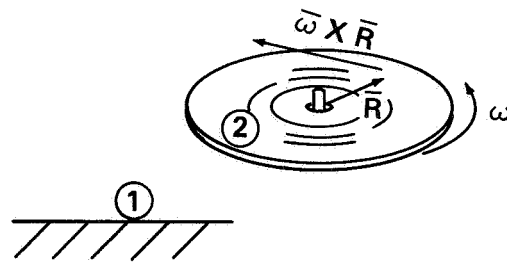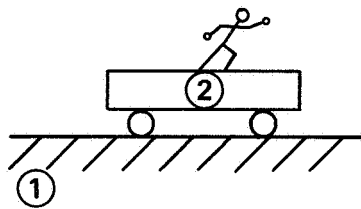
FIGURE 1

$$\overline{M}_c = p_i\overline{H} = p_b\overline{H} + \overline{\omega}_{ib} \times \overline{H}$$

WHERE

$$\overline{H} = [J]\,\overline{\omega}_{ib} \quad \text{AND} \quad \overline{\omega}_{ib}^b = \begin{Bmatrix} \omega_x \\ \omega_y \\ \omega_z \end{Bmatrix}$$

OR

$$\overline{H}^b = \begin{bmatrix} J_x & 0 & 0 \\ 0 & J_y & 0 \\ 0 & 0 & J_z \end{bmatrix} \begin{Bmatrix} \omega_x \\ \omega_y \\ \omega_z \end{Bmatrix}$$

$$= \begin{Bmatrix} J_x\,\omega_x \\ J_y\,\omega_y \\ J_z\,\omega_z \end{Bmatrix}$$

$$p_b\overline{H}^b = \begin{Bmatrix} J_x\,\dot{\omega}_x \\ J_y\,\dot{\omega}_y \\ J_z\,\dot{\omega}_z \end{Bmatrix}$$

AND

$$\overline{\omega}_{ib}^b \times \overline{H}^b = \begin{bmatrix} 0 & -\omega_z & \omega_y \\ \omega_z & 0 & -\omega_x \\ -\omega_y & \omega_x & 0 \end{bmatrix} \begin{Bmatrix} J_x\,\omega_x \\ J_y\,\omega_y \\ J_z\,\omega_z \end{Bmatrix} = \begin{Bmatrix} -\omega_z\,\omega_y J_y + \omega_z\,\omega_y J_z \\ \omega_z\,\omega_x J_x - \omega_z\,\omega_x J_z \\ -\omega_x\,\omega_y J_x + \omega_x\,\omega_y J_y \end{Bmatrix}$$

$$= \begin{Bmatrix} (J_z - J_y)\,\omega_z\,\omega_y \\ (J_x - J_z)\,\omega_x\,\omega_z \\ (J_y - J_x)\,\omega_y\,\omega_x \end{Bmatrix}$$

OR

$$\overline{M}_c^b = \begin{Bmatrix} T_x \\ T_y \\ T_z \end{Bmatrix} = \begin{Bmatrix} J_x\,\dot{\omega}_x \\ J_y\,\dot{\omega}_y \\ J_z\,\dot{\omega}_z \end{Bmatrix} + \begin{Bmatrix} (J_z - J_y)\,\omega_z\,\omega_y \\ (J_x - J_z)\,\omega_x\,\omega_z \\ (J_y - J_x)\,\omega_y\,\omega_x \end{Bmatrix} \quad , \text{ EULER'S EQS.}$$

FIGURE 2

150

J

SYSTEM DESIGN RATIONALE

(1) IF THE CROSS PRODUCT TERMS, ARE SMALL COMPARED TO THE ACCELERATION TERMS,

$$J_3 \dot{\omega}_3 >> (J_2 - J_1) \, \omega_1 \omega_2$$

I.E., DIFFERENCES OF LARGE NUMBERS MULTIPLIED BY PRODUCT OF TWO SMALL NUMBERS,

WE MAY WRITE:

$$T_x = J_x \, \dot{\omega}_x$$

$$T_y = J_y \, \dot{\omega}_y \qquad \qquad \underline{\text{DECOUPLED}} \, \underline{\text{AXES}}$$

$$T_z = J_z \, \dot{\omega}_z$$

(2) IF ANGULAR DISPLACEMENTS PER CALCULATION ARE KEPT SMALL, WE MAY SAY $\omega \approx \dot{\bar{\theta}}$, AND THE SYSTEM CONTROL RELATES TORQUE TO ANGLE BY A SIMPLE DOUBLE INTEGRAL. NOTE THAT FOR LARGE ANGLES, AN ANGLE IS NOT A VECTOR.

"NON—COMMUTATIVITY OF ANGLES."

FIGURE 3

151

- FOR <u>SMALL</u> ANGLES, $\theta = \dfrac{1}{J} \iint \overline{T} dt^2$

- ANGLES KEPT SMALL PER CALCULATION BY 12.5 Hz ITERATION RATE OF DAP

- DRIFT OF ACTUAL ORIENTATION FROM DESIRED BECAUSE OF ASSUMPTIONS (1) AND (2) IS SENSED BY IMU AND NEW COMMAND ISSUED AT EACH ITERATION

ACTUAL STATE →
DESIRED STATE → **GUIDANCE LAW** → $\overline{ERROR}$ → **RCS ERRORS** → $\bar{\omega}_E$ / $\bar{\theta}_E$ TO PHASE PLANE

COMMAND → **DAP** → **JETS AND/OR OMS** → THRUST AND TORQUE → **EULER'S EQUATIONS (RIGID BODY DYNAMICS)** → RESPONSE

IMU

FIGURE 4

J
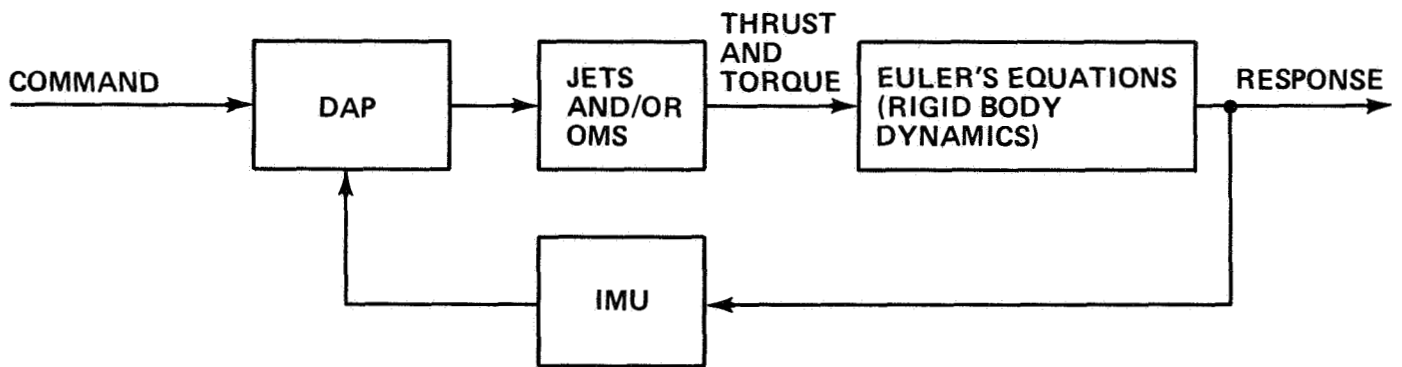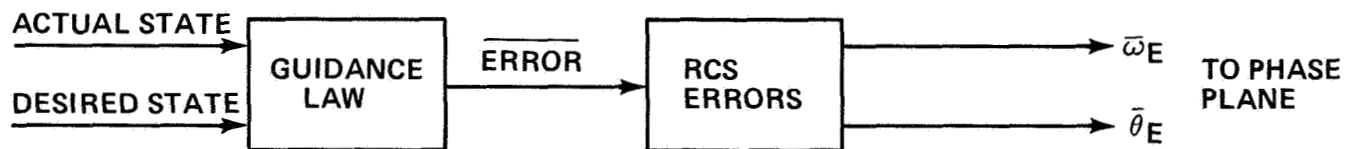
PHASE PLANE

$$\frac{T}{J} = u = \ddot{\theta} = \dot{\omega}$$

$$\dot{\theta} = \omega$$

IF u = 0, NO TORQUE, $\dot{\omega}$ = 0 OR ω = CONSTANT AND θ <u>INCREASES</u> FOR POSITIVE ω AND <u>DECREASES</u> FOR NEGATIVE ω
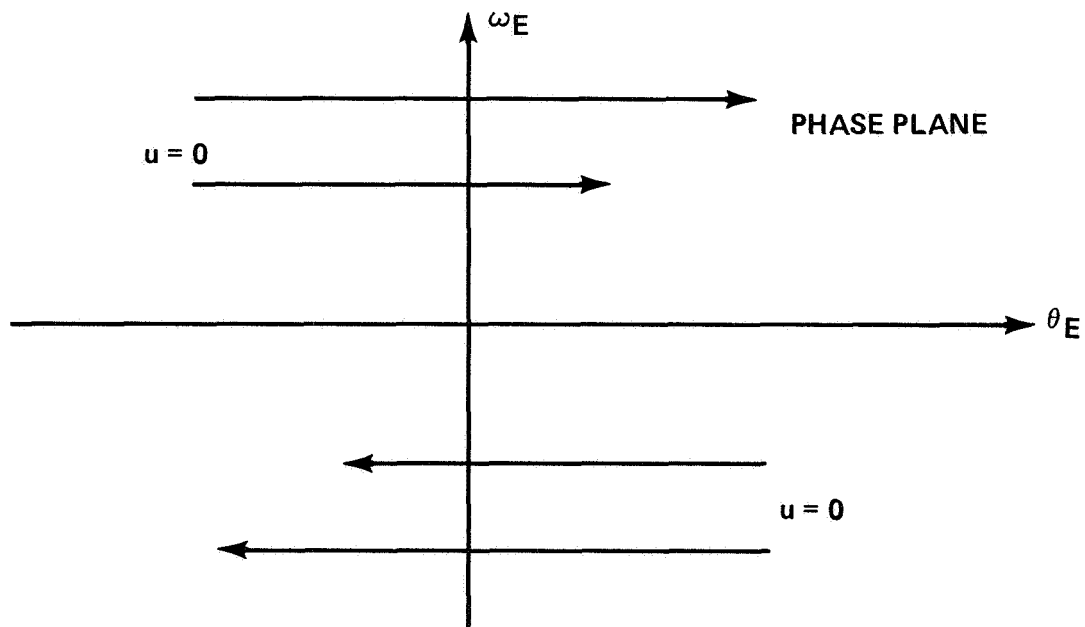
FIGURE 5

$$\frac{T}{J} \;=\; u = \dot{\omega}$$
$$\dot{\theta} = \omega$$

$$\text{SLOPE} \;=\; \frac{d\omega}{d\theta} \;=\; \frac{d\omega/dt}{d\theta/dt} \;=\; \frac{\omega}{\dot{\theta}} = \frac{u}{\omega}$$

$$\text{ASSUME } u = \frac{T}{J} \;=\; \underline{\text{CONSTANT}} \text{ FOR JETS:}$$

$$\frac{d\omega}{d\theta} = \frac{u}{\omega}$$

$$\omega d\omega = u d\theta$$

$$\frac{1}{2}\left(\omega^2 - \omega_0^2\right) \;=\; u\,(\theta - \theta_0)$$
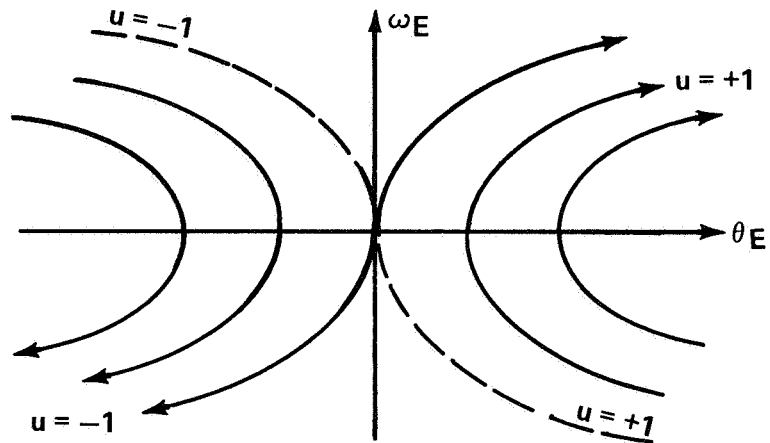
$u = +1,\ \omega_E$ MUST INCREASE (HEAD UPWARDS)

$u = -1,\ \omega_E$ MUST DECREASE (HEAD DOWNWARDS)

ω_E IS $+,\ \theta_E$ MUST INCREASE (HEAD TO RIGHT)

ω_E IS $-,\ \theta_E$ MUST DECREASE (HEAD TO LEFT)

TO HIT ZERO ERROR, DOTTED TRAJECTORY DESIRED.

FIGURE 6

154
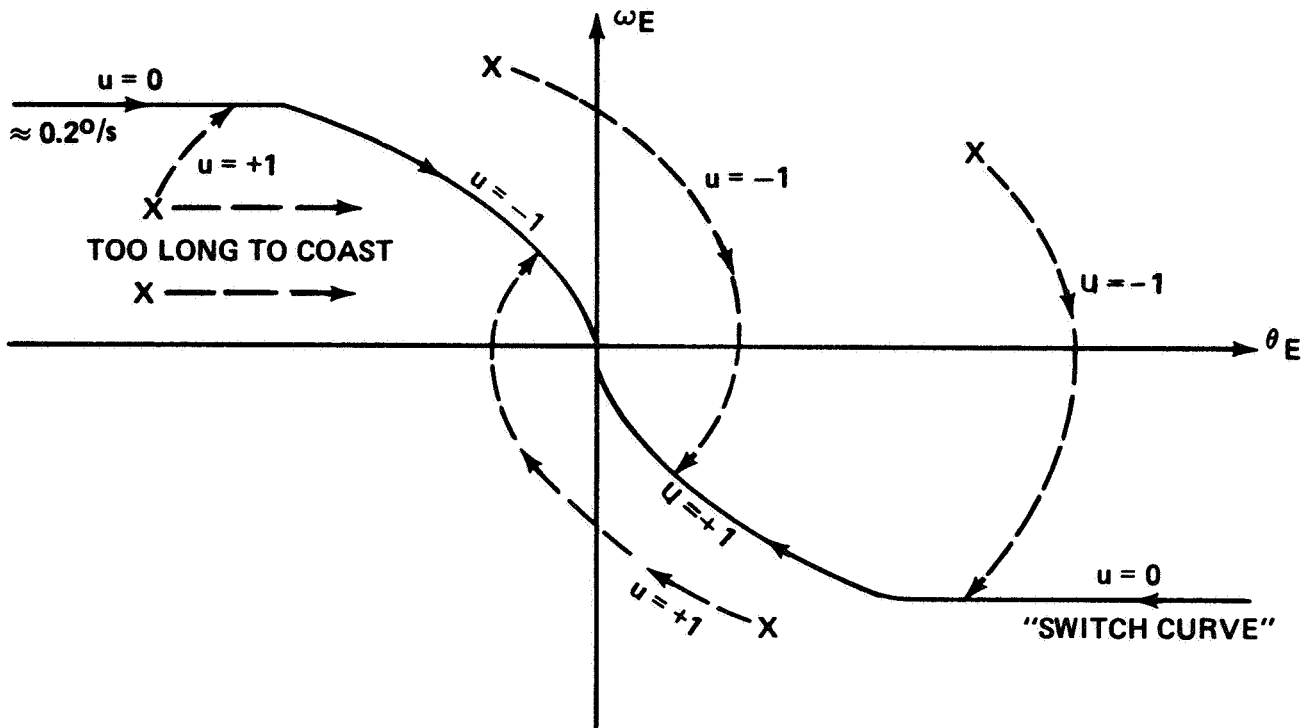
u = +1, ω_E INCREASES, MOVE UP PAGE

u = −1, ω_E DECREASES, MOVE DOWN PAGE

MOVEMENT ALWAYS CLOCKWISE

NEVER HIT ZERO EXACTLY BECAUSE:

1. ATTITUDE MEASUREMENT ERRORS
2. RATE MEASUREMENT ERRORS
3. MEASUREMENT DISTURBANCES OR NOISE
4. JET QUANTIZATION FIRING TIME

RESULT:

1. CONTINUOUS LIMIT CYCLE AROUND ZERO
2. FUEL WASTE

FIGURE 7

DEAD BAND:
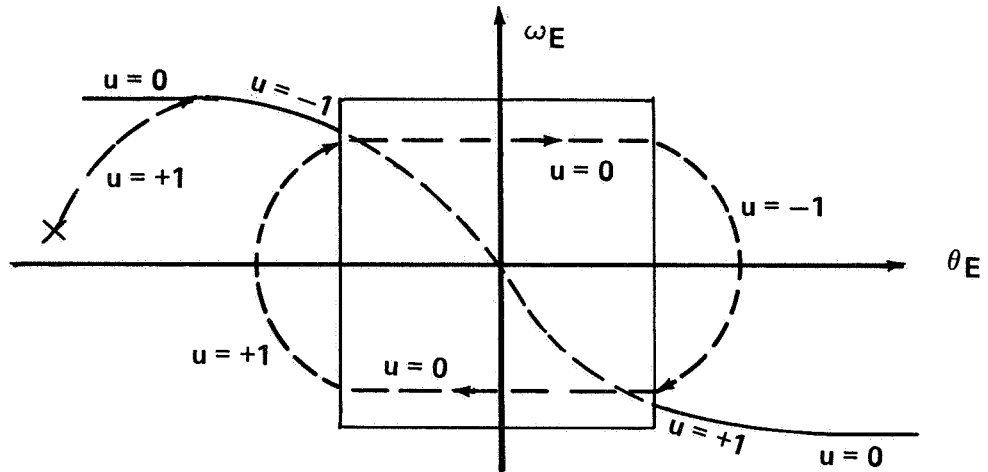
TO ATTENUATE LIMIT CYCLE RATE AND SAVE FUEL:
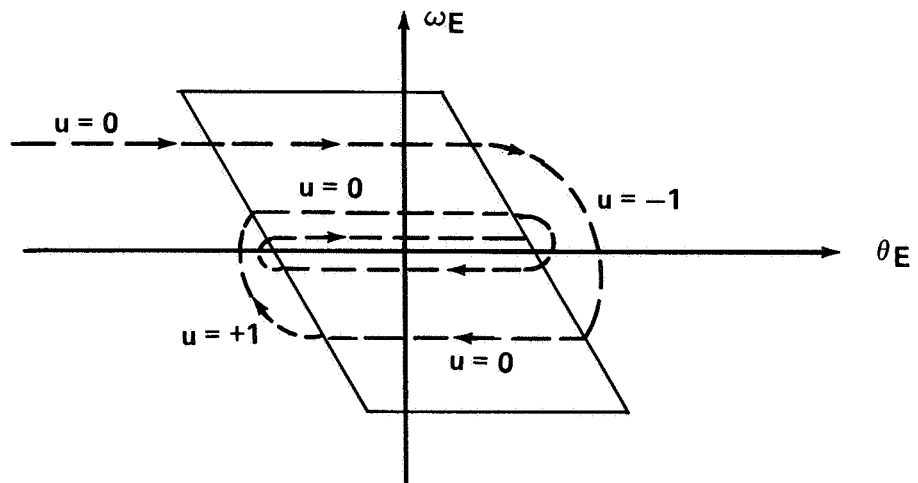
SMALLEST LIMIT CYCLE DETERMINED BY MIN IMPULSE OF JETS

$$\text{IMPULSE} = \int_0^T F\,dt = F\int_0^T dt = FT; \qquad T = 80 \text{ MS}$$

$$F_{pri} = 870 \text{ LB}$$

$$F_{vern} = 25 \text{ LB}$$

FIGURE 8

156

TO HIT SMALLEST LIMIT CYCLE IN ONE PASS:

INSIDE BOX:

IF SGN (u) = − SGN (ω_E) CONTINUE TO FIRE

OTHERWISE u = 0
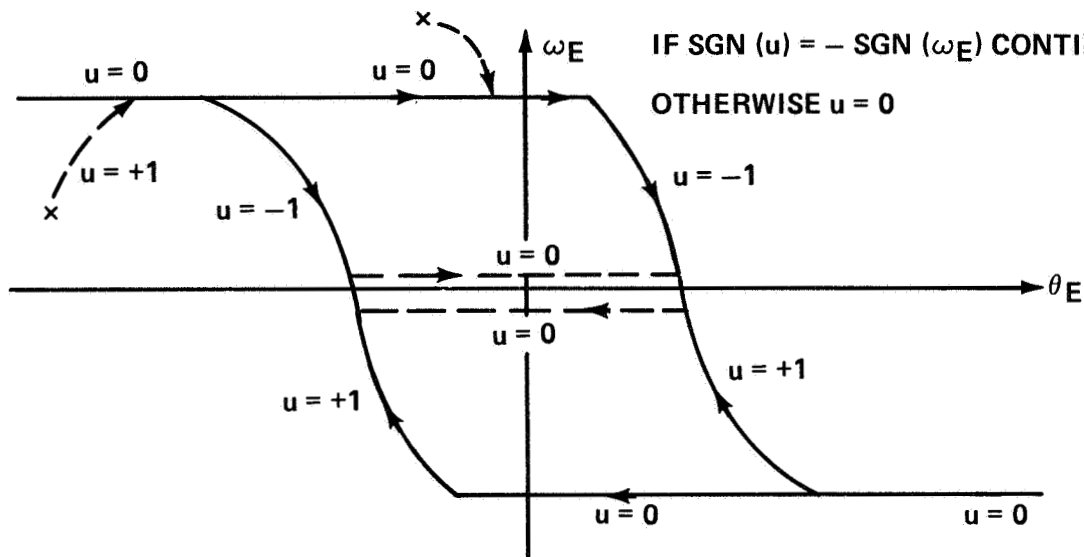
ADDITION OF SHELF DUE TO QUANTIZATION OF MEASUREMENT OF θ AND ω (GRANULARITY OF A/D CONVERTER FROM IMU)·

FIGURE 9

157
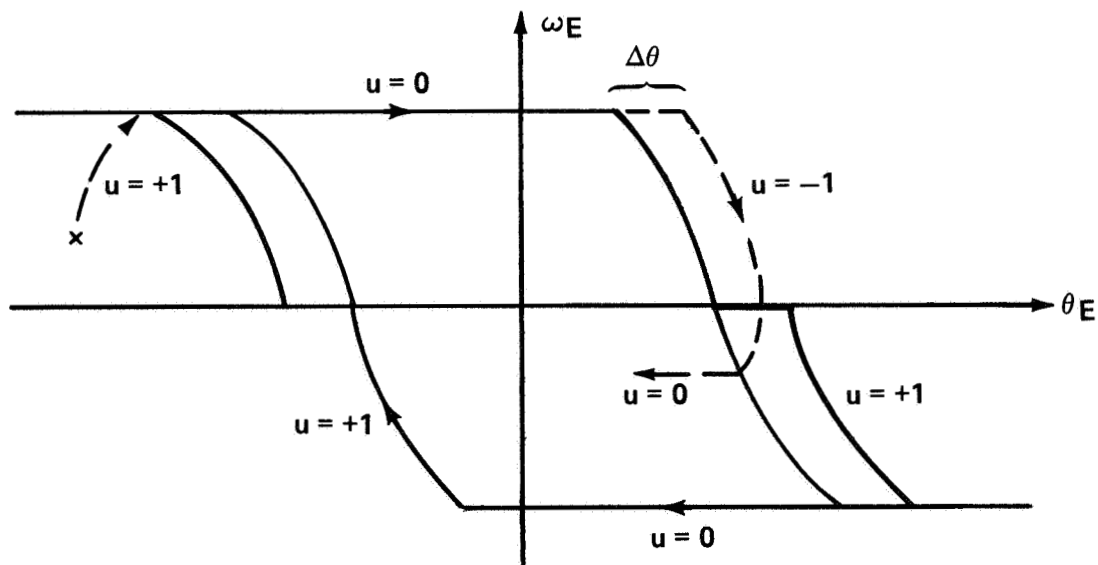
ONE SIDE OF DEAD BAND LIMIT CYCLING

JET IMPULSE:
$$-T_j\Delta t = J\Delta\Omega \tag{1}$$
(JET FIRED IN AN ASSUMED NEGATIVE DIRECTION)

DISTURBANCE TORQUE:
$$+T_d = J\frac{d\Omega}{dt} \tag{2}$$
(DISTURBANCE TORQUE IS IN AN ASSUMED POSITIVE DIRECTION)

FROM (2):
$$\frac{d\Omega}{dt} = \frac{T_d}{J}$$

$$\Omega = \frac{T_d}{J}\, t + \Omega_0 \tag{3}$$

WHERE $\Omega_0 = 1/2\ \Delta\Omega = -\ 1/2\ \dfrac{T_j\Delta t}{J}$ FROM (1)

INTEGRATING (3):
$$\theta = 1/2\ \frac{T_d}{J}\, t^2 + \Omega_0 t + \theta_0 \tag{4}$$

WHERE AT $t = 0$, $\theta = \theta_0 = \theta_{DB}$
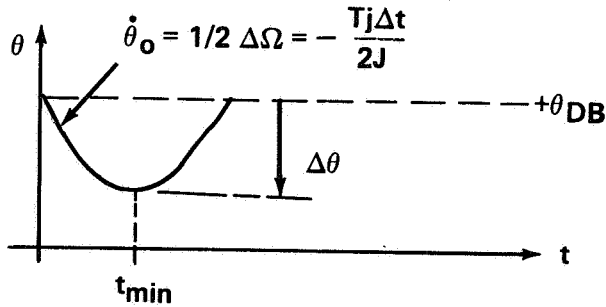
$$\dot{\theta}_0 = 1/2\ \Delta\Omega = -\ \frac{T_j\Delta t}{2J}$$

DIFFERENTIATING (4): $\dot{\theta} = \dfrac{T_d}{J} t + \Omega_0 = 0$ OR $t_{min} = \dfrac{\Omega_0 J}{T_d} = \dfrac{T_j\Delta t J}{2JT_d} = \dfrac{T_j\Delta t}{2T_d}$

PERIOD OF LIMIT CYCLE, $T = \dfrac{T_j\Delta t}{T_d} = \dfrac{\text{JET IMPULSE}}{T_d}$

FIGURE 10

ﾠ

AMPLITUDE OF LIMIT CYCLE:

FROM (4): $\quad \Delta\theta = \theta_{DB} - \theta_{min} = -1/2 \, \dfrac{T_d}{J} \, t^2_{min} - \Omega_0 t_{min}$

$$= -1/2 \, \frac{T_d}{J} \, \frac{T_j^2 \Delta t^2}{4 T_d^2} \; + \; 1/2 \; \frac{T_j \Delta t}{J} \; \frac{T_j \Delta t}{2 T_d}$$

$$= 1/8 \; \frac{T_j^2 \Delta t^2}{T_d J}$$

$$= 1/8 \; \frac{(\text{JET IMPULSE})^2}{T_d J}$$

NOTE: LARGER T_d YIELDS SMALLER $\Delta\theta$

APPROXIMATE NUMERICAL VALUES:

$\quad F_{j_{vernier}} = 25$ LB, $\Delta t = 80$ MS

$\quad$ MOMENT ARMS: $\quad$ ROLL, 10 FT
$\qquad\qquad\qquad\qquad\quad$ PITCH, YAW, 40 FT

ROLL $J_x = 9 \times 10^5$ FT LB S^2

PITCH $J_y = 72 \times 10^5$ FT LB S^2

YAW $J_z = 75 \times 10^5$ FT LB S^2

FIGURE 11

159

J

YAW AXIS

$\Delta\theta$	T_d	T
1°	0.006 FT LB	3.7 H
2°	0.003 FT LB	7.4 H
3.4 SEC	6.5 FT LB	12 S *

GRAVITY GRADIENT
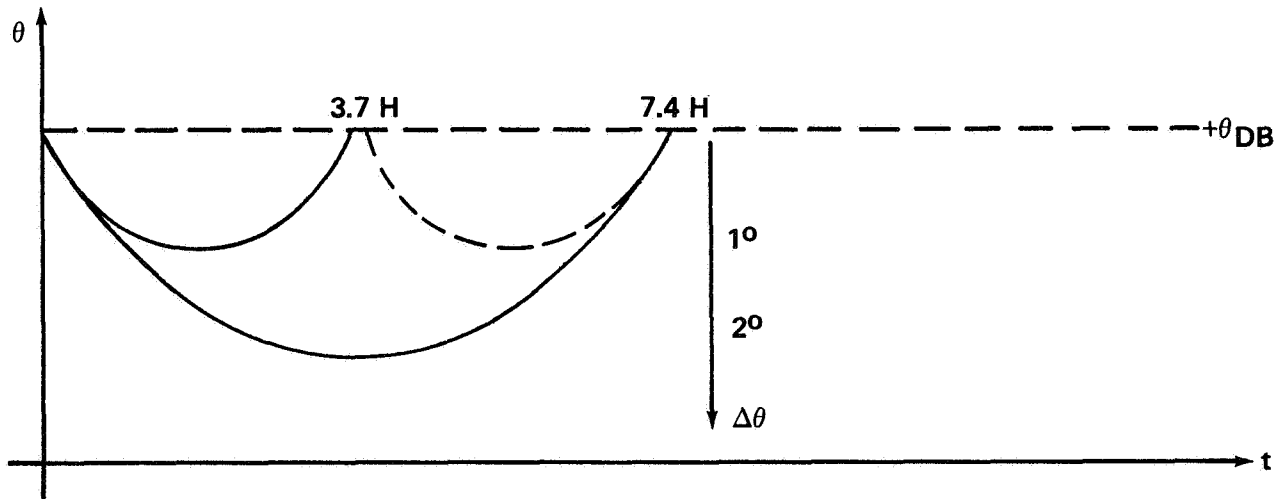
* TO LENGTHEN TIME BETWEEN JET FIRINGS, THE ACTUAL ADJUSTMENT IS FOR 1½ X DEAD BAND BY FIRING MORE THAN ONE JET.

MIN θ_{DB} = 0.1°

FIGURE 12

SHUTTLE FACTS

1. **38 MAIN JETS, 900 LB THRUST, TRANSLATION AND ATTITUDE**
   6 VERNIER JETS, 25 LB THRUST, ATTITUDE ONLY

   44

1a. APPROXIMATE MOMENT ARMS OF JETS FROM C.M.

   ROLL, 10 FT
   PITCH, YAW, 40 FT

2. OMS ENGINES (TWO), GIMBALED, FIXED THRUST $\approx$ 6,000 LB

   6° PITCH
   7° YAW

3. ORBITER ANGULAR RATES: 0.1^o/S TO 5°/S

4. ATTITUDE DEAD BAND: 0.1^o TO 5°

5. ORBITER MASS APPROXIMATELY: $\dfrac{200,000 \text{ LB}}{g} = 6,500$ SLUGS

6. ORBITER MOMENTS OF INERTIA:

   ROLL (FORWARD), $J_x \approx 1.2 \times 10^6$ KG METER$^2 = 9 \times 10^5$ FT LB S^2

   PITCH (RIGHT WING), $J_y \approx 9.7 \times 10^6$ $\qquad = 72 \times 10^5$

   YAW (DOWN), $J_z \approx 10 \times 10^6$ $\qquad = 75 \times 10^5$

FIGURE 13

ATTITUDE STABILIZATION

1. SHUTTLE JETS: ±0.1° DEAD BAND

2. BOLT—DOWN CMG PACKAGE $\begin{cases} \text{ACCURACY} \pm 50 \text{ SEC} \\ \text{JITTER RATE} \pm 25 \text{ SEC/S} \end{cases}$

3. STABILIZED GIMBAL SYSTEM $\begin{cases} \text{ACCURACY} \pm 1 \text{ SEC} \\ \text{JITTER RATE} \pm 1 \text{ SEC/S} \end{cases}$

EXAMPLE: APOLLO TELESCOPE MOUNT (ATM) ON SKYLAB

— ATM TWO GIMBAL REQUIREMENTS:

	POINTING (RAD)	STABILITY (RAD/15 MIN)	
ROLL	$\pm$ 29 X 10^{-4}	$\pm$ 22 X 10^{-4}	(VEHICLE AXIS)
PITCH & YAW	$\pm$ 12 X 10^{-6} (2.5 SEC)	$\pm$ 12 X 10^{-6}	(PLATFORM AXES)

— SKYLAB ATTITUDE VIA CMG

	POINTING (RAD)	STABILITY (RAD/15 MIN)
ROLL	$\pm$ 29 X 10^{-4}	$\pm$ 22 X 10^{-4}
PITCH & YAW	$\pm$ 12 X 10^{-4} (250 SEC)	$\pm$ 26 X 10^{-4}

FIGURE 14

162

ACCELERATION DISTURBANCES
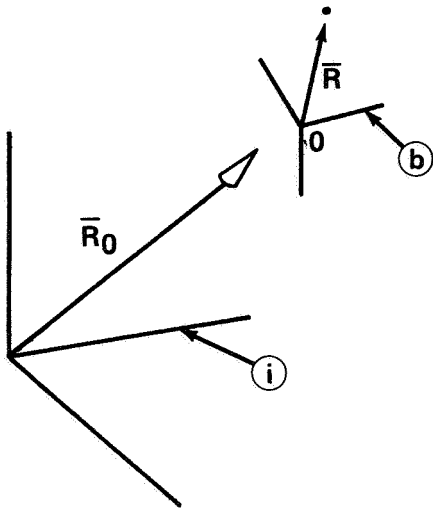
ORIGIN OF BODY FRAME AT VEHICLE C.M.

$$\bar{R}_i = \bar{R}_0 + \bar{R}$$

$$p_i^2 \, \bar{R}_i = \bar{a}_0 + p_b^2 \, \bar{R} + 2\bar{\omega}_{ib} \times p_b \, \bar{R} + p_b\bar{\omega}_{ib} \times \bar{R} + \bar{\omega}_{ib} \times (\bar{\omega}_{ib} \times \bar{R})$$

EXAMPLE: *SINGLE* VERNIER JET FIRING ONE MINIMUM IMPULSE

$$\bar{a}_{exp} = \bar{a}_0 + \dot{\bar{\omega}} \times \bar{R} + \bar{\omega} \times (\bar{\omega} \times \bar{R})$$
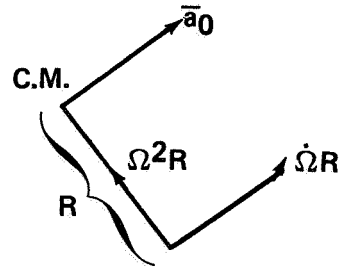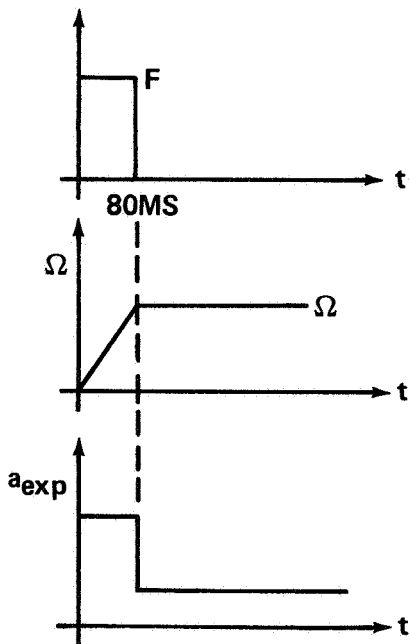
$$[a_{exp}] = \sqrt{(a_0 + \dot{\Omega}R)^2 + (\Omega^2 R)^2}$$

FIGURE 15

163

ROLL AXIS: F = 25 LB
ℓ = 10 FT
R = EXPERIMENT DISTANCE FROM C.M. $\approx$ 2 FT
J_{ROLL} = 9 X 10^5 FT LB S^2
m = 6,500 SLUGS

$a_0 = \dfrac{F}{m} = \dfrac{25}{6,500}$ = 3.85 X 10^{-3} FT/S^2 = 1.2 X 10^{-4}g

$\dot{\Omega} = \dfrac{F\ell}{J} = \dfrac{(25)\,(10)}{9 \times 10^5}$ = 2.78 X 10^{-4} RAD/S^2

$\Omega = (\dot{\Omega})\,(0.08)$ = 2.22 X 10^{-5} RAD/S

$\Omega^2 R$ = 9.86 X 10^{-10} FT/S^2 = 3 X 10^{-11}g

$\dot{\Omega}R$ = 5.56 X 10^{-4} FT/S^2 = 1.74 X 10^{-5}g
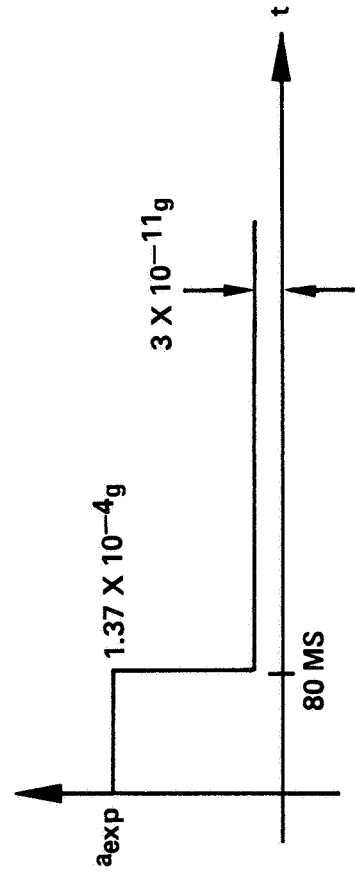
FIGURE 16

DRAG DECELERATION
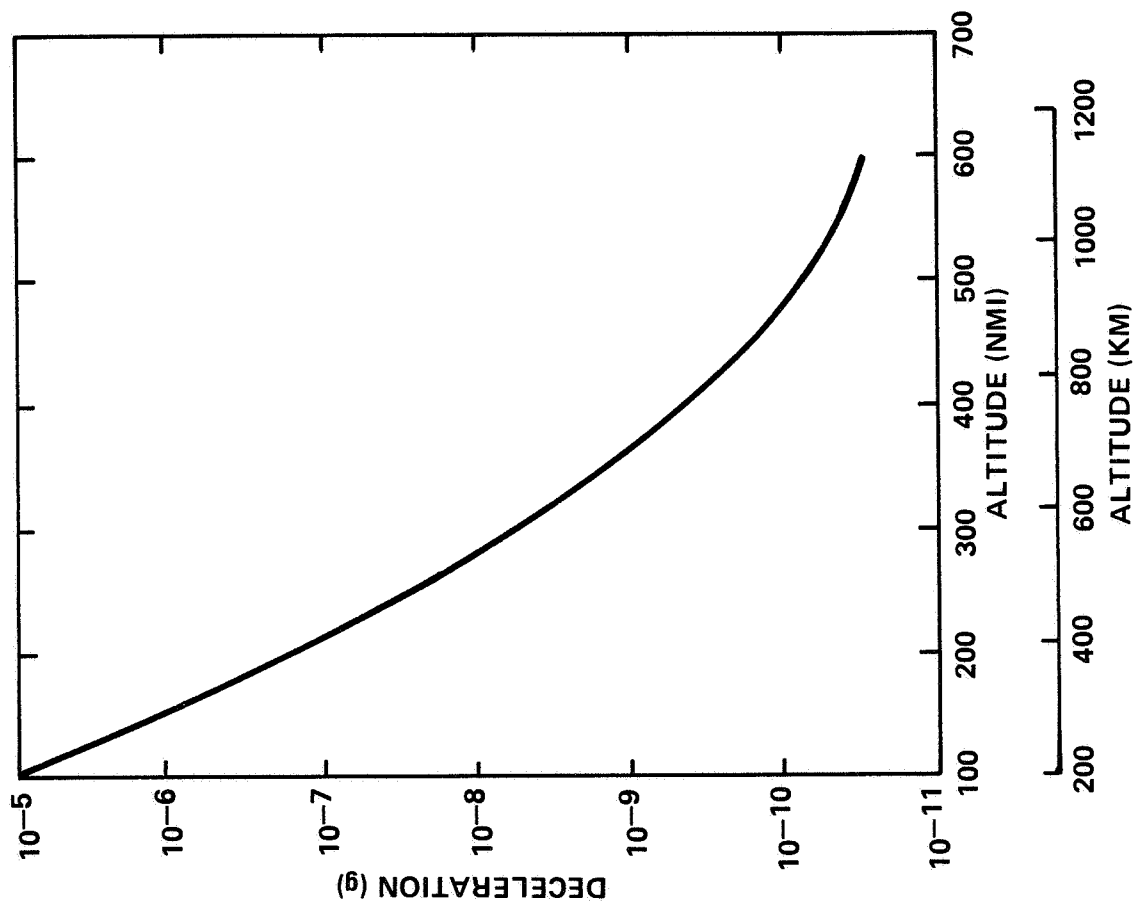
FIGURE 17

ACCELERATIVE g—LEVELS AND SOURCES

SOURCE	DISTURBANCE VALUE (g)	FREQUENCY BAND:
GRAVITY GRADIENT	8×10^{-7}	
AERODYNAMIC DRAG	2×10^{-7}	
LEFT, RIGHT FLASH EVAPORATORS	2.5×10^{-7}	
BOTH FLASH EVAPORATORS	1×10^{-7}	
WATER DUMP	8×10^{-6}	
VFT SPIN—UP	7×10^{-7}	
THRUSTERS	$6 \times 10^{-5} - 6 \times 10^{-4}$	
CREW MOTION		
BREATHING	$10^{-5} - 10^{-4}$	
COUGHING	$5 \times 10^{-5} - 2 \times 10^{-4}$	
SNEEZING	$2 \times 10^{-5} - 3 \times 10^{-4}$	
CONSOLE OPERATION	$10^{-5} - 3 \times 10^{-5}$	0.3 TO 2 HERTZ
BODY BENDING	$9 \times 10^{-5} - 3 \times 10^{-4}$	
ARM ROTATION (90°)	$4 \times 10^{-5} - 2 \times 10^{-4}$	
LEG ROTATION (45°)	$7 \times 10^{-5} - 2 \times 10^{-4}$	
CROUCH AND STAND	$3 \times 10^{-4} - 5 \times 10^{-4}$	

FIGURE 18

EXCEEDANCE STATISTICS OF ACCELERATIONS

RESULTING FROM THRUSTER FIRINGS ON

THE APOLLO-SOYUZ MISSION

by
George H. Fichtl
Robert L. Holland
NASA/George C. Marshall Space Flight Center

INTRODUCTION

Spacecraft acceleration resulting from firings of vernier control system thrusters is an important consideration in the design, planning, execution and post-flight analysis of laboratory experiments in space. In particular, scientists and technologists involved with the development of experiments to be performed in space in many instances required statistical information on the magnitude and rate of occurrence of spacecraft accelerations. Typically, these accelerations are stochastic in nature, so that it is useful to characterize these accelerations in statistical terms. This paper summarizes statistics of spacecraft accelerations associated with thruster firings that occurred during the Apollo-Soyuz mission. The motivation for performing this statistical analysis was simply to obtain an idea of the kind of exceedance statistics one might expect for vehicle accelerations associated with vernier control system thruster firings. To the best of our knowledge statistical data of spacecraft accelerations resulting from thruster firings are not available. The statistics of spacecraft accelerations for any given space mission depend on characteristics of the spacecraft (mass, control systems, etc.) mission profile, and a host of other parameters unique to the mission.

Estimates of exceedance statistics of spacecraft accelerations can be obtained via Monte Carlo simulation of the mission, wherein the statistics of the forcing functions and other stochastic parameters germane to the mission enter the simulation via random selection from populations which possess statistical attributes of these forcing functions and parameters.

THRUSTER ACCELERATION TIME HISTORIES

Acceleration at time t at a given point in a spacecraft as a result of thruster firings is given by

$$\vec{g}(t) = \dot{\vec{\Omega}} \times \vec{r} + \vec{\Omega} \times (\vec{\Omega} \times \vec{r}) + \vec{a} \qquad (1)$$

where $\vec{\Omega}$ is the rigid body angular velocity vector of the spacecraft, $\vec{r}$ is position vector relative to the spacecraft center of mass, $\vec{a}$ is rectilinear acceleration, and ($\cdot$) denotes time differentiation. During a thruster firing event $\vec{\Omega}$ and $\vec{a}$ are nonzero. After the event, these quantities vanish. Furthermore, the second term on the right side of equation (1) is usually two to three orders of magnitude smaller than the remaining terms (at least for the Apollo-Soyuz mission and typical Shuttle missions). In addition, the typical thruster event duration time for attitude vernier control is less than a second. Thus, a time history of the magnitude of spacecraft acceleration, at a given point in the spacecraft, as a result of vernier control system thruster firings would be like a series of Dirac delta function-like acceleration spikes, corresponding to the thruster firings, with essentially zero acceleration between the spikes (see Figure 1). Of course, the total time history would have additional contributions from crew activity, venting of gases and liquids, atmospheric drag, etc. This paper does not consider these additional contributions.

Time histories of the kind depicted in Figure 1 were calculated for specific periods of time during the Apollo-Soyuz Mission for postflight analysis of the experiments performed on that mission. The calculations involved the estimation of $\vec{\Omega}$ and $\vec{a}$ via the calculation of the net force and net torque associated with each thruster firing event. This was possible because the location and reaction force of each thruster relative to the center of mass was known. A discussion of the Apollo-Soyuz vernier control system and thrusters is provided in the reference cited at the end of this paper

Four acceleration time histories were selected for analysis, namely those associated with experiments MA-044, 085, 041 and the science demonstration (Sci-Dem). These runs were approximately 3 to 17 hours in duration. The thruster firing time for each thruster firing event was 0.015 or 0.031 sec.

168

STATISTICAL CALCULATIONS

The quantity $\vec{g}$ is a vector. We have performed statistical calculations on the individual components and the magnitude of $\vec{g}$. In this section we present our statistical calculations on the magnitude of $\vec{g}$. We seek the answer to two questions. First, what is the average rate of exceedance of vehicle acceleration at some assigned level g_1? (See Figure 1). Second, what is the statistical distribution of the time interval between adjacent acceleration events?

The answer to the first question would provide an experimenter an estimate of the average number of times a critical acceleration level would be exceeded during an experiment with duration time t_e. Furthermore, by making assumptions about the distribution of the number of times a critical acceleration level is exceeded in time t_e an estimate can be made of the risk of exceeding a critical acceleration level during the experiment.

The answer to the second question would provide the experimenter with an estimate of the probability of the time interval between acceleration events being less than or equal to some critical time.

ACCELERATION EXCEEDANCE STATISTICS

We define the exceedance rate N of the magnitude of the acceleration vector, g say, to be the average number of acceleration events that exceed level g_1 per unit time. To calculate this quantity from the data we merely count the number of events that exceed level g_1. In an attempt to combine the exceedance calculation for the four time histories that were examined we (1) scaled the exceedance rate N with the standard deviation, σ_T, of the time interval between acceleration events (t_1, t_2, t_3, ... in Figure 1) and (2) subtracted the mean value of g, $\bar{g}$ say, from g and scaled the resulting difference with the standard deviation of g, σ_g say. Thus, Figure 2 provides plots of results of calculations of nondimensional exceedance rate $N\sigma_T$ as a function of the non-dimensional unbiased accelerations, $(g - \bar{g})/\sigma_g$.

169

DISTRIBUTION OF TIME INTERVALS

To calculate the distribution of time interval between acceleration events, T say, straightforward counting procedures were used. Here again in an attempt to combine the results of our calculations we subtracted the mean time interval, $\bar{T}$ say, from the time interval and scaled the resulting difference with σ_T. Thus, Figure 3 provides plots of the distribution function of unbiased time interval between acceleration events, $(T - \bar{T})/\sigma_T$.

DISCUSSION

It appears that some order can be brought about in the statistics of spacecraft vernier control thruster firing statistics via the scaling introduced in the previous section. This is especially true for the thruster time interval distribution function. The thruster acceleration exceedances do not collapse as well as the time interval distribution functions for $(g - \bar{g})/\sigma_g < -1$. However, this may not be important because the important part of the curve is for $(g - \bar{g})/\sigma_g > 0$, i.e., the part for $g > \bar{g}$. The part associated with $(g - \bar{g})/\sigma_g < 0$ encompasses $0 \leq g < \bar{g}$.

We do not claim these results to be universal because of variation in mass, crew activity, control system parameters, etc., from one spacecraft to the next. If results like these could be derived for planned missions, they could play a useful role in the planning of experiments which are sensitive to spacecraft dynamics. These statistics permit the calculation of the risk associated with $g \geq g_c$ for a given experiment duration time t_e, where g_c is a critical value of g to the experiment. To do this one needs to assume that the exceedances of the g process above level g_c arrive independently. We note by $Q(t_e)$ the number of exceedances of g at level g_c over the experiment duration time t_e. Clearly, the process $Q(t_e)$ is a Poisson process, and the probability of $Q(t_e)$ being less than or equal to an assigned value (for example q) is given by

$$P(Q(t_e) \leq q \,,\, t_e) = \frac{(\lambda t_e)^q}{q!} e^{-\lambda t_e} \tag{2}$$

where λ is a parameter. The probability of no exceedance of the g process above the critical value g_c in time interval t_e

follows by setting q = 0 in the above equation, so that

$$P(Q)(t_e) = 0 , t_e) = e^{-\lambda t_e} \qquad (3)$$

By definition of the Poisson process we set

$$\lambda = N$$

Now the risk R that the g process will exceed the critical value of g_c at least once during an experiment of duration time t_e is thus

$$R = 1 - e^{-Nt_e} \qquad (4)$$

Upon specifications of risk R and t_e the value of N can be calculated. A curve like that shown in Figure 2 can be used to calculate g upon specification of σ_T, $\bar{g}$, and σ_g. These latter parameters as well as the $N\sigma_T$ versus $(g - \bar{g})/\sigma_g$ curve will in all likelihood vary from mission to mission of a given spacecraft and possibly vary within a mission. A curve like that shown in Figure 3 can be used to estimate the distribution of time intervals between g-events upon specification of $\bar{T}$ and σ_T. This distribution would provide an estimate of extreme values and typical values of T. Thus, the scientist obtains a statistical description of the dynamic environment in terms of the risk of exceeding a critical g-level and the distribution of time intervals between g-events.

REFERENCE

Apollo Test Project Operation Data Book, Vol. 1, MSC 07765, Lyndon B. Johnson Space Center, Houston, Texas, 1973.
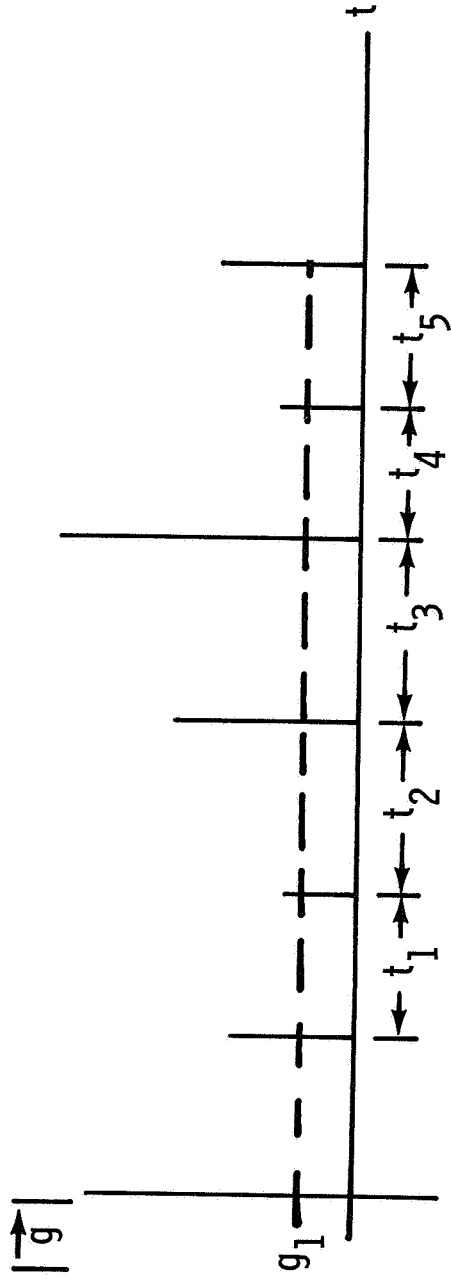
CALCULATE

• EXCEEDANCE RATE OF $g > g_1$, i.e. NUMBER OF THRUSTER FIRING EVENTS PER UNIT TIME

  IN WHICH $g > g_1 : N[(g-\bar{g})/\sigma_g]$

• DISTRIBUTION OF TIME INTERVAL BETWEEN THRUSTER FIRING EVENTS: $P[(t-\bar{t})/\sigma_t]$

FIGURE 1   CALCULATION OF THRUSTER FIRING STATISTICS

172
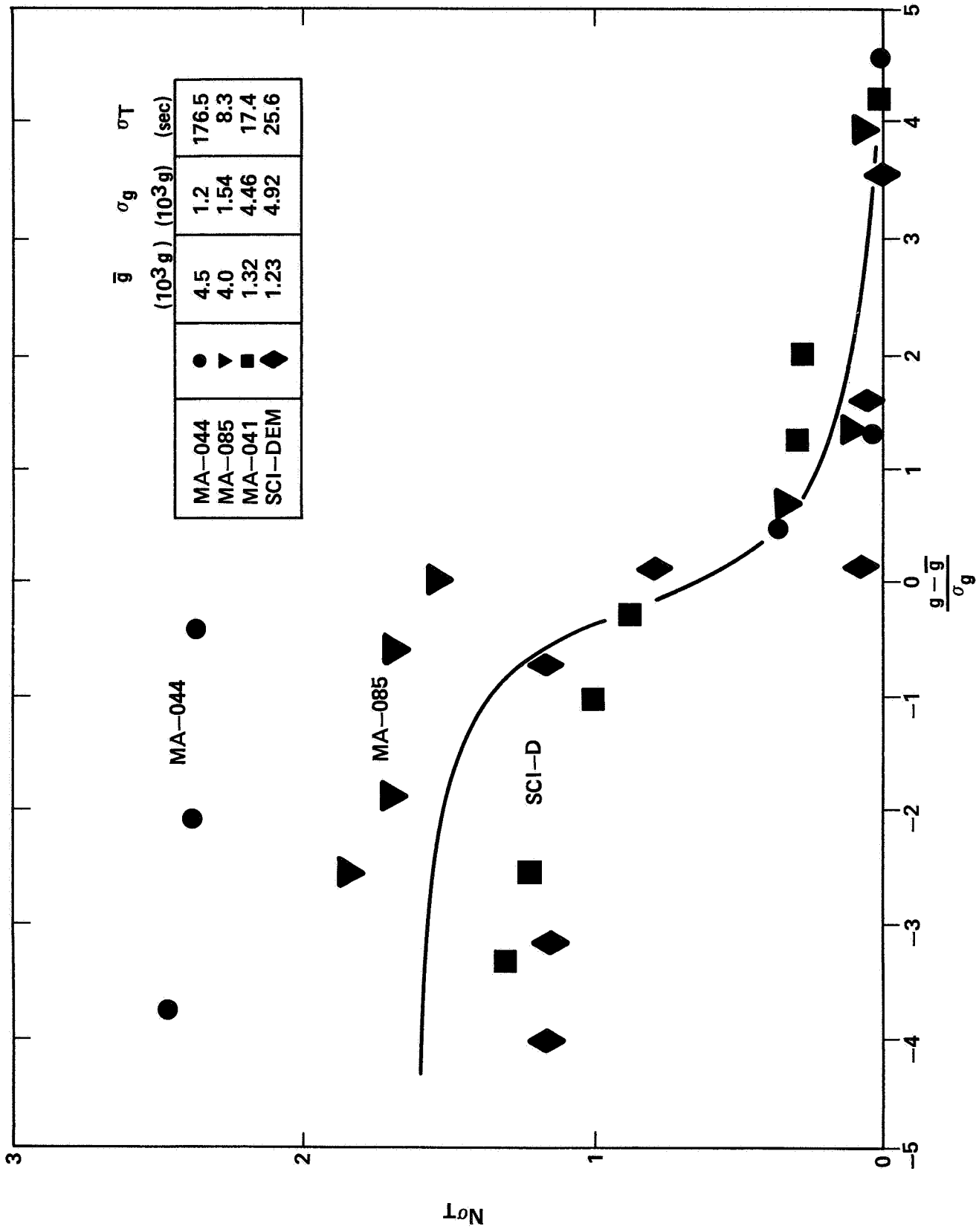
FIGURE 2 ASTP THRUSTER ACCELERATION EXCEEDANCES
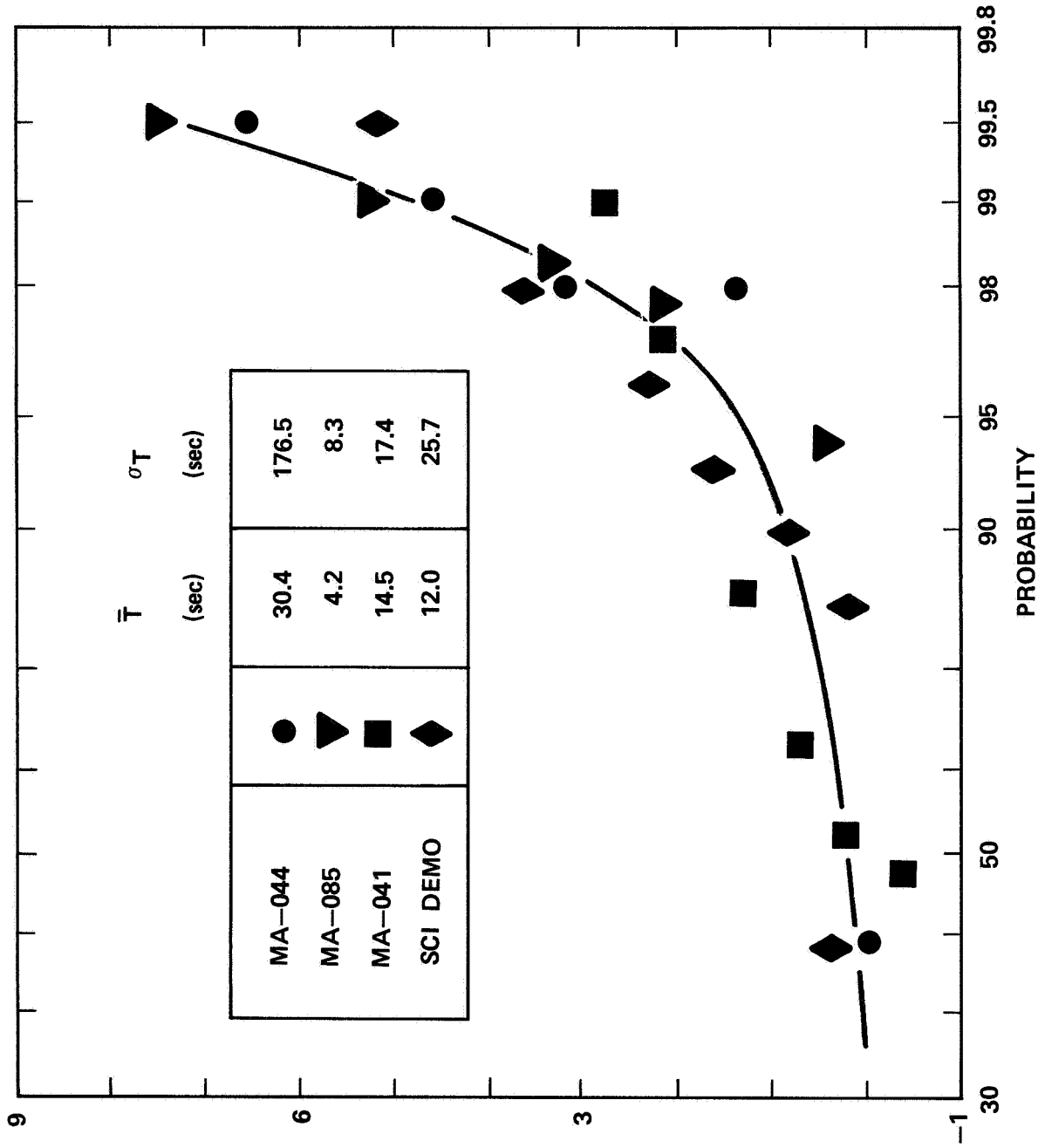
FIGURE 3   ASTP THRUSTER TIME INTERVAL DISTRIBUTION FUNCTION

174

ELASTIC BODY DYNAMICS

by
Ben W. Holder
NASA/Lyndon B. Johnson Space Flight Center

Most of the structural dynamics resources allocated to the Space Shuttle have been concentrated on the flight events which result in critical structural loads and/or minimum control stability margins. Since these events are primarily sub-orbital, the data base of interest to those involved in orbital experimentation is somewhat limited. A brief discussion of available data is given in the following paragraphs.

Three types of on-orbit thrusting are planned. These involve the reaction control system (RCS), vernier reaction control system (VRCS), and the orbital maneuvering system (OMS). Of the three, the OMS provides the largest acceleration levels and in all likelihood, the most severe elastic responses. However, the OMS is used primarily for orbital insertion and de-orbit maneuvers and, therefore, is not likely to be a major source of disturbance during on-orbit experimentation. The RCS was designed as the primary system to be used for on-orbit control. However, present planning calls for use of the VRCS rather extensively for this purpose since it is more efficient from a fuel usage standpoint. The VRCS also provides small control system deadbands and lower acceleration levels. A disadvantage of this system is its lack of redundancy. Loss of a thruster can render the system ineffective. For this reason commitments to use only the VRCS for protracted periods has been discouraged. Other on-orbit disturbance sources which can produce elastic responses are on-board mass movements, most of which are associated with crew motion or remote manipulator system activity.

Two major structural configurations will exist while on-orbit: Orbiter payload bay doors open and Orbiter payload bay doors closed. Up-to-date structural math models are easily developed for the latter case since it represents minor changes to models that are required for response analyses for several mission phases. An up-to-date open door structural dynamic math model does not presently exist. However, a model which was developed for studies concerned with the Spacelab IPS is available for preliminary analysis purposes.

The development of the on-orbit elastic response environment requires a detailed knowledge of the disturbance inputs as well as the structural math models and disturbance sources, some of which were discussed earlier. As far as the author can determine, data describing crew motions and thrusting duty cycles for the Orbiter are not presently available. Certain basic information can be derived from available data sources which should be of interest to those involved in on-orbit experimentation. First, the rigid body acceleration levels due to OMS, RCS, and VRCS firings are given in Figures 1 and 2. These levels contain an allowance for elastic response. Second, Figures 3 and 4 provide examples of transfer function information for the closed-door math model. The transfer functions show the ratio of the acceleration response in the Orbiter mid-bay to steady-state sinusoidal force input at the various thruster locations. These data are useful in determining the frequency content of the response. Similar data exist for the open-door math model.

In summary, information regarding structural responses during on-orbit operations is limited. Although estimates of peak acceleration levels and the associated frequency spectrum in the payload bay due to thrusting of the various control system thrusters have been made, the actual levels and time histories must be based on updated structural math models and a detailed knowledge of the input forcing functions.

SIGNIFICANT ON—ORBIT FORCING FUNCTIONS

● ORBITAL MANEUVERING SYSTEM

LOAD FACTOR i = $\dfrac{\text{EXTERNAL FORCE IN i DIRECTION}}{\text{VEHICLE WEIGHT}}$

CARGO MAXIMUM LIMIT LOAD FACTORS/ANGULAR ACCELERATIONS FOR OMS OPERATION

CARGO WEIGHT	LOAD FACTOR			ANGULAR ACCEL. RAD/SEC^2		
	N_x	N_y	N_z	$\ddot{\theta}_x$	$\ddot{\theta}_y$	$\ddot{\theta}_z$
⩽ 32K	−0.27	±0.005	−0.09	±0.01	±0.005	±0.005
> 32K	−0.24	±0.004	−0.07	±0.01	±0.005	±0.004

FIGURE 1

ᶦ

● REACTION CONTROL SYSTEM

CARGO MAXIMUM LIMIT LOAD FACTORS/ANGULAR ACCELERATIONS FOR RCS/VRCS OPERATION

SYSTEM	LOAD FACTOR			ANGULAR ACCEL. RAD/SEC^2		
	N_x	N_y	N_z	$\ddot{\theta}_x$	$\ddot{\theta}_y$	$\ddot{\theta}_z$
RCS (870 LBS)	0.019 −0.016	±0.022	0.034 −0.040	±0.021	0.024 −0.026	±0.014
VRCS (25 LBS)	+0 −0	±0.0002	+0.0002 −0.0	±0.0007	0.0005 −0.0003	±0.0003

CENTER—OF—MASS AT (1080, 0, 400)
ANGULAR ACCELERATIONS MAY OCCUR SIMULTANEOUSLY

FIGURE 2

178

EMPTY M54D ATTACH POINT ACCEL TF
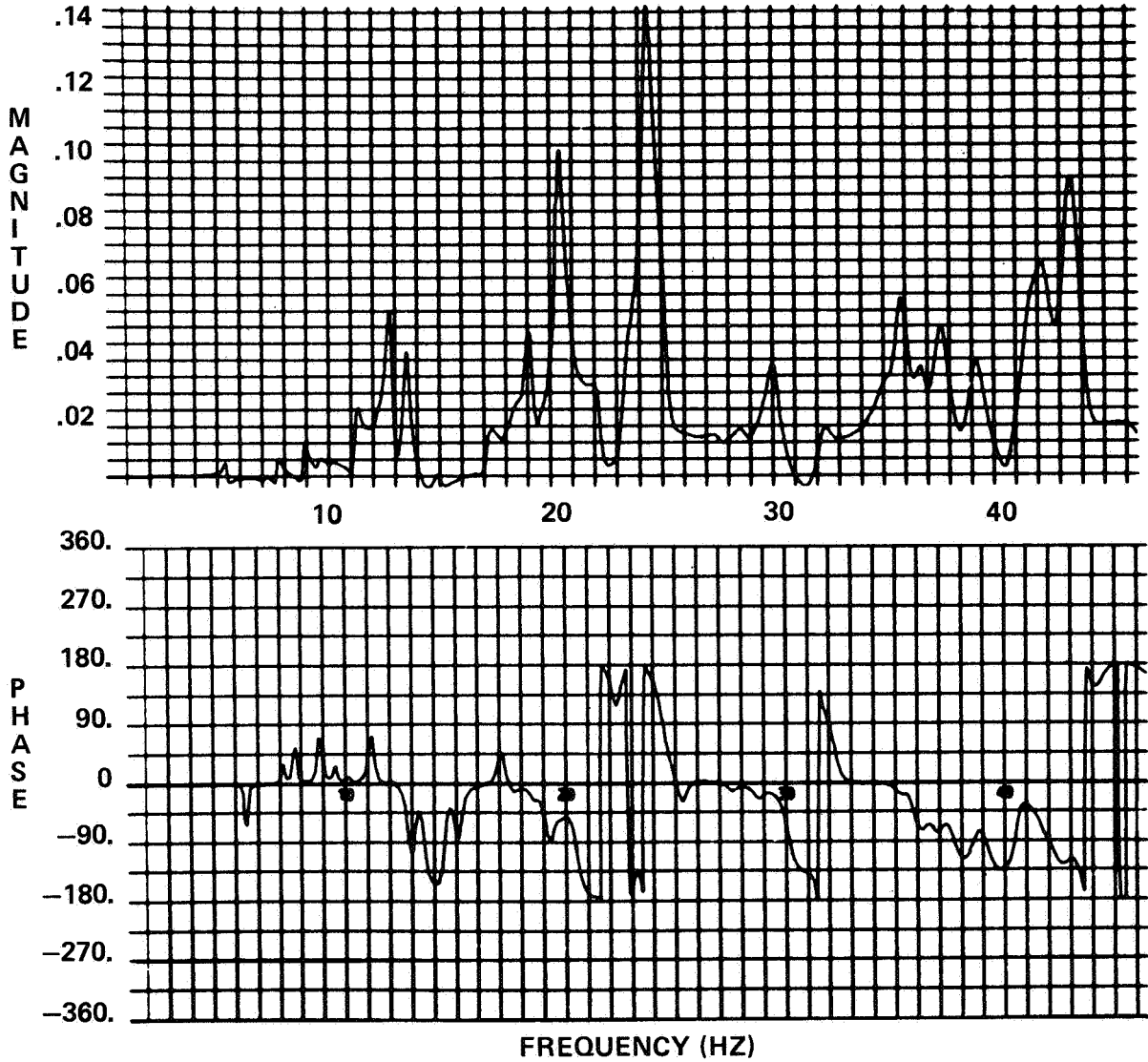
X RESPONSE AT X = 1002.13.y = −94.. z = 414.
TWO SINUSOIDAL THRUST FORCES WITH UNIT
AMPLITUDE AT OMS POD CG ALONG X−AXIS

FIGURE 3

EMPTY M54D ATTACH POINT ACCEL TF
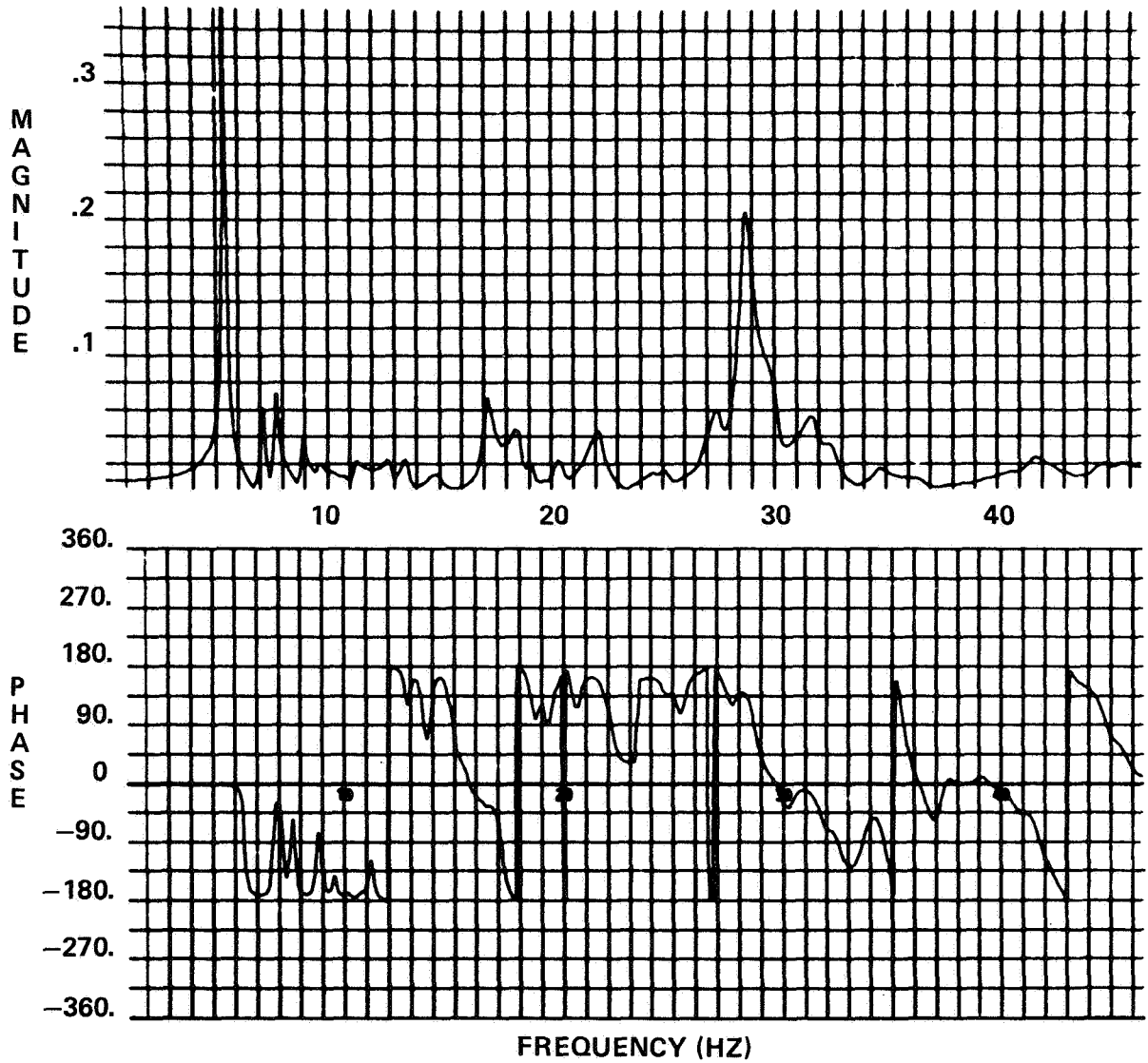
Z RESPONSE AT x = 1002. 13. y = 94. .z = 414.
TWO SINUSOIDAL FORCES WITH UNIT AMPLITUDE
AT TWO NOSE GEAR TRUNNIONS ALONG Z−AXIS

FIGURE 4

CREW ACTIVITIES IN SPACE

by
Lt. Col. Guión S. Bluford, Jr.
NASA/Lyndon B. Johnson Space Flight Center

INTRODUCTION

One of the mission requirements of the Space Shuttle is to serve as a working platform for experiments in space. Many of these experiments will be performed by crewmembers (mission specialists and payload specialists) in a general-purpose laboratory called Spacelab. Part of Spacelab consists of a pressurized module, accessible from the Orbiter cabin through a transfer tunnel, which will provide a shirt-sleeve environment for performing experiments in space. All nonexperiment-related activities or housekeeping activities will be done in the Orbiter, while most of the mission-related activities (experiments) will be done in Spacelab.

In order for experimenters to design their experiments to best utilize the capabilities of the Orbiter, the Spacelab, and the crew, it is necessary that they understand the working environment in the Orbiter and in Spacelab. In addition, the experimenters must be knowledgeable of the housekeeping activities required of the crew.

ORBITER

The Orbiter is the crew and payload carrying section of the Space Shuttle. It is a delta-winged spacecraft/aircraft, about the size of a DC-9 airliner. The forward part of the Orbiter contains the pressurized section in which the crew works, while the aft five-sixths of the Orbiter consists of a payload bay in which the Spacelab module will sit (see Figure 1).

During launch and entry, the acceleration stresses on the crew and payloads will never exceed three g's. On orbit the acceleration levels will be much lower (<.06 g) and will be based on mission requirements and Orbiter capability.

The Orbiter will also be subject to random vibrations on its exterior surfaces, particularly during launch. These vibrations will be generated by acoustic noise (generated by

the engine exhaust) and by aerodynamic noise (generated by airflow). These fluctuating pressure loads will cause structural vibrations which will be transmitted to the mid-fuselage payload section of the Orbiter and eventually to the payload. The magnitude of these vibrations will be based on the transmission characteristics of the Orbiter payload support structure and the interactions between each payload's mass, stiffness, and center of gravity. The estimated values of thermal, pressure, contamination, and electro-magnetic environments in the payload bay for various aspects of flight are given in Space Shuttle System Payload Accommo-dations, JSC-07700, Volume XIV, for user reference.

The pressurized portion of the Orbiter provides separate working and living quarters for the crew with ordinary air (21% oxygen, 79% nitrogen) provided at standard sea-level pressures of 14.7 psi and temperatures of 11°C to 27°C (Figure 2). The humidity is controlled, and odors and carbon dioxide are continuously filtered out.

The upper section of the cabin is the flight deck, from which the Shuttle is controlled and most external payloads are handled. During on-orbit operations, the crew monitors and controls Shuttle systems, performs rendezvous and stationkeeping, operates the payload bay doors and radiator systems, and manages the Orbiter's interface with payloads and Spacelab. Below the flight deck is the crew living area or mid-deck. In this mid-deck area are the sleeping stations, the galley, and the washroom. From the back of the mid-deck is a hatch which leads to the tunnel for entry into the pressurized module of Spacelab.

SPACELAB

Spacelab consists of a module and pallet sections used in various configurations to suit the needs of a particular mission (Figure 3). The pressurized module provides a shirtsleeve working environment for four crewmembers. The Spacelab subsystem equipment, such as environmental control system, power systems, data-handling systems, etc., are located in the forward end of the module, leaving about 60% of the volume available for experiments. In addition, some mission-dependent equipment, such as a top airlock and an optical window/viewport assembly can also be flown. More detailed information on accommodations can be found in the Spacelab Payload Accommodations Handbook (European Space Agency SLP/2104).

The pallets accommodate experiment equipment for direct exposure to space. Each standard pallet segment is 3 meters long, and two or three pallets can be connected together to form a single pallet train. When no module is used with the pallets, a cylindrical "igloo" mounted on the end of the forward pallet provides a controlled, pressurized environment for Spacelab subsystems normally carried in the module. A mission-dependent instrument pointing subsystem can be attached to a pallet for precision payload instrument pointing. Pallet equipment, without a Spacelab module, is operated remotely from the Orbiter aft flight deck or from the ground.

CREW OVERHEAD ACTIVITIES

Besides performing mission-related experiments in space, the crew will have collateral duties to be performed in the Orbiter. These activities include sleeping, eating, exercising, communicating with the ground, and Orbiter systems management. These activities must be integrated into the daily routine or timeline of the crew. A synopsis of these overhead activity requirements is given as follows:

Pre-sleep/Post-sleep Activities

Approximately 45 minutes will be allotted for each pre-sleep and post-sleep activity period. These activities include stowing or unstowing equipment, reviewing checklists and crew activity plans, and personal hygiene.

Sleep

Eight hours per day of uninterrupted sleep will be allotted to each crewman. The sleep stations in the mid-deck of the Orbiter can accommodate four crewmembers simultaneously.

Meals

One hour per meal (three meals per day) will be allotted to each crewmember for food preparation and dining. Four crewmembers can be accommodated simultaneously in the galley area.

Exercise

A limited amount of physical exercise is anticipated for each crewman on flights exceeding eight

days. Exercise will be performed on a portable treadmill or isokinetic exerciser.

Communications/Handover (Two-Shift Operations Only)

Approximately 15 minutes per day will be allotted to reporting Orbiter systems and consumables status to the ground. The crew required for this status report will be the commander and/or pilot and a mission specialist.

For two-shift operations, 15 minutes per day will be required for hand-over operations on which the old shift will brief the new shift on spacecraft status, continuing activities, and any changes in mission operations to be performed during the new shift.

Orbiter Systems Management

Most Orbiter systems management functions will be performed by the commander and/or pilot with some collateral duties being performed by a mission specialist. These collateral duties include fuel cell purging (5 minutes in the auto mode or 25 minutes in the manual mode every 8 hours), CO_2 absorber changeout (5 minutes every 12 hours for four crewmen), water dumps (as scheduled), inertial measuring unit alignments (15 minutes every 8 hours), trash management (as required), and housekeeping duties (at least one hour per day).

MISSION PLANNING

In preparing a crew activity plan for payload activities on a Spacelab mission, it should be anticipated that crew work efficiency will initially be low but will rapidly increase as the crew adjusts to the zero-g environment. Payload specialists will be dedicated full time on Spacelab experiments, while mission specialists will be dedicated approximately 80% of the time. Orbiter activities and detailed test objectives will be integrated with payload activities.

184

X_O 1307
(33 198)

X_O 1302
(33 071)

X_O 576
(14 630)

X_O 582
(14 783)

60 FT
(18.3 M)

CENTER LINE
OF CARGO BAY

Z_O 400
(10 161)

X_O 235
(5969)

15 FT
(4 6 m)
DIAM

Z_O = 0

X_O = 0

CARGO BAY DOORS

FIGURE 1

185

FLIGHT DECK

MID DECK

AIRLOCK

EQUIPMENT BAY

FIGURE 2

FORWARD END CONE
WITH THERMAL INSU—
LATION TENT

VIEWPORT
ASSEMBLY

INSULATION

AIRLOCK

PALLET SEGMENT

TRANSFER
TUNNEL

PALLET/ORBITER
ATTACH FITTINGS

MODULE/ORBITER
ATTACH FITTINGS

EXPERIMENT SEGMENT

CONE SEGMENT

ORBITER

UTILITY SUPPORT STRUCTURE

COVER PLATE

VIEW PORT

AFT END CONE

PROVISIONS FOR
SCIENTIFIC AIRLOCK

PALLET SEGMENTS

UTILITY CONNECTIONS

IGLOO (PALLET—ONLY CONFIGURATIONS)

UTILITY FEEDTHROUGHS

PROVISIONS FOR
VIEWPORT ASSEMBLY

FORWARD END CONE

SMALL EXPERIMENT
VENT ASSEMBLY

EVA AIRLOCK
(ORBITER ELEMENT)

TUNNEL

TUNNEL ADAPTER
(ORBITER ELEMENT)

AFT FLIGHT DECK CONTROLS & DISPLAY

EXPERIMENT SEGMENT

EXPERIMENT RACKS
(DOUBLE AND SINGLE)

FLOOR

CORE SEGMENT

SUBFLOOR FOR SUBSYSTEMS

UTILITY CONNECTIONS

UTILITY FEEDTHROUGHS

INSTRUMENT
POINTING SYSTEM (IPS)

VIEW PORT ASSEMBLY

AIRLOCK
1 M DIAMETER
1 M HEIGHT

IPS AND COMMON PAYLOAD SUPPORT EQUIPMENT (CPSE)

FIGURE 3

187

ACOUSTICS AND VIBRATION ENVIRONMENTS FOR

LABORATORY EXPERIMENTS IN SPACE

by
W. P. Rader
Martin Marietta Corporation
Denver, Colorado

INTRODUCTION

This paper briefly describes some of the basic parameters of random noise and vibration, and presents typical environments for the launch phase and orbital operations. For the latter, both acoustically induced and structure-borne, thruster-induced vibration are addressed, using data obtained during the Skylab and Titan programs.

LAUNCH ENVIRONMENTS

In order for experiments to perform the scientific functions for which they were designed, the equipment must first survive the launch/boost environments. Typical acoustic and random vibration criteria [1] for Spacelab equipment are presented in Figure 1. In Figure 1a, the acoustic levels internal to the payload bay are applicable to pallet-mounted experiments. The noise reduction of the Spacelab module attenuates the environment to the lower level shown (Figure 1a, curve B). Typical predicted random vibration criteria for pallet- and module-mounted equipment are shown in Figure 1b. Note that the pallet specification is applicable for equipment mounted at pallet hard points. For experiments with large, lightweight surface areas, the response of the experiment to direct acoustic excitation must be considered also, since the vibration levels produced may be higher than those transmitted from the pallet.

ORBITAL ENVIRONMENTS

The primary emphasis in this paper is on the acoustic and vibration environments which may interfere with experiment function or scientific data acquisition during operations in space. Very limited measured data are available,

j

since, in the past, the emphasis for conventional launch vehicles has been on defining the severe launch environments, and the data acquisition systems used had inadequate dynamic range to measure the low-level orbital environments. The reusable Shuttle, with suitable instrumentation systems and on-board recording capability, provides the potential to alleviate the problems associated with the limitation of telemetry systems.

Data obtained in the Multiple Docking Adapter (MDA) during the Skylab Missions have been selected as typical of the acoustical environment which may be expected in Spacelab. As points of reference, the overall sound pressure levels in the MDA ranged from roughly equivalent to those in a noisy office or department store to those on a noisy, busy street. The noise-producing equipment in Skylab included fans and pumps associated with the refrigeration and environmental control systems, the rate gyro package, and gears and stepper motors associated with experiments.

Unfortunately, no random vibration measurements were obtained during Skylab orbital operations. Therefore, estimates of the vibration levels have been made based on ground test data and adjustments for differences in acoustic levels measured during the ground test and during the mission. The general technique is often used in predicting random vibration environments for components on new programs. The applicable data were obtained from References 2 and 3, and the results are shown in Figure 2.

THRUSTER-INDUCED VIBRATION

The response of spacecraft to thruster actuation is potentially more detrimental to science experiments than is the equipment noise. Propulsion systems used for orbital/ attitude control typically range in thrust capability from a few pounds to several thousand pounds. One might expect the effect to be limited to a steady-state acceleration; however, the actuation of valves and of pressure fluctuations in the propulsion process produces a dynamic forcing function. The effect is illustrated by an example using data from a Titan transtage.

Data were obtained from several low-frequency (0 to 50 Hz) accelerometers mounted on primary airframe structure during the transtage engine firing. A typical vibration time history is shown in Figure 3. The resulting vibration spectrum is presented in Figure 4. Since experimenters are often concerned with displacements rather than accelerations,

the maximum displacement of the vibration has been estimated. Note that the vibration spectrum has a significant peak at approximately 8 Hz. Referring to the acceleration time history (Figure 3), the maximum acceleration amplitude at this frequency is approximately .05 g peak and the associated maximum displacement is approximately 0.0008 in., 0 to peak.

CONCLUSIONS

Some of the basic parameters associated with random noise and vibration have been briefly discussed, and typical acoustic and vibration environments for both the launch phase and orbital operations have been presented. Too little information is available on the orbital environments. Clearly, measurement systems to acquire these data are needed on early shuttle flights, as well as improved data analysis techniques to determine sources of excitation and transmission of noise as a function of frequency.

It is hoped that the information presented will provide experimenters with a clearer understanding of acoustics and random vibration. Clearly, we dynamicists need to develop a better understanding of the experiments and interaction with the environments in order to recognize what may be detrimental and how to alleviate the problems.

REFERENCES

1. Lipff, J. V. D.: Natural and Induced Environment, VFW-Fokker ERNO Modular Spacelab Specification SR-ER-0008, April 2, 1976.

2. Baratono, John R., and Rader, W. Paul: Skylab Interior Acoustic Environment Report, ED-2002-1200-10, Contract NAS8-24000, Martin Marietta Corporation, Denver, Colorado, March 31, 1972.

3. Anon.: Skylab Vibroacoustic Test Program Phase II, Payload Assembly Acoustic Test, Volumes I and III, Report S&E ASTN-ADD (72-79), NASA/MSFC, January, 1972.
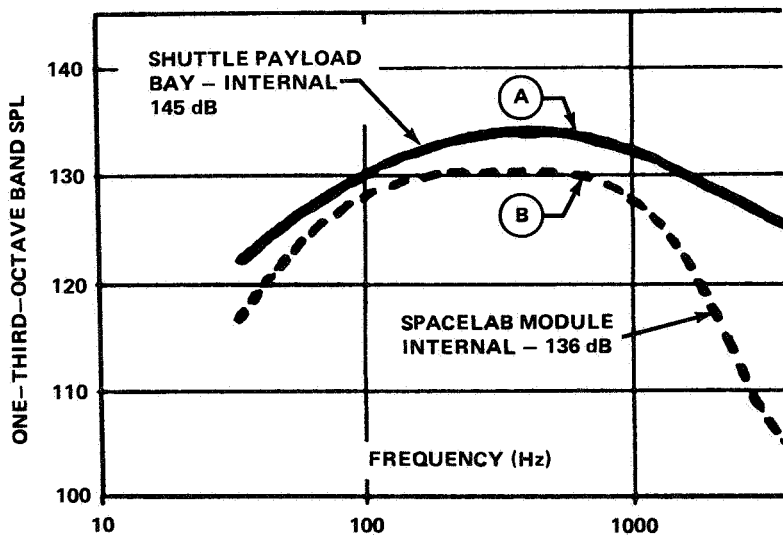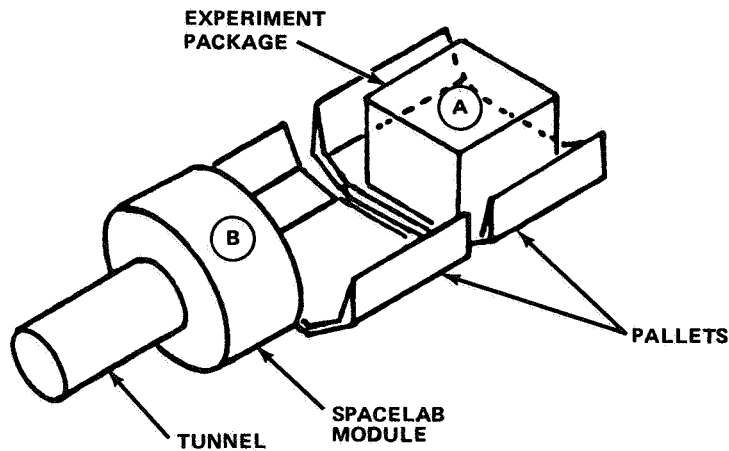
FIGURE 1a. LAUNCH ACOUSTIC LEVELS

FIGURE 1. SPACELAB LAUNCH ACOUSTIC AND VIBRATION ENVIRONMENTS.

191
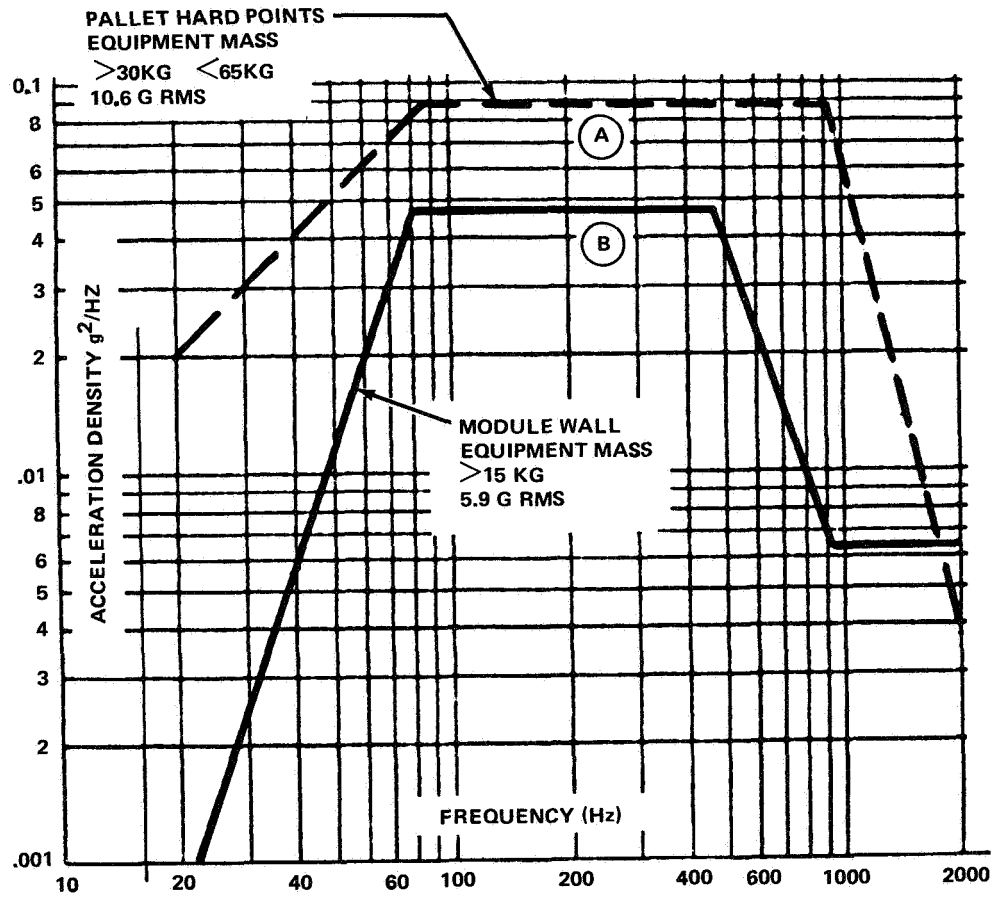
FIGURE 1b. LAUNCH VIBRATION LEVELS

FIGURE 1. SPACELAB LAUNCH ACOUSTIC AND VIBRATION ENVIRONMENTS.

192
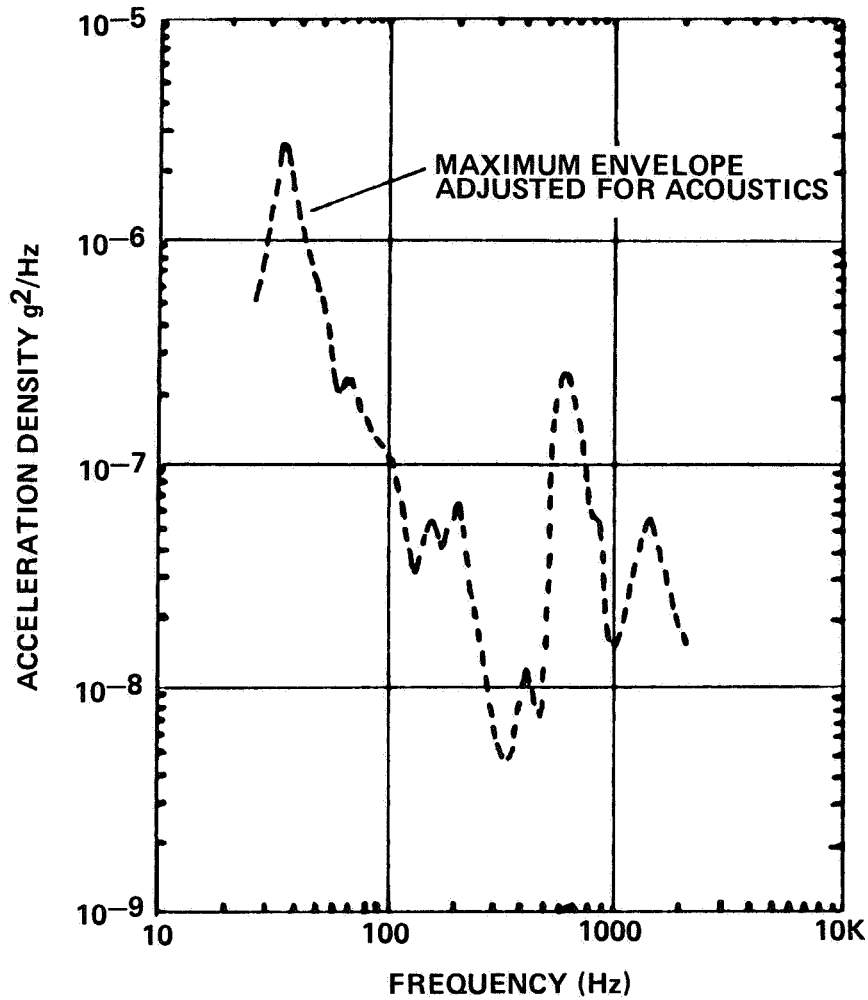
FIGURE 2. ESTIMATED VIBRATION LEVELS DUE TO
NOISE FROM EQUIPMENT OPERATION.

193
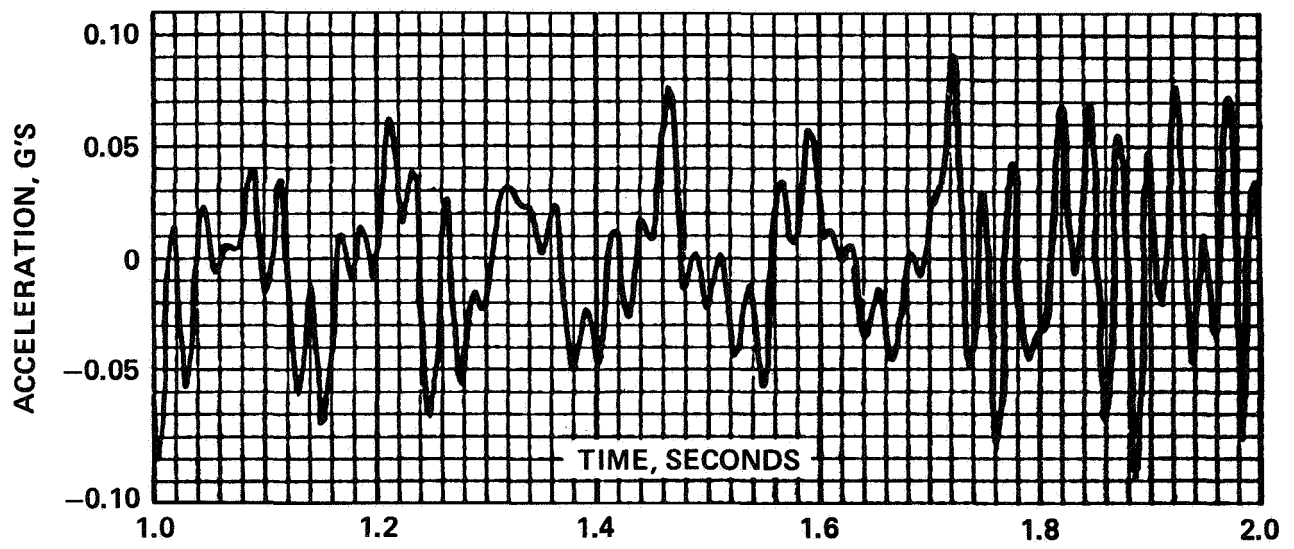
FIGURE 3. ACCELERATION TIME HISTORY
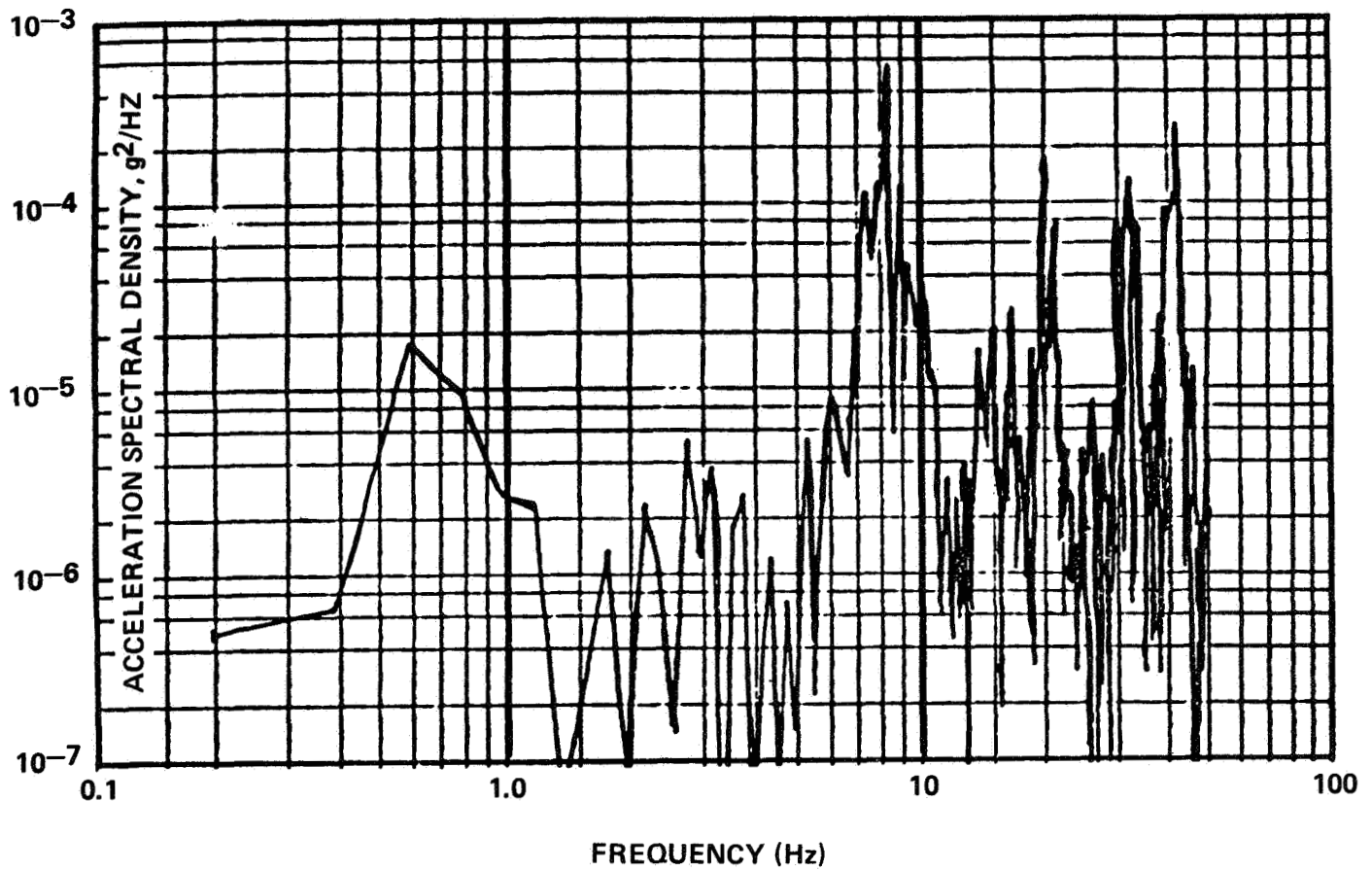
FIGURE 4. VIBRATION RESPONSE TO THRUSTER FIRING.

APPENDIX A

AGENDA FOR WORKSHOP ON SPACECRAFT DYNAMICS
AS RELATED TO LABORATORY EXPERIMENTS IN SPACE

<u>May 1, 1979</u>

Time	Topic	Speaker
8:00	Registration	
8:30	Welcome	W. W. Vaughan
8:35	Workshop Objectives and Plan	G. H. Fichtl

<u>MORNING SESSION</u> Flight Experiments
<u>Chairperson:</u> B. Antar

Time	Topic	Speaker
8:55-9:00	Introduction.	B. Antar
9:00-9:15	Critical Point Experiment .	M. Moldover
9:15-9:30	Liquid Helium Experiments	P. Mason
9:30-9:45	Geophysical Fluid Dynamics	W. Fowlis
9:45-10:00	Drop Dynamics	D. Elleman
10:00-10:15	Atmospheric Cloud Physics	J. Anderson
10:15-10:30	Break	
10:30-10:45	Combustion Processes . . .	A. Berlad
10:45-11:00	Boiling Heat Transfer . . .	W. Frost
11:00-11:15	Tribology Experiment. . . .	R. Gause
11:15-11:30	Materials Processing in Space	R. Naumann
11:30-12:15	Convection in Fluids at Reduced Gravity	S. Ostrach
12:15-1:15	Lunch	

AFTERNOON SESSION Spacecraft Dynamics and Low Gravity
                   Fluid Mechanics
Chairperson: F. Collins

1:15-1:20   Introduction . . . . F. Collins

1:20-1:40   Rotational Fluid
                      Mechanics . . . . R. Gans

1:40-2:00   Vehicle Motion Induced-g
                      Effects on Fluids . . . . R. Dressler

2:00-2:10   Orbital Density
                      Environment . . . . R. Smith

2:10-2:40   Orbital Mechanics . . . . . L. Mullins

2:40-3:00   Relative Motions Inside
                      Spacecraft . . . . B. S. Perrine

3:00-3:15   Break

3:15-4:00   Spacecraft Rigid Body
                      Dynamics . . . . S. Fay

4:00-4:30   Elastic Body Dynamics . . . B. W. Holder

4:30-4:50   Crew Activity . . . . F. Bluford

4:50-5:05   Measurement of Spacecraft
                      Dynamics . . . . S. Fay

5:05-5:30   Acoustics and Vibration . . P. Radar

5:30   Adjourn

6:00   Social . .   Redstone Arsenal Officers Club

May 2, 1979

MORNING SESSION
Chairperson: G. H. Fichtl

9:00-9:05   Introduction . . . . G. H. Fichtl

9:05-9:30   Miniature Electrostatic
                      Accelerometer . . . . . . W. Lang

9:30-9:50   Gravity Wave Detection . . R. Drever

9:50-10:00	ORI Activities in Materials Processing in Space . . .	E. Eller
10:00-10:30	Summary of Previous Day's Meeting	G. H. Fichtl
10:30-12:30	Group Discussion	
12:30	Adjourn	

APPENDIX B
LIST OF PARTICIPANTS

Jeffrey Anderson	NASA Marshall Space Flight Center
Basil Antar	University of Tennessee Space Institute
A. L. Berlad	State University of New York, Stony Brook
Guion S. Bluford, Jr.	NASA Johnson Space Center
Warren Campbell	NASA Marshall Space Flight Center
Al Chirby	Rockwell International, Downey, CA
Thomas H. Cochran	NASA Lewis Research Center
Frank Collins	University of Tennessee Space Institute
Aaron Copeland	Bell Aerospace Textron, Buffalo, NY
Franklin T. Dodge	Southwest Research Institute
Robert F. Dressler	NASA Headquarters
Ronald W. V. Drever	California Institute of Technology
Evan Eller	ORI, Inc., Silver Spring, MD
Stanley Fay	MIT Draper Lab.
Terry Feagin	University of Tennessee, Knoxville
George H. Fichtl	NASA Marshall Space Flight Center
William W. Fowlis	NASA Marshall Space Flight Center
Walter Frost	University of Tennessee Space Institute
Roger F. Gans	University of Rochester
A. C. Giere	NASA Marshall Space Flight Center
Ben Holder	NASA Johnson Space Center
Jae Hyun	NASA Marshall Space Flight Center

201

Vernon W. Keller	NASA Marshall Space Flight Center
William G. Lange	Bell Aerospace - Textron, Bullalo, NY
Peter Mason	Jet Propulsion Lab.
Jim McQuire	NASA Marshall Space Flight Center
Mike Moldover	National Bureau of Standards, Washington, D.C.
Larry Mullins	NASA Marshall Space Flight Center
Robert Nauman	NASA Marshall Space Flight Center
Simon Ostrach	Case Western Reserve University
Scott Perrine	NASA Marshall Space Flight Center
Paul Radar	Martin Marietta, Denver
Mel Saffren	Jet Propulsion Lab.
Charles F. Schafer	NASA Marshall Space Flight Center
R. E. Smith	NASA Marshall Space Flight Center
E. Pat Symons	NASA Marshall Space Flight Center
Richard E. Valentine	NASA Marshall Space Flight Center
William W. Vaughan	NASA Marshall Space Flight Center
Bill Wall	NASA Marshall Space Flight Center
Bill Wilcox	Clarkson College of Technology
Robert S. Witte	TRW

1 REPORT NO. NASA CP- 2199	2. GOVERNMENT ACCESSION NO.	3 RECIPIENT'S CATALOG NO.

4 TITLE AND SUBTITLE	5. REPORT DATE November 1981
SPACECRAFT DYNAMICS AS RELATED TO LABORATORY EXPERIMENTS IN SPACE	6. PERFORMING ORGANIZATION CODE

7 AUTHOR(S) G. H. Fichtl, B. N. Antar, and F. G. Collins, Editors	8. PERFORMING ORGANIZATION REPORT #

9. PERFORMING ORGANIZATION NAME AND ADDRESS	10. WORK UNIT NO. M-362
George C. Marshall Space Flight Center Marshall Space Flight Center, Alabama 35812	11 CONTRACT OR GRANT NO.
	13. TYPE OF REPORT & PERIOD COVERED

12. SPONSORING AGENCY NAME AND ADDRESS	Conference Publication
National Aeronautics and Space Administration Washington, D C. 20546	14. SPONSORING AGENCY CODE

15. SUPPLEMENTARY NOTES

16. ABSTRACT

This report provides summary results of the Workshop on Spacecraft Dynamics as Related to Laboratory Experiments in Space which was held at the Marshall Space Flight Center in Huntsville, Alabama, May 1-2, 1979. Prior to the meeting, the subject of spacecraft dynamics in the context of laboratory experiments in space had not been considered in a unified manner. The Physics and Chemistry Experiments in Space (PACE) Working Group sponsored this meeting for scientists and engineers to discuss the nature of spacecraft dynamics and its impact on the design and performance of laboratory experiments in space and to identify engineering and scientific deficiencies in our knowledge of the subject. The proceedings can serve as an introduction to the subject for those new to the use of space as a laboratory environment and can serve as a reference for those currently planning to use space for scientific experimentation. The workshop was organized by NASA Marshall and the University of Tennessee Space Institute, Tullahoma, Tenn.

17 KEY WORDS	18. DISTRIBUTION STATEMENT
Spacecraft Dynamics — Spaceflight Experiment Definition Low-Gravity Fluid Mechanics	Unclassified - Unlimited STAR Category: 18

19. SECURITY CLASSIF (of this report)	20. SECURITY CLASSIF. (of this page)	21 NO. OF PAGES	22 PRICE
Unclassified	Unclassified	211	A10